Proximity labeling approaches to mitochondrial import receptors TOMM20 and TOMM70

Dissertation

der Mathematisch-Naturwissenschaftlichen Fakultät

der Eberhard Karls Universität Tübingen

zur Erlangung des Grades eines

Doktors der Naturwissenschaften

(Dr. rer. nat.)

vorgelegt von

Saira Akram

aus Faisalabad, Pakistan

Tübingen

2025

Gedruckt mit Genehmigung der Mathematisch-Naturwissenschaftlichen Fakultät der Eberhard Karls Universität Tübingen.

Tag der mündlichen Qualifikation:	15.04.2025
Dekan:	Prof. Dr. Thilo Stehle
1. Berichterstatter/-in:	Prof. Dr. Ralf-Peter Jansen
2. Berichterstatter/-in:	Prof. Dr. Jeffrey Gerst

Erklärung / Declaration:

Ich erkläre, dass ich die zur Promotion eingereichte Arbeit mit dem Titel:

“Proximity labeling approaches to mitochondrial import receptors TOMM20 and TOMM70’’

Selbstständig verfasst, nur die angegebenen Quellen und Hilfsmittel benutzt und wörtlich oder inhaltlich übernommene Stellen als solche gekennzeichnet habe. Ich versichere an Eides statt, dass diese Angaben wahr sind und dass ich nichts verschwiegen habe. Mir ist bekannt, dass die falsche Abgabe einer Versicherung an Eides statt mit Freiheitsstrafe bis zu drei Jahren oder mit Geldstrafe bestraft wird.

I hereby declare that I have produced the work entitled:

“Proximity labeling approaches to mitochondrial import receptors TOMM20 and TOMM70’’

submitted for the award of a doctorate, on my own (without external help), have used only the sources and aids indicated and have marked passages included from other works, whether verbatim or in content, as such. I swear upon oath that these statements are true and that I have not concealed anything. I am aware that making a false declaration under oath is punishable by a term of imprisonment of up to three years or by a fine.

Augsburg, 10.03.2025

Table of Contents

Summary

In yeast, import of most mitochondrial proteins requires that their precursor proteins are bound by the peripheral receptor proteins Tom20, Tom22, and Tom70, a process conserved from yeast to mammals. For budding yeast Tom20 and Tom70, there is evidence of specific yet overlapping substrate recognition, however, no such data is available for the metazoan cells. Although mitochondrial protein import has been extensively studied in past years, the cytosolic stage of this process remains enigmatic. The cytosolic ribosomes interacting with the TOM complex have been found at the mitochondrial outer membrane (MOM). mRNA localization to specific subcellular compartments is an essential process in the eukaryotic cells, allowing precise and targeted distribution of mRNAs to particular site, where proteins can be synthesized locally, exactly where they are needed. Numerous nuclear-encoded mitochondrial mRNAs are increasingly recognized to be localized to MOM. mRNA localization to the mitochondria is well documented in polarized cells like neurons but global occurrence of mRNA localization in other mammalian cells remains to be analyzed. The key players involved in this process mainly include RNA binding proteins (RBPs), which presumably regulate the targeting and local translation of their putative targets at MOM. In my project, I aimed to identify the association profiles for TOMM20 and TOMM70 in mammals. I particularly focused on identifying novel RBPs, associating with these receptors and probably being involved in localized translation at the TOM complex. For that, I established an APEX2-based proximity labeling methodology, and targeted it to human TOMM20 and TOMM70 receptors in HeLa cells. This approach allowed me to capture the distinct interactomes of TOMM20 and TOMM70 receptors within their nano-environments. Each receptor showed enrichment of a unique set of proteins, though several RBPs and translation factors were preferentially more enriched in TOMM20 interactome over TOMM70 interactome. These include SYNJ2BP, a previously identified MOM-localized RBP that binds and protects mRNAs encoding mitochondrial proteins. Translational inhibition by puromycin resulted in an even increased association of these RBPs with TOMM20 compared to TOMM70, suggesting that TOMM20 but not TOMM70 might play a role in preserving cellular homeostasis during translation stress by retaining protective RBPs and translation-related proteins at

the MOM. Further validation of identified interactors by orthogonal experiments could potentially identify their complex interaction and function at TOM complex. Then, nearby mRNAs biotinylated by TOMM20 bait protein were identified in a preliminary RNA-seq analysis. Not any particular enrichment of nuclear-encoded mitochondrial transcripts over non-mitochondrial ones was identified. It appears like RNA-Seq pipeline requires further optimization to identify local transcriptome at the TOM complex. However, I established an APEX2 based methodology for studying the local proteome of the human TOMM20 and TOMM70 receptors at MOM in HeLa cells. In future, this methodology could be further applied in other cells, such as neurons, to identify receptor specific interactomes. The identified interactomes could be further characterized and compared with analyses of other TOM receptors to reveal complex interactions at MOM, and provide deeper insights into localized translation processes and their contribution to mitochondrial import.

Zusammenfassung

Der Import der meisten mitochondrialen Proteine setzt voraus, dass ihre Vorläuferproteine von den peripheren Rezeptorproteinen Tom20, Tom22 und Tom70 gebunden werden. In der Bäckerhefe gibt es für Tom20 und Tom70 Hinweise auf spezifische, allerdings überlappende Substraterkennung; solche Daten gibt es nicht für Zellen aus Metazoen. Obwohl mitochondrialer Proteinimport in den letzten Jahren ausgiebig untersucht wurde, bleibt die zytosolische Phase dieses Prozesses rätselhaft. Die zytosolischen Ribosomen, die mit dem TOM-Komplex interagieren, wurden der äußeren mitochondrialen Membran (MOM) zugeordnet. Die mRNA-Lokalisierung an spezifischen, subzellulären Kompartimenten ist ein wesentlicher Prozess in eukaryotischen Zellen, der eine präzise und gezielte Verteilung der mRNAs auf spezifische Orte erlaubt, an denen die Proteine lokal, dort wo sie gebraucht werden, synthetisiert werden. Zunehmend werden kernkodierte mitochondriale mRNAs an der äußeren mitochondrialen Membran lokalisiert. Die mRNA-Lokalisierung in Mitochondrien ist in polarisierten Zellen wie Neuronen gut dokumentiert, doch generell muss die mRNA-Lokalisierung in anderen Säugetierzellen noch analysiert werden. Die Hauptakteure schließen RNA-Bindeproteine ein (RBPs), die vermutlich das Targeting und die lokale Translation ihrer mutmaßlichen Targets regulieren. Mit APEX2-basierter Nachbarschaftsmarkierung habe ich daher Assoziationsprofile für TOMM20 und TOMM70 in menschlichen HeLa-Zellen erstellt. Insbesondere habe ich mich auf die Identifizierung neuer RBPs konzentriert, die mit diesen Rezeptoren assoziiert sind und wahrscheinlich in die lokalisierte Translation am TOM-Komplex involviert sind.

Unsere Experimente legen die präferenzielle Assoziation mehrere RBPs und Translationsfaktoren mit TOMM20 im Vergleich zu TOMM70 nahe. Dazu gehört SYNJBP2, ein zuvor identifiziertes, MOM-lokalisiertes RBP, das an mRNAs für mitochondriale Proteine bindet und diese schützt. Die Hemmung der Translation mit Puromycin führt zu erhöhter Assoziation dieser RBPs mit TOMM20 im Vergleich zu TOMM70. Somit liegt nahe, dass TOMM20, nicht aber TOMM70 eine Rolle bei der Etablierung der zellulären Homöostase während des translationalen Stresses spielt, indem protektive RBPs und translationsbezogene Proteine an der äußeren mitochondrialen Membran gehalten werden.

Die weitere Validierung der identifizierten Interaktoren durch orthogonale Experimente könnte potenziell ihre komplexe Interaktion und Funktion am TOM-Komplex aufklären. Anschließend wurden in einer vorläufigen RNA-Seq-Analyse nahegelegene mRNAs identifiziert, die durch das TOMM20-Köderprotein biotinyliert wurden. Bisher wurde keine spezifische Anreicherung von nukleär kodierten mitochondrialen Transkripten gegenüber nicht-mitochondrialen Transkripten festgestellt. Es scheint, dass die RNA-Seq-Pipeline einer weiteren Optimierung bedarf, um das lokale Transkriptom am TOM-Komplex präziser zu identifizieren. Jedoch habe ich eine auf APEX2 basierende Methodik etabliert, um das lokale Proteom und Transkriptom der humanen TOMM20- und TOMM70-Rezeptoren in HeLa-Zellen zu untersuchen. Zukünftig könnte diese Methodik auch auf andere Zelltypen, wie beispielsweise Neuronen, angewendet werden, um rezeptorspezifische Interaktome zu identifizieren. Die ermittelten Interactome könnten weiter charakterisiert und mit Analysen anderer TOM-Rezeptoren verglichen werden, um komplexe Interaktionen an der äußeren mitochondrialen Membran (MOM) aufzudecken und weitere Einblicke in lokalisierte Translationsprozesse sowie deren Beitrag zum mitochondrialen Import zu gewinnen.

List of publications

Akram, S., Zittlau, I. K., Maček, B., & Jansen P. R. Proximity labeling reveals differential interaction partners of the human mitochondrial import receptor proteins TOMM20 and TOMM70. bioRxiv 2024.10.25.620316. DOI: 10.1101/2024.10.25.620316 (under review at Journal of Proteome Research)

Weissinger, R., Heinold, L., **Akram, S**., Jansen, R.-P., & Hermesh, O. (2021). RNA Proximity Labeling: A New Detection Tool for RNA–Protein Interactions. Molecules, 26(8), 2270. DOI: 10.3390/molecules26082270

Personal contribution to the publications

Akram, S., Zittlau, I. K., Macek, B., & Jansen P. R. Proximity labeling reveals differential interaction partners of the human mitochondrial import receptor proteins TOMM20 and TOMM70. bioRxiv 2024. DOI: 10.1101/2024.10.25.620316.
(Under review at Journal of Proteome Research)

I formulated research questions and performed experiments, including Western blotting, subcellular fractionation, immunoprecipitation, microscopy analysis, and initial mass spectrometry (MS) sample preparation (biotinylation and streptavidin pull-down to enrich biotinylated proteins) for downstream mass spectrometry (LC-MS/MS) analysis. The project was conducted in close collaboration with Boris Macek and Katharina Zittlau at the Proteome Center Tubingen (PCT), University of Tübingen, Germany. Katharina Zittlau designed the MS pipeline to analyze the samples under the supervision of Boris Macek. Subsequent MS-sample preparation was also done at PCT by Silke Wahl under the supervision of Katharina Zittlau and Boris Macek. MS data processing and analysis were performed by Katharina Zittlau under the supervision of Boris Macek. I wrote the manuscript with the support of Ralf-Peter Jansen, Katharina Zittlau, and Boris Macek. The manuscript is integrated into chapters 3, 4, and 5 of this thesis. In summary, I am responsible for Figure 1–13, Figure 16, Figure 19, Figure 20, and Supplementary Figure 1 in this thesis.

Weissinger, R., Heinold, L., **Akram, S**., Jansen, R.-P., & Hermesh, O. (2021). RNA Proximity Labeling: A New Detection Tool for RNA–Protein Interactions. Molecules, 26(8), 2270. DOI: 10.3390/molecules26082270.

I wrote chapter 1 of this review article with the help of Ralf-Peter Jansen.

Chapter 1: Introduction

1.1 Mitochondria- a snapshot of cell´s powerhouse

Eukaryotic cells have distinctly organized themselves into many unique membrane-enclosed compartments, each maintaining a specific microenvironment and performing their intracellular, compartment-specific function (Diekmann & Pereira-Leal, 2012). According to the 'endosymbiosis theory' by Lynn Margulis (Sagan, 1967), mitochondria are traced back 1.5 billion years ago to the free-living, aerobic alpha-proteobacteria that were engulfed by the ancestor of the eukaryotic cells and gradually evolved into the present-day organelles (reviewed by Dyall, Brown, and Johnson 2004; Gray, Burger, and Lang 1999). These semi-autonomous organelles retain their own small 16.6 kb (in humans) DNA genome (mtDNA) that resides in multiple copies and can independently replicate, transcribe, and is also translated in the organelle (Taanman, 1999). In mammals, only 13 of the mitochondrial proteins are encoded by mtDNA, they form the core subunits of the mitochondrial oxidative phosphorylation (OXPHOS) system together with the nuclear-encoded subunits. The rest (~99%) of the mitochondrial proteins are contributed by the nucleus. Hence, the biogenesis of functional mitochondria fully depends on the efficient synthesis and import of those precursor proteins into the organelle. Mitochondria were first purified in the early 1950s and characterized as unique structures surrounded by the two membranes, a mitochondrial outer membrane (MOM) and an inner mitochondrial membrane (IMM; Palade, 1953; Sjöstrand, 1953). Both of the membranes are proximal to each other, with a 12-40 nm space exists between them, known as intermembrane space (IMS). The mitochondrial matrix comprises membrane-enclosed space within the IMM. Both membranes exhibit significant differences in their protein and lipid composition (Giacomello et al., 2020). MOM is semi-permeable for the small molecules, while the IMM is a densely-protein enriched membrane with strictly controlled permeability (Vogel et al., 2006). Further, the IMM further invaginates into the mitochondrial cristae, or sometimes tubuli, to enhance surface areas creating microdomains with specific protein composition (Vogel et al., 2006).

Mitochondria, being highly dynamic organelles of the cell maintain the metabolic homeostasis of the cells. They are capable of changing their morphology and

continuously undergo fusion reactions in order to substitute their damaged proteins or replenish their mitochondrial contents. On the other hand, mitochondrial fission is a process that allows the elimination of impaired organelles by activating autophagy pathways leading to apoptosis during cellular stress (Youle & van der Bliek, 2012). A balanced interplay between mitochondrial biogenesis and degradation of the defective ones is necessary in maintaining functional mitochondria and, therefore, cell survival. All these processes depend entirely on the mitochondrial protein biogenesis and import.

1.2 Mitochondrial import – a highly versatile and tightly regulated mechanism

The vast majority (~99%) of the mitochondrial proteins are nuclear encoded (Meisinger et al., 2008). Hence, the biogenesis of functional mitochondria fully depends on the effective synthesis and import of those precursor proteins into the organelle. These nuclear-encoded precursors are imported into the organelle either post- or co-translationally and eventually sorted to their final destination by defined targeting signals, which can be either internally situated or located at N-terminus (Meisinger et al., 2008; Wiedemann & Pfanner, 2017). Around 60% of the mitochondrial proteome in their precursor form carry a N-terminal cleavable segment of variable length, ranging between 10 and approximately 100 amino acid residues, designated as matrix targeting signal (MTS) or mitochondrial targeting peptide (Chacinska et al., 2009; Roise et al., 1986). Preproteins carrying specific targeting signals are recognized by the mitochondrial import machinery, a highly versatile and tightly regulated system that governs their transport and distribution to the corresponding mitochondrial sub-compartments (Neupert & Herrmann, 2007; Wiedemann & Pfanner, 2017).

Mitochondria tailors protein transfer in dual directions, including precursors from the cytosol into MOM or other sub-compartments like IMS, IMM or matrix, along with the mitochondrial genome-encoded proteins from the matrix to the IMM. MOM permits the free movement of ions and water-soluble molecules with a size limit of 2-6 kDa, which mainly shuttle through the voltage-dependent anion channel (VDAC; Rosencrans et al., 2021). Due to the free flow of the ions and small molecules, the composition of IMS remains comparable to the cytoplasm. Any molecule larger than this size limit is transported into the mitochondria only

via translocases of the outer membrane (TOMs). Therefore, the TOM complex is the main entry gate for all mitochondrial proteins. After crossing the TOM complex, these precursor proteins are further sorted into their corresponding mitochondrial sub-compartments i.e. MOM, IMM, and matrix (**Figure 1**). Mitochondrial precursors take different pathways, which primarily depends on if they cross the mitochondrial membrane either once or multiple times, as well as which end of the protein is directed towards MOM. Precursors imported into various mitochondrial sub-compartment may take different routes, described as follows:

1.2.1 Import of the matrix and IMM proteins via the 'classical' presequence pathway

The majority of the matrix and IMM proteins carry a N-terminal targeting signal and are imported and subsequently sorted through this classical presequence pathway (Roise et al., 1986; Vögtle et al., 2009). Their import signals form positively charged, amphiphilic α-helical structures with a hydrophobic face (Abe et al., 2000), and are recognized specifically during translocation specifically by the complexes of the import machinery including TOMs, and TIMs (TIM23 complex), as well as the translocase-associated motor (PAM; Dudek et al., 2013; Wiedemann & Pfanner, 2017). Structural studies using X-ray crystallography showed that these N-terminal presequences consist of a consensus, encrypted motif ("ϕχχϕϕ", where ϕ corresponds to a hydrophobic amino acid and χ represents any amino acid). In yeast, these precursors are first recognized by Tom20, then further transferred to Tom22. Afterwards these are translocated via the translocation pore known as Tom40 channel. (Bolliger et al., 1995; Moczko et al., 1997; Mossmann et al., 2012; Yamano et al., 2008). The inner membrane translocase or Tim23 (TIMM23 in mammals) complex, along with the import motor, ensures targeted protein translocation into the matrix (Becker et al., 2012; Bolender et al., 2008; Kühlbrandt, 2015). The translocases of the MOM and IMM (TOMMs and TIMMs) transiently interact with each other: When a presequence-carrying precursor protein crosses the Tom40 channel to the IMS side, the TIM50, which is an integral subunit of the Tim23 channel, binds it as a receptor and further shuttles the protein over to the Tim23, which in turn is closely associated with Tim17 (Albrecht et al., 2006; Chacinska et al., 2005). This shuttling utilizes an electrochemical hydrogen ion gradient in the form of a membrane potential

(Δψ) to translocate proteins further to the matrix (Meinecke et al., 2006). While the IMM proteins carrying a stop-transfer signal are arrested during import to be laterally sorted into IMM (Schendzielorz et al., 2016), the precursors destined to be sorted into the matrix, are imported completely through their interaction with the PAM motor, driven by an ATP-dependent process. The presequences of both, matrix-targeted as well as IMM-sorted preproteins, are cleaved off by the matrix processing peptidase (MPP), either during transit or after transport via the TIM23 complex, and are further degraded by the presequence peptidase (PreP; Dudek et al., 2013; Mossmann et al., 2012; Wiedemann & Pfanner, 2017)

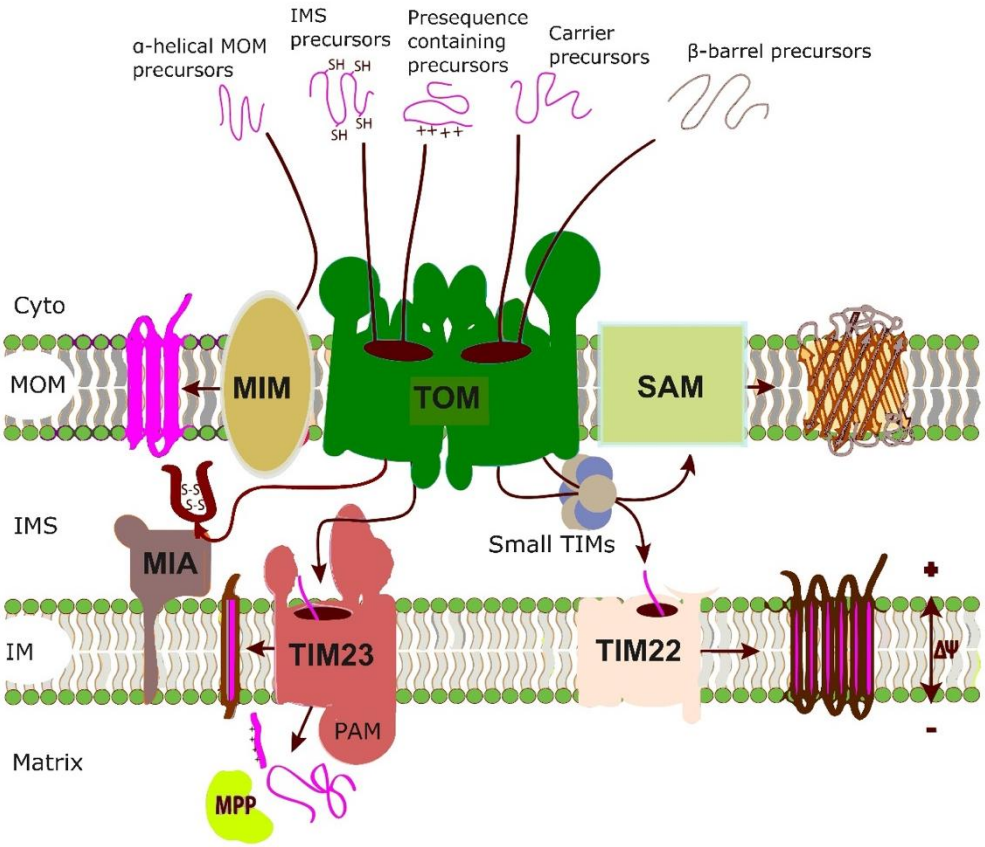

Figure 1. Pathways of mitochondrial protein import inside the organelle.
Nuclear encoded mitochondrial precursors adopt various routes depending on their structure and target destination in mitochondrial sub-compartments. After their synthesis on cytosolic or MOM localized ribosomes, all precursor proteins are imported through the TOM complex. Afterwards, precursors are directed to four specific mitochondrial compartments namely MOM, IM, IMS, and Matrix and utilize various machineries including mitochondrial import machinery (MIM), sorting and assembly machinery (SAM), mitochondrial intermembrane space import and assembly machinery (MIA), translocase of the inner mitochondrial membrane 23 (TIMM23) machinery, translocase of the inner mitochondrial membrane 22 (TIMM22) machinery, and a presequence-associated motor (PAM) (figure is modified from Gupta & Becker, 2021).

1.2.2 Import of multi-spanning IMM proteins through the carrier pathway

A large number of mitochondrial proteins like hydrophobic carrier proteins consist of multiple α-helical TM domains, are synthesized without cleavable presequences. Instead, they contain internal targeting signals (internal MTS-like signal sequence; iMTS-LS) located in their mature region (Brix et al., 1997; Endres et al., 1999). Such hydrophobic proteins are prone to aggregate; hence they need specialized chaperones. In yeast, these precursors bind first to the cytosolic chaperones, the ATP-dependent heat-shock proteins Hsp70/Hsp90, which recruit them to the receptor Tom70 (Backes et al., 2021), which then transfers these precursors to the receptor Tom22. Afterwards they translocate across the Tom40 channel, while maintaining a loop form with their both termini still in the cytosol, while the middle portion has already made its way to the intermembrane space. After translocation through the TOM channel, another set of IMS resident TIM chaperones, the Tim9-Tim10 complex, takes over. These chaperones recruit to the MOM, bind to the precursors, which in turn are eventually delivered to the carrier translocase of the inner membrane, the TIM22 complex. TIM22 mediates the Δψ-dependent, lateral release and insertion of the precursors driven by the inner membrane potential (Harbauer et al., 2014; Kurz et al., 1999; Rehling et al., 2003; Wiedemann & Pfanner, 2017).

1.2.3 The MIA pathway: protein sorting to the IMS

Numerous proteins in the mitochondrial IMS possess specific cysteine motifs inside their IMS sorting signals. These cysteine motifs form intramolecular disulfide bonds, and further on, the proteins need to be correctly folded. These proteins translocate in their reduced form, do not possess cleavable targeting sequences, and entirely depend on the TOM complex and the oxidoreductase Mia40- based oxidative protein folding machinery (Chatzi et al., 2016; Gornicka et al., 2014; Herrmann & Riemer, 2010; Stojanovski et al., 2008; Wiedemann & Pfanner, 2017). After crossing the Tom40 channel, the unfolded precursors in their reduced form are quickly handled over to the mitochondrial intermembrane space import and assembly protein 40 (Mia40), that oxidizes these precursors and further facilitates translocation into the IMS. It is considered that the MIA pathway has larger spectrum than initially expected. It also contributes to the biogenesis and quality control of matrix and IMM proteins. These include Tim17, Tim22, and the mitochondrial ribosomal subunit Mrp10 (Longen et al., 2014;

Wrobel et al., 2013, 2016).

1.2.4 Protein sorting at MOM

The MOM proteome is essential for mitochondrial-cytoplasmic crosstalk. MOM proteins exist either as α-helical or β-barrel membrane proteins. These structurally distinct proteins follow two different import routes as follows.

1.2.4.1 The β-barrel pathway: import of β-barrel anchors

The β-barrel MOM proteins are integrated into the MOM via multiple transmembrane β- sheets, which twist and roll up together forming a barrel like structure. Mitochondria in yeast are reported to contain four primary β-barrel proteins in yeast including Tom40, the SAM complex channel Sam50, the voltage-dependent anion channel (Vdac), and Mdm10, the integral subunit of mitochondrial-ER contact sites (Imai et al., 2011; Walther et al., 2009). Their targeting signal mainly comprises a β-hairpin element and is recognized by theTOM receptor, although the exact targeting sequence recognized is not yet known (Dudek et al., 2013; Jores et al., 2016). All three TOM receptors, Tom70, Tom20, and Tom22 are crucial for their import (Krimmer et al., 2001; J. Qiu et al., 2013). Once β-barrel substrates are recognized, they are further imported into the IMS through the Tom40 channel, and bound to TIM chaperones of the IMS. These Tim chaperones including the Tim9–Tim10 and Tim8–Tom13 complexes appear in heterohexameric complexes, also associate to the MIA pathway, and preserve the hydrophobic proteins including β-barrels from aggregation in the aqueous IMS surroundings (Dudek et al., 2013; Wiedemann & Pfanner, 2017). Ultimately, the β-barrels precursors are handled to the sorting and assembly machinery (SAM) and are further inserted into the MOM (Diederichs et al., 2020; Takeda et al., 2021).

The human SAM complex comprises cytosolically exposed, peripheral membrane proteins including MTX2 (Sam35 in yeast), MTX3 (Sam37 in yeast), MTX1, and a MOM associated β-barrel core subunit SAMM50 (yeast Sam50; Diederichs et al., 2020). The exact mechanisms behind the insertion of β-barrel proteins into the MOM are still not fully known. In yeast, the direct translocation of the β-barrel precursors from the TOM complex to the SAM complex is also reported (Kutik et al., 2008). Here, the cytosolic domain of Tom22 interacts with Sam37, resulting in a transient TOM-SAM supercomplex (Qiu et al., 2013; Wenz et al., 2015). Meanwhile, Sam35 recognizes the sorting signal in the last strand

of the β-barrel precursor. This binding induces a conformational change in the supercomplex as a result of which channel protein Sam50 is opened, allowing the insertion of the β-barrel precursors into the Sam50 channel and lateral release into the lipid phase of the MOM (Kutik et al., 2008; Wenz et al., 2015).

1.2.4.2 The MIM pathway: import of the α-helical proteins into MOM

Similar to the IMM proteins, the import of the α-helical proteins into MOM depends on the targeting signal positioned outside or within the transmembrane domain of these proteins. The α-helical proteins are grouped in three main classes: signal-anchored (SA) proteins, tail-anchored (TA) proteins, and polytopic or multispanning MOM proteins (Haastrup et al., 2023; Wiedemann & Pfanner, 2017). The SA and TA proteins possess the α-helical transmembrane domains at the corresponding N- or C-terminus, respectively. These transmembrane domains exhibit modest average hydrophobicity and are flanked by positively charged amino acid residues. They also perform a dual function as both, targeting signals and membrane anchors. While polytopic proteins possess multiple transmembrane domains spanning the MOM multiple times, their exact targeting signals are still unknown (Kanaji et al., 2000; Waizenegger et al., 2003). In yeast, the protein insertase for SA and polytopic MOM proteins is the mitochondrial import complex (MIM) that itself comprises multiple copies of the small single-spanning MIM1 and one or two copies of MIM2 (Wiedemann & Pfanner, 2017). None of the TOM receptors are involved in the import of SA proteins (Ahting et al., 2005; Meineke et al., 2008). In yeast, the polytopic α-helical MOM proteins are recognized by the Tom70 receptor that shuttle them to the MIM complex for their subsequent insertion into the MOM (Becker et al., 2012; Papić et al., 2011). The majority of TA proteins do not employ proteinaceous import machinery, rather their import may be facilitated by the lipid composition of the MOM (Kemper et al., 2008; Setoguchi et al., 2006). However, the impaired import of the precursor of the tail-anchored α-helical Fis1 protein in yeast was observed in isolated *mim1*Δ and *mim1-23 deficient* mitochondria (Doan et al., 2020). Hence, the MIM complex is necessary for the import of all kinds of α-helical proteins. In addition, the low ergosterol content of the MOM also facilitates the import of TA proteins into the MOM (Kemper et al., 2008). Yeast Tom20 and Tom70, both being SA proteins follow a MIM-dependent insertion (Becker et al., 2008, 2011; Dimmer et al., 2012; Hulett et al., 2008; Popov-Čeleketić et al., 2008). Whereas

both TA precursors Mim1 and Tom22 contain internal targeting sequences, as their C-termini embedded in the IMS. Both proteins are reported to be imported by the TOM receptors and the SAM complex, although their final insertion steps differ with each other (Keil & Pfanner, 1993; Papić et al., 2013; Stojanovski et al., 2007). Interestingly, few MOM proteins follow distinct import routes. For example, the MOM protein Mcp3 in yeast, which possesses a N-terminal presequence including a stop-transfer signal, and is imported by the TOM and TIM23 complexes. It is first inserted laterally into the inner membrane and further processed by an inner-membrane peptidase (IMP). Afterwards, it is released into the IMS and then exported into the MOM by the MIM complex (Sinzel et al., 2016).

1.3 The TOM complex- the entry gate of mitochondria

The nuclear-encoded mitochondrially destined precursors are recognized by a heterooligomeric protein complex known as TOM complex, which constitutes the main entry gate for all precursors. The TOM complex was first identified in 1989, however, its detailed structure remained inconclusive for about three decades (Söllner et al., 1989; Vestweber et al., 1989). Recent advancements in cryo-EM helped to reveal the structures of the TOM complex, particularly in *Neurospora crassa* (Bausewein et al., 2017), humans (Guan et al., 2021; Su et al., 2024; Wang et al., 2020), and yeast (Araiso et al., 2019; Tucker & Park, 2019). The structure of the TOM complex is highly conserved among species. It consists mainly of seven different subunits, which are either α-helical or β-barrel membrane proteins (Brix et al., 1997; Wang et al., 2020). In mammals, the central poreforming channel is made by β-barrel protein TOMM40 and works as an import channel for shuttling of the precursors into the organelle. The other subunits are α-helical structures (Meisinger et al., 2001). In mammals, these include two peripheral receptors, TOMM20 (yeast homolog: Tom20) and TOMM70 (yeast homolog: Tom70), a central preprotein receptor subunit, TOMM22 (yeast homolog: Tom22)", and three supplementary subunits including TOMM5 (Tom5 in yeast), TOMM6 (Tom6 in yeast), and TOMM7 (Tom7 in yeast; Araiso et al., 2019; Harbauer et al., 2014; Su et al., 2022; Wang et al., 2020). In mammals, two TOMM22 receptors reportedly tether and stabilize the TOMM40 adjacent pores at the dimer interface and constitute a TOM core complex (TOM-CC) together with the supplementary small TOM subunits **(Figure 2A, left**).

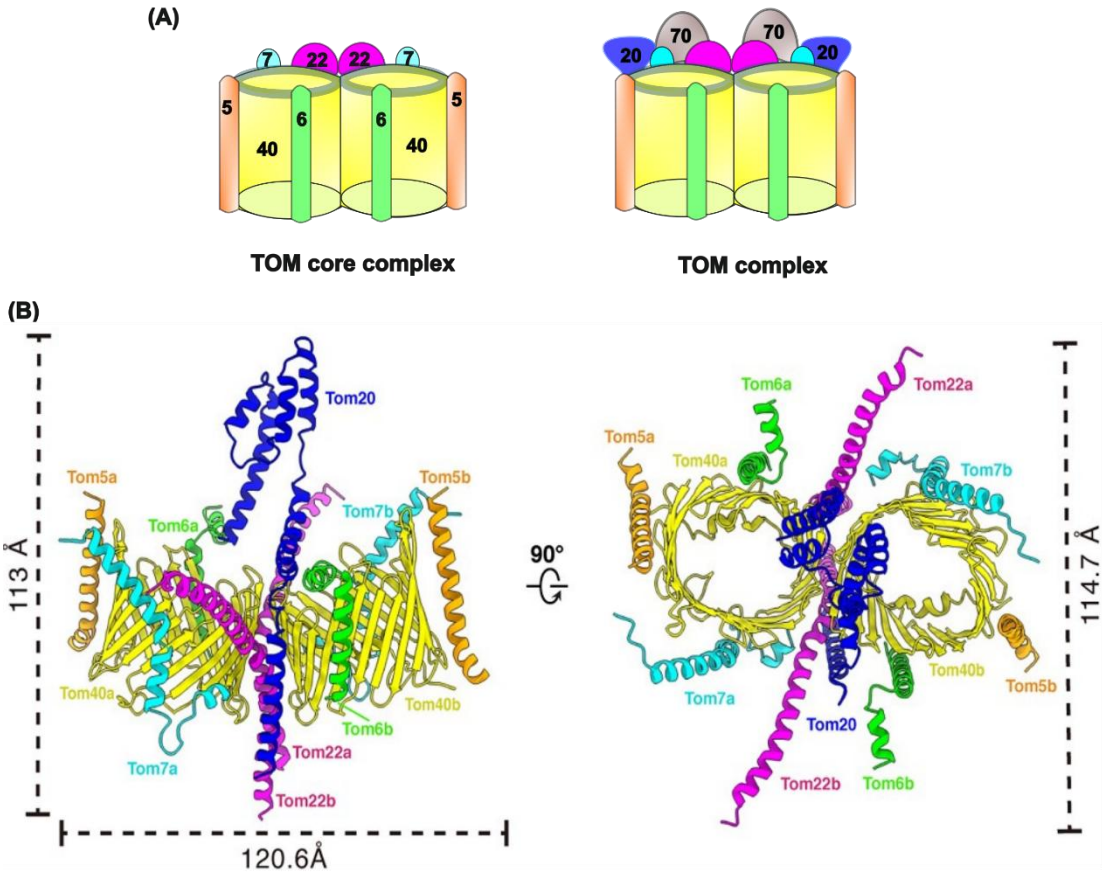

Figure 2. Structure and organization of the TOM complex.
(A) The TOM core complex or TOM-CC (left) in humans consists of dimeric TOMM40, stabilized by TOMM22 and supplementary subunits including TOMM55, TOMM6, and TOMM7. The TOM core complex together with the peripheral receptors TOMM20 and TOMM70 forms the TOM complex (right). **(B)** Ribbon diagram of a predicted cryo-EM model (PBD: 8XVA) of the dimeric TOM holo complex in humans, containing the TOMM20 subunit at the center (Su et al., 2022, 2024).

TOM-CC after binding with the regulatory peripheral receptors, TOMM20 and TOMM70, is termed as the TOM complex **(Figure 2A, right)**. The precise location of TOMM20 in the TOM complex is inconclusive. Recently, authors captured the TOMM20 subunit located right in the middle of the TOM holo complex, interacting extensively with TOMM22 (**Figure 2B**; Su et al., 2024). Through its C-terminal TOMM22 spans into the IMS and may facilitate the TOM complex interaction with the translocase of the inner membrane. In *Neurospora crassa,* the supplementary small subunits (Tom5, Tom6, and Tom7) surround Tom40 and together with Tom22 are necessary for assembly and stability of the complex (Dembowski et al., 2001; Yamano et al., 2008). In yeast mitochondria, the cytosolic domain of the Tom22 possesses docking sites for Tom20 and Tom70 (Araiso et al., 2019;

Tucker & Park, 2019). In yeast, there exists another paralogue of Tom70, known as Tom71, though its distinct role and preference in protein import is not yet well defined (Backes et al., 2018; Schlossmann et al., 1996). Recently, many studies based on cryo-EM highlighted the dynamic dimeric, trimeric and tetrameric conformations of **t**he TOM complex in *Saccharomyces cerevisiae* and *Neurospora crassa* (Araiso et al., 2019; Bausewein et al., 2017; Tucker & Park, 2019).

1.3.1 TOMM20 and TOMM70 - preprotein receptors of the TOM complex

The human TOMM20 and TOMM70, like their yeast counterparts, are the peripheral receptors of the TOM complex. Both contribute to targeting and import of corresponding substrates in their unique ways. The human TOMM20 is a membrane-anchored α-helix receptor, possessing a N-terminal transmembrane (TM) domain, together with a C-terminus domain that contains a cytosolically exposed, hydrophobic groove (**Figure 3**, **A**). By its C-terminus hydrophobic groove, fungal Tom20 interacts and recognizes the amphipathic helices of the mitochondrial targeting sequence (MTS) embedded in presequences (Abe et al., 2000; Saitoh et al., 2007). It specifically recognizes precursors containing N-terminal presequences mainly of matrix and IMM proteins, and directs them further to the Tom40 pore. NMR studies of fungal Tom20 binding elements showed that sequences, usually recognized by hydrophobic groove of the Tom20, can be as short as 8 amino acids but also longer than 40 residues. However, there often exists a consensus motif consisting of 5-residues, ϕXXϕϕ, where ϕ represents a hydrophobic amino acid, and X is any amino acid residue (Moczko et al., 1997; Obita et al., 2003). The presequences exhibit an unstable structure in the free state, however, they adopt a helical confirmation when interacting with Tom20. This binding mode is known as templated folding, as their interaction and recognition by Tom20 drives the confirmation changes (Han et al., 2022; Toto et al., 2016).

The human TOMM70, like its yeast homolog, is also an α-helix, the N-terminally anchored receptor in the MOM (**Figure 3**, B). Authors reported the secondary structure of yeast Tom70 in the form of a bundle of 26 α-helices (helices A1 to A26). The majority of helices are involved in the formation of 11 tetratricopeptide repeat (TPR) motifs (Kreimendahl & Rassow, 2020; Wu & Sha, 2006). The N-terminal TPRs of Tom70 mainly interact with the chaperones, the C-terminal

TPRs capture the mitochondrial precursors for import. TPR4 to TPR9 are mainly involved in the formation of the preprotein-binding pocket (Gao et al., 2021; Wu & Sha, 2006). Tom70 works as scaffold protein and tethers cytosolic heat shock protein (HSP) family chaperones to MOM. These chaperones mainly stabilize and retain the hydrophobic, multispanning precursors belonging to the inner membrane (known as bona fide carrier proteins) in a non-aggregated form at MOM, which in turn are further imported by the carrier pathway as described in chapter 1.2.2 (Backes et al., 2018, 2021; Fan et al., 2011; Hoseini et al., 2016; Q. Xue et al., 2017; Young et al., 2003; Zanphorlin et al., 2016). The TOM complex shares similarities as well as differences when comparing yeast and human mitochondria. For example, yeast Hsp70 delivers proteins to Tom70, and its homolog HSP70 forms a multi-chaperone complex together with HSP90 (human) and delivers preproteins to TOMM70 respectively (Araiso et al., 2019). In-vitro import assays showed that Tom70 is indeed essential against proteotoxicity of carrier proteins (Backes et al., 2021). Moreover, yeast Tom70 also regulates the transcription of mitochondrial proteins, ultimately mitochondrial protein biogenesis. Age-related retardation in the same organism leads to increased degradation and reduces biogenesis of Tom70, which results into loss of mtDNA, mitochondrial membrane potential, and mitochondrial proteins (Liu et al., 2022). Although both, human TOMM20 and TOMM70 receptors, are dynamically associated with the TOMM40/TOMM22 core complex, it is considered that TOMM70 is more loosely associated with the core complex compared to TOMM20 (Araiso et al., 2019; Kreimendahl & Rassow, 2020; Morgenstern et al., 2021; Tucker & Park, 2019). TOMM70 typically migrates as a homodimer on Blue Native PAGE, indicating less stable interaction with the core complex (Ryan et al., 1999; Wiedemann et al., 2001). TOMM20, when solubilized with mild detergents, also exhibits a loose association with the core complex. In Blue Native PAGE, a portion of TOMM20 migrates as a high-molecular-weight complex of ~ 400 kDa, together with TOMM40 and TOMM22, and additional free TOMM20 migrates in smaller forms ranging from ranging between ~40 and ~100 kDa (Abdul et al., 2000; Dekker et al., 1997; Fan et al., 2011; Mossmann et al., 2012).

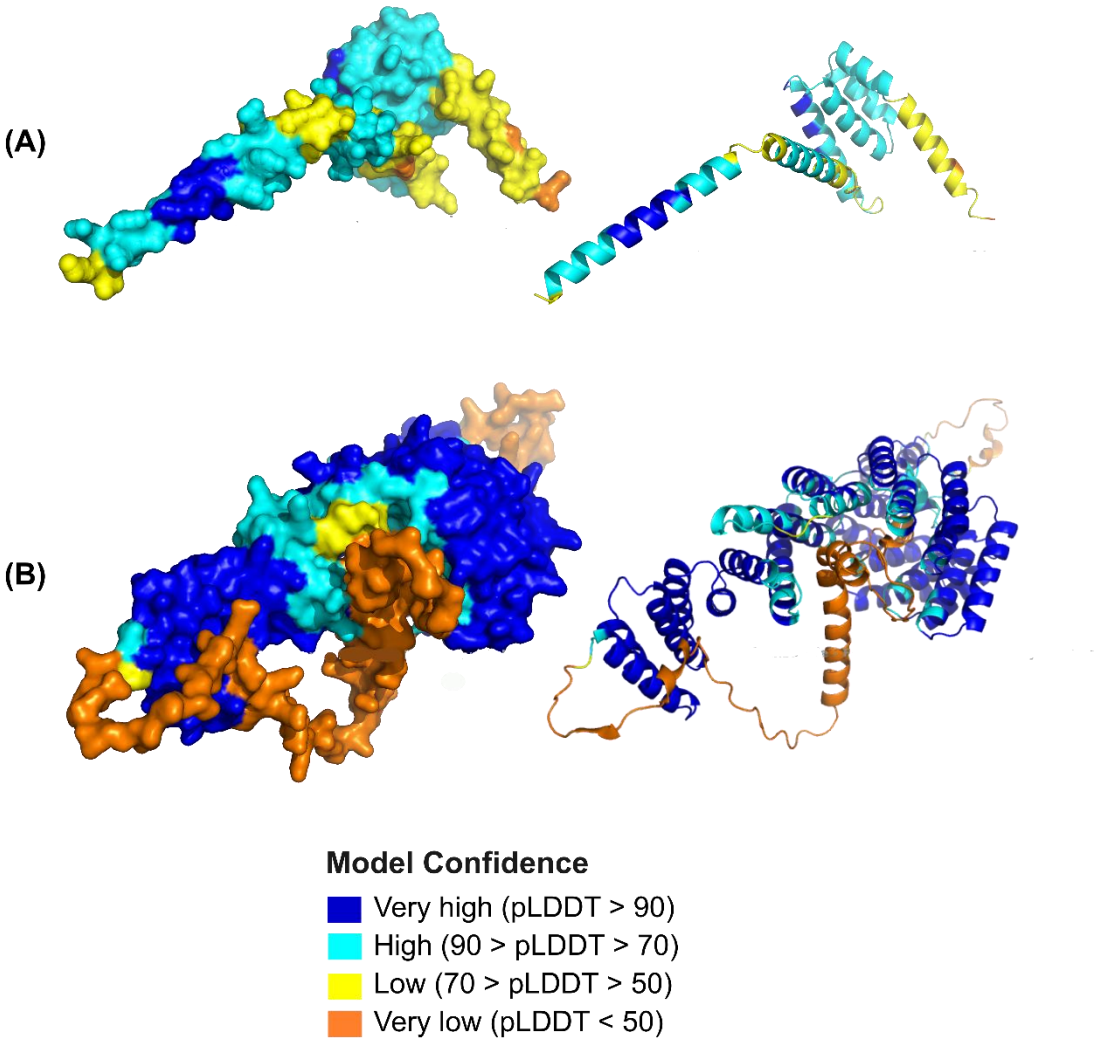

Figure 3. Predicted structure of human TOMM20 and TOMM70.
AlphaFold2 structure prediction model of human TOMM20 **(A)** (Uniport accession number: Q15388) and human TOMM70 **(B)** (UniProt accession number: O94826).

1.3.2 Substrate spectrum of TOM receptors

Human TOMM20 and TOMM70 dynamically associate with the TOM complex and recognize and import specific substrates. TOMM22 accepts its substrates from both, TOMM20 or TOMM70, and transfers them to the translocating TOMM40 pore. TOMM20 and TOMM70 recognize the targeting signals but differ in their substrate specificity, although overlaps can be observed (Brix et al., 1997; Kanaji et al., 2000; Yamamoto et al., 2011). TOMM20 binds to preproteins targeted to the inner mitochondrial membrane (MIM) and the matrix, whereas

TOMM70 prefers substrates that are α-helical proteins and destined to the outer or inner mitochondrial membrane (Abe et al., 2000; Araiso et al., 2019; Komiya et al., 1998; Tucker & Park, 2019). It is considered that 60% of mitochondrial precursors are matrix proteins, containing a MTS, and are imported via the classical presequence pathway by TOMM20/TOMM22. However, the loss of Tom70 in yeast affects the import of a wide variety of precursors, including the matrix and MIM proteins (Backes et al., 2021; Chan et al., 2006; Sayyed & Mahalakshmi, 2022). Yeast Tom20, through its C-terminal conserved DDVE motif, interacts with Tom70 (Araiso et al., 2019), and Tom70 is not essential provided that Tom20/Tom22 are complementary (Ramage et al., 1993). Yeast Tom20/Tom22 may complement Tom70 function and compete with chaperones, thus aiding in preprotein release from the chaperones (Fan et al., 2011). There is evidence of specific yet overlapping substrate recognition, particularly for budding yeast Tom20 and Tom70 receptors, but no such data is available for mammalian cells.

1.4 mRNA localization to mitochondria

Mitochondria, particularly in extensively polarized cells like neurons, serve as crucial signaling hubs and facilitate localized protein translation events to meet required protein turnover, quality control, and synaptic plasticity (Altman et al., 2021; Gershoni-Emek et al., 2018; Rangaraju et al., 2019; Spillane et al., 2013). Of the around approximately 1100 proteins found in mitochondria of various mammalian cell types (Rath et al., 2021), only 13 polypeptides are mitochondrial are encoded by mitochondrial genome, while the vast majority of all mitochondrial proteins are synthesized from the nuclear-encoded mRNAs and need to be delivered to the mitochondria.

Several studies suggest that some of the nuclear-encoded mitochondrial mRNAs are localized at the MOM in mammalian cells, not only in neurons or yeast but also in the HeLa cells (Chen & Collart, 2024; Golani-Armon & Arava, 2016; Sharma & Fazal, 2024). At the organelle surface, these specific mRNAs presumably are locally translated by MOM-localized ribosomes (Cohen et al., 2024; Vardi-Oknin & Arava, 2019; Williams et al., 2014). mRNA localization to mitochondria has been extensively studied in the budding yeast *Saccharomyces cerevisiae* (Arceo et al., 2022; Gadir et al., 2011; Saint-Georges et al., 2008;

Tsuboi et al., 2020; Zabezhinsky et al., 2016; Zipor et al., 2009). Biochemical fractioning together with transcriptomic studies showed that nearly half of the nuclear-encoded mitochondrial mRNA population is co-fractionating with mitochondria in yeast (Marc et al., 2002; Saint-Georges et al., 2008).

Cellular state and energy requirements greatly influence abundance and repertoire of the localized mRNAs at the MOM (Tsuboi et al., 2020). In yeast, mitochondrial dynamics change, when the cells undergo transition from fermentation mode of energy production to the respiratory mode. This transition also greatly influences mRNA localization. Particularly, the volume of mitochondria increases, when cells switch to the respiratory mode, which also facilitates the mitochondrial localization of mRNAs including the genes *ATP3 and TOM22* (Arceo et al., 2022; Tsuboi et al., 2020).

The sequence elements present in the open reading frame region (ORF) of the transcript are also likely to be essential for RNA targeting. Some of the RNAs e.g. *TIM50* is reported as constitutively localized to mitochondria even under fermentative conditions, when mitochondria have a smaller volume (Tsuboi et al., 2020). The ORF of *TIM50* comprises a sequence for polyproline, a consecutive stretch of 7 proline codons, situated roughly 60 amino acids downstream of the MTS. Nevertheless, during translation the polyproline stretch causes ribosomal stalling, leading to slowness or accumulation of ribosomes. It increases the likelihood for recognition of *TIM50* MTS, and consequently promotes the constitutive localization of *TIM50* RNA to the mitochondria (Tsuboi et al., 2020).

In a study utilizing HEK293T cells, thousands of mRNAs were shown to be at close proximity of the MOM (Fazal et al., 2019). The authors applied a proximity-labeling approach to identify the MOM-localized transcripts. Here, APEX2 was targeted to MOM by fusing it with the mitochondrial tethering domain of the mitochondrial antiviral-signaling protein (MAVS; Fazal et al., 2019). At MOM, an enrichment of nuclear-encoded mitochondrial transcripts over non-mitochondrial ones was reported (Fazal et al., 2019). Multiple factors influencing the RNA localization to the mitochondria have been identified (Fazal et al., 2019). These include poly(A) tail length, lengths of the UTRs, and short sequence motifs.

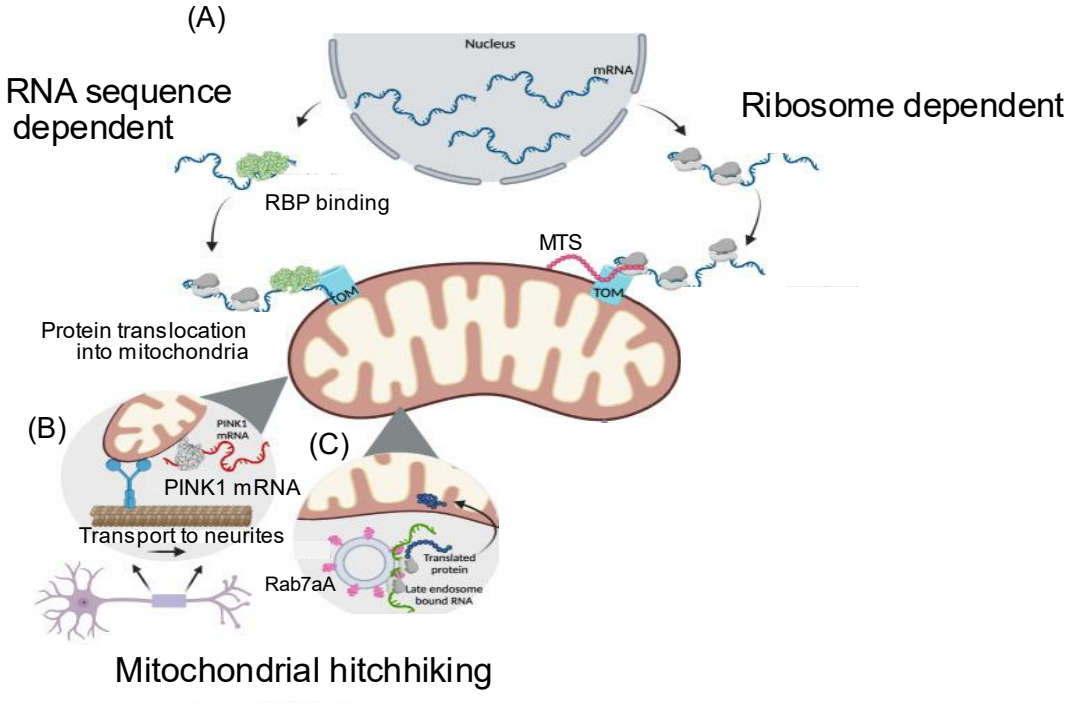

Figure 4. Modes of mRNAs localization to mitochondria.
Nuclear-encoded mitochondrial transcripts localize to mitochondria after adopting different routes depending upon their category. **(A)** RNA-sequence dependent transcripts are recognized by RNA binding proteins (RBPs). RBPs recognize sequence elements in the 3′-UTR region of the transcripts, and further escort them at MOM. The ribosome-dependent mRNAs require the translation of the N-terminal peptide sequence. The TOM complex mediates mRNA localization, presumably by its interaction with the translating MTS of the nascent chain. **(B)** Several mitochondrial transcripts hitchhike on mitochondria and co-localize to reach distant cellular locations by leveraging cytoskeletal microtubule networks. **(C)** mitochondrial mRNAs selectively bind and tether to the endosomal membrane, and these mitochondrial mRNAs carrying endosomes often pause near mitochondria and are locally translated (modifed from Sharma & Fazal, 2024).

The MOM-localization pattern of these transcripts is changed when the cells are treated with translation inhibitors, including puromycin and cycloheximide. Two different sub-populations of mRNAs were identified: ribosome-dependent and RNA-sequence-dependent transcripts (Fazal et al., 2019).

1.4.1 Ribosome-dependent transcript and their localization to the mitochondria

Cycloheximide treatment enriched the population of ribosome-dependent transcripts by preserving the transcripts bound to stalled ribosomes, while the nascent peptide was still localized to the MOM together with the translating mRNAs (**Figure 4A**; Fazal et al., 2019). Ribosome-dependent mRNAs at the

MOM require their translation, especially of the MTS peptide for their MOM-localization. The mitochondrial precursors encoded by mRNAs belonging to this category are likely to be imported co-translationally after the MTS is translated, while the translating ribosomes remain bound to the nascent chain (Fazal et al., 2019; G. Wang et al., 2018). The translated MTS might be recognized by the TOM complex after exiting of ribosomes and the ribosome/nascent chain/mRNA complex, thus interacting with the MOM during import into the mitochondria (**Figure 4A**). Evidence for this comes from localization of *ATP2* mRNA in yeast, which is reported as dependent on translation of the MTS sequence. The RNA was delocalized when a premature stop-codon was introduced in the sequence, leading to the detachment of ribosomes from the transcript (Garcia et al., 2010). Ribosome-dependent RNAs were greatly influenced by drugs leading to ribosome detachment from the transcripts. For example, treatment of yeast with the translation-inhibitor puromycin delocalized approximately 200 mRNAs coding for mitochondrial proteins (Saint-Georges et al., 2008).

1.4.2 RNA-sequence dependent transcripts and their localization to the mitochondria

Authors treated HEK293T cells with puromycin and identified a different sub-population of mRNAs at MOM (Fazal et al., 2019). These mRNAs did not require an intact ribosome and nascent-chain-complex. This subpopulation of the transcripts represents presumably the RNA sequence-dependent transcripts (**Figure 4A**).

Mitochondrial localization of these RNA sequence-dependent transcripts in diverse cell types, ranging from yeast to mammalian cells, is regulated by the specific sequences elements known as zip codes or RNA localization elements, presumably located in their 3´-untranslated region (UTR; Engel et al., 2020; Gadir et al., 2011; Kaltimbacher et al., 2006; Sharma & Fazal, 2024; Sylvestre et al., 2003).

These transcripts were targeted to the MOM, without requiring translation or ribosome recognition, and perhaps being anchored and subsequently regulated by RNA binding proteins (Fazal et al., 2019). mRNAs that showed translation-independent targeting to the MOM, contained shorter 3′ UTRs and poly(A) tails in comparison to RNAs showing translation-dependent localization (Fazal et al., 2019). Supporting this observation, translation-dependent mRNAs at

mitochondria identified by RNA-seq in zebrafish larvae comprised longer 3′-UTRs and ORFs (Saint-Georges et al., 2008).

1.4.3 RNA binding proteins are involved in mRNA targeting and stability at MOM

RNA binding proteins (RBPs) bind their mRNA targets after recognizing sequence elements located in 3'-UTR. RBPs subsequently escort their targets to the MOM, where they are translated, and resulting precursors are imported into the organelle. In yeast, the PUF family RBP, Puf3p, mediates localization of its targets to the MOM, while its deletion disturbs this pattern (Eliyahu et al., 2010; Gadir et al., 2011; Lapointe et al., 2018). Mutating the RNA motif of the *bcs1* transcript, needed for Puf3p binding, results in its mis-localization (Saint-Georges et al., 2008).

In mammals, the repertoire of corresponding RBPs involved in mRNA localization, their stability and local translation at MOM is limited. Few RBPs involved in RNA stability at MOM have been identified including clustered mitochondria homolog (CLUH; Gao et al., 2014), the Synaptojanin 2 binding protein (SYNJ2BP; Qin et al., 2021), La ribonucleoprotein 4 (LARP4; Lewis et al., 2024), A-kinase anchor protein 1 (AKAP1; Gabrovsek et al., 2020), and PTEN-induced kinase 1 (PINK1; Gehrke et al., 2015).

CLUH preferentially stabilizes a specific subset of nuclear-encoded mitochondrial mRNAs (J. Gao et al., 2014). CLUH depletion leads to faster decay of target mRNAs, and the corresponding mitochondrial proteins were decreased in abundance. These proteins belong to oxidative phosphorylation (OXPHOS), the tricarboxylic acid (TCA) cycle, and multiple metabolic mitochondrial pathways (Gao et al., 2021; Schatton et al., 2017; Wakim et al., 2017; Yang et al., 2022). It also associates with the translation machinery components including translation initiation factors as well as several ribosomal subunits, and presumably regulates local translation (Hémono et al., 2022; Pla-Martín et al., 2020; Schatton et al., 2017; Zaninello et al., 2024).

Proximity labeling by the APEX2 based approach, applied to capture the interactome of MOM in HEK293T cells, identified around 28 MOM-localized RBPs including SYNJ2BP (Qin et al., 2021). SYNJ2BP has been identified as a component of RNA-protein complexes at MOM and is essential for localization of its targets (Qin et al., 2021). It retains ∼100 transcripts at MOM including the

transcripts of the genes *UQCR11*, *PET117*, *RAB5IF, MRPS17, and MTFP1. UQCR11*, *PET117*, and *RAB5IF* encoding corresponding oxidative phosphorylation related proteins. *MRPS17* encodes a key mitochondrial ribosome protein, and *MTFP1* codes for a mitochondrial fission factor (Qin et al., 2021). In addition, SYNJ2BP is involved in piggy-back traveling of *PINK1* mRNA with mitochondria in neurons (Harbauer et al., 2022). Here, SYNJ2BP knockdown redistributes *PINK1* mRNA to RNA granules and inhibits local mitophagy (Harbauer et al., 2022). It specifically anchors its target mRNAs at the MOM under translation stress, facilitating their local translation and further import into mitochondria. Furthermore, its loss in HEK293 cells compromises the function of the OXPHOS complex (Qin et al., 2021).

Recently, a proximity labeling based approach, applied directly to TOMM20, also identified a number of enriched RBPs including LARP4 and AKAP1 in its vicinity (Meurant et al., 2023). AKAP1 is a well-documented MOM-localized RBP (Gabrovsek et al., 2020; Merrill & Strack, 2014), whereas LARP4 is also involved in positive regulation of nuclear-encoded mitochondrial mRNAs belonging to OXPHOS or mitochondrial ribosomal proteins. LARP4 depletion resulted in reduced translation of the protein products of its targets and affected mitochondrial function (Lewis et al., 2024).

In *Drosophila melanogaster,* local translation at MOM is selectively mediated by the AKAP1 protein MDI that recruits a translation stimulator known as Larp at MOM, and the MDI-Larp complex promotes local protein synthesis (Zhang et al., 2019). A mitochondrial fitness sensor in cultured mammalian cells is PINK1. PINK1 degrades rapidly in healthy mitochondria but selectively stabilizes at MOM of depolarized mitochondria to initiate the autophagic removal of defective mitochondria, a mechanism called as mitophagy (Lin & Kang, 2008; Narendra et al., 2010). PINK1 promotes the translation of mRNAs encoding proteins of the electron transport chain (Gehrke et al., 2015). PUF homlogs in human, PUM1 and PUM2 act as translational repressors and capture mitochondrial mRNAs, particularly in the cytosol (Uyhazi et al., 2020; Vessey et al., 2006). After reaching MOM, the PUM-bound, translationally repressed mitochondrial mRNAs undergo derepression of translation, and this whole mechanism is promoted by PINK1. Here, PINK1 at MOM triggers a cascade that directly leads to the displacement of the PUM repressors. As a result, derepressed mRNAs are locally translated,

directly at a site where they are needed (Gehrke et al., 2015).

1.4.4 RNA targeting by hitchhiking

Mitochondria utilize cytoskeletal microtubule networks extensively, particularly in polarized cells like neurons, where mitochondria are assisted by the motor proteins dynein and kinesin to deliver themselves at distant locations including axonal terminals. Several mRNAs including *COX7C* mRNA hitchhike on mitochondria where they co-localize together, leveraging cytoskeletal-mediated transport to reach distant cellular locations. *Cox7c* hitchhiking is reported mainly in distant axons of primary motor neurons in mice, and this co-transport depends on ORF and MTS regions of the transcript (Harbauer et al., 2022). Similarly, the *PINK1* transcript is also reported to travel via mitochondrial hitchhiking in distal neurites. Here, SYNJ2BP and its interactor SYNJ2 (Synaptojanin-2) are required to tether the *PINK1* mRNA to mitochondria (**Figure 4B**; Harbauer et al., 2022).

1.4.5 Endosome-coupled translation of mitochondrial proteins

Few studies also reported that some of the nuclear-encoded mitochondrial transcripts are translated in the vicinity of mitochondria, rather than directly at MOM (Müntjes et al., 2021; Schuhmacher et al., 2023). In retinal ganglion cells, such mitochondrial mRNAs selectively bind and tether to the endosomal membrane, and these mitochondrial mRNAs carrying endosomes often pause near mitochondria (Figure 4C; Müntjes et al., 2021). The proximity between endosomes and mitochondria makes sure that the corresponding translated protein products are imported into the mitochondria.

1.5 The need for future studies to analyze organelle-coupled translation at the mitochondria

Though past studies have demonstrated that co-transport and local translation of mRNA can occur while tethered at mitochondria, further research is needed to analyze mRNA localization and local translation at MOM. This may not only occur in neurons but also in other cell types to understand general principles and consequences of mRNA localization to mitochondria. The mechanisms and key players the cell utilizes to ensure that these transcripts get safely localized to the mitochondria, as well as co-translational import of the encoded precursors into the organelle are still not thoroughly investigated, especially in mammals.

Translation of nuclear encoded mitochondrial mRNAs might occur locally at the

TOM complex with some of its subunits participating in the co-translational import. Previous studies have shown that yeast Tom20 facilitates the localization of mRNAs to the organelle and contributes to the co-translational import of the mitochondrial proteins in a translation dependent manner (Eliyahu et al., 2010). Tom70 may also contribute to some level to localized translation at the MOM, as Tom70 depletion in yeast and mammalian cells led to a reduction in the levels of mitochondrially-localized mRNAs (Eliyahu et al., 2010; Gadir et al., 2011), or to dissociation of ribosomes associated with a subset of nuclear-encoded mitochondrial mRNAs (Vardi-Oknin & Arava, 2019).

It still needs to be verified if TOM complex mediates localization of mRNAs to the MOM. If it recruits some of the RBPs or other components of the translation and if this recruitment is differential, RBPs or other players somehow are localized to one of its subunits more than others. Hence, the role of the TOM complex as a direct or indirect mediator of localized translation is yet to be specified.

1.6 Proximity labeling techniques

Conventional methods that allow to map protein-protein interactions (PPI) include affinity purification or immunoprecipitation followed by mass spectrometry. These methods have limitations, since the native cellular context is lacking, and transient interactions are often lost due to harsh lysis conditions or either during washing steps in the purification process or due to long incubation times (Liu et al., 2024). Recently, many enzyme-catalyzed proximity labeling (PL) approaches, also coupled with mass spectrometry, have been developed that overcome these limitations. In a PL method, the protein of interest (POI or bait) is fused to a promiscuous labeling enzyme that converts an inert substrate into a reactive radical species, which due to its high reactivity, diffuses over short distances and covalently tags nearby proteins promiscuously. These covalently tagged biotinylated proteins are subsequently extracted and analyzed by mass spectrometry. PL methods are employed in live cells to analyze interactions in their native cellular environment, and characterize transient interactions as well as the low abundance protein. Stringent washing conditions during the pull-down are also allowed, reducing background noise substantially in following mass spectrometry analysis. Furthermore, PL methods are efficiently useful for studying PPI in insoluble cell compartments like mitochondria or nucleus (Hung

et al., 2017; Wang et al., 2024; Zhou et al., 2023). The two major enzymes utilized for proximity labeling approaches are engineered ascorbate peroxidase, and biotin ligase.

1.6.1 Engineered ascorbate peroxidase (APEX)

Engineered ascorbate peroxidase (APEX) is an 28 kDa enzyme derived from soybean or pea (Martell et al., 2012). APEX is fused to a bait protein, and the cells expressing recombinant APEX2-bait protein are first incubated with an inert substrate (biotin-phenol or BP). After adding H_2O_2, APEX transforms substrates into highly reactive phenoxyl radicals, which particularly target aromatic, electron-rich amino acids (tyrosine, tryptophan) as well as cysteine and histidine, present on the surface of nearby proteins, if these are located in the vicinity of approximately 10–20 nm (Martell et al., 2012). The initially used APEX had low catalytic activity. Later, the more efficient, mutated form A134P, known as APEX2 was developed (Rhee et al., 2013). APEX2, due to its strong labeling activity, has been widely used in proteomic profiling of subcellular compartments, particularly mitochondria (Hung et al., 2017; Lee et al., 2016; Qin et al., 2021; Wang et al., 2024). APEX2 permits labeling times as short as 1 min, rendering it suitable to study time-resolved temporal and transient PPIs in living cells. However, the APEX2 biotinylation demands H_2O_2 treatment of cells, which may cause cellular stress by affecting redox-sensitive cellular processes (Lennicke et al., 2015). APEX2-generated biotin-phenoxyl radicals are membrane-impermeable, hence APEX2 can be efficiently targeted to characterize the proteome of membrane-enclosed organelles like mitochondria or nuclei. The split version of APEX2 has also been developed that reduces the number of false positives, due to the fact that split-APEX2 biotinylation depends on correct localization of both split factors (Y. Han, Branon, et al., 2019; M. Xue et al., 2017).

1.6.2 Proximity ligase enzyme- BirA* and other variants

The proximity ligase BirA* utilizes biotin, and in the presence of ATP, it converts biotin into highly reactive biotinoyl-5′-adenylate (bioAMP) radicals, which diffuse to a radius of around 10 nm, and target lysine residues of promiscuous proteins. The covalently labeled proteins are then efficiently captured by streptavidin beads. One disadvantage of BirA* is its relatively big size (35 kDa). Due to its size, it may disturb the function and interfere with the localization of the bait protein. Due to slow kinetics, BirA* requires biotin labeling for nearly 16–18 h.

However, numerous modified enzymes with better labeling efficiencies have been developed including BioID2 (Kim et al., 2016), TurboID (Branon et al., 2018) and UltraID (Kubitz et al., 2022). TurboID is one of the most efficient enzymes, it offers a labeling time of 10 min and has been widely employed for proteomics studies.

1.6.3 General consideration for implementing proximity ligation approach

Proximity labeling emerged as a powerful tool to identify interaction partners of particular bait proteins. Nevertheless, PL enzymes possess relatively large sizes (28-35 kDa) that may influence the localization and physiological function of the bait protein (Kim et al., 2016; Lam et al., 2015; Roux et al., 2012). The exact labeling radius is uncertain, especially for biotin ligases, since reactive bioAMP generated by biotin ligase may readily diffuse away from the biotin ligase (Roux et al., 2012). Due to the very strong biotin-streptavidin interaction, the biotinylated proteins bound to streptavidin beads often prone to insufficient elution. In such cases, on-bead digestion could be beneficial, though it could also result in false positives, as non-biotinylated proteins, interacting non-specifically with the streptavidin beads, may be cleaved off. Hence, appropriate controls are necessary to cope with false positive and false negative proteins. Control fusion proteins should ideally be expressed at a similar level as bait proteins. Biotinylation of a protein mainly depends on the type and accessibility of the exposed amino acids. APEX2 favors aromatic amino acids like tyrosine, whereas BioID enzyme targets lysine residues. This shows that proximity labeling may be affected when targeting a small protein that does not possess enough corresponding residues to be addressed by a particular PL enzyme. For example, intrinsically disordered proteins often contain more lysine residues, and are more favored by biotin ligases than by APEX2 (Minde et al., 2020).

Chapter 2: Research questions

1. Studying the local interactome of TOMM20 and TOMM70 receptors of the TOM complex at the mitochondrial outer membrane (MOM) in mammalian cells via proximity labeling approaches.
2. Comparing the local differential interactome (interaction profile) of TOMM20 and TOMM70 in their particular nano-environment in mammalian cells.
3. Probing the substrate spectrum of TOMM20 and TOMM70 with a major focus on identifying differential recruitment of RNA binding proteins (RBPs) and other effectors of translation.
4. Identifying nuclear-encoded mitochondrial transcripts in the proximity of the TOM complex.

Specific research objectives

1. Establishing the APEX2 based proximity labeling technology in the mammalian cells for studying and comparing the local proteomes of the TOMM20 and TOMM70 receptors at the MOM.
2. Extending the APEX2 methodology to study the mitochondrially localized nuclear-encoded mitochondrial transcripts at the TOM complex.

Chapter 3: Results

To characterize the local interactome of two main receptor subunits of the TOM complex, I applied an APEX2 based proximity labeling approach (PL) and fused the APEX2 enzyme (Lam et al., 2015) to either TOMM20 or TOMM70 proteins in HeLa cells. TOMM20 emerged as a compelling bait to be fused with APEX2, since it is the major player of the pre-sequence pathway to import mitochondrial proteins. Additionally, previous studies have shown that this subunit contributes to the co-translational import of mitochondrial proteins in yeast cells (Eliyahu et al., 2010). In parallel, TOMM70 was labeled with APEX2 since it may contribute to some level to localized translation at the MOM, as TOMM70 depletion in yeast and mammalian cells led to a reduction in the levels of mitochondrially-localized mRNAs (Eliyahu et al., 2010; Gadir et al., 2011), and the dissociation of ribosomes associated with a subset of nuclear-encoded mitochondrial mRNAs has also been described (Vardi-Oknin & Arava, 2019).

3.1. Designing and characterization of TOMM20-APEX2 and TOMM70-APEX2 fusion proteins

The N-terminal corresponding regions of both TOMM20 and TOMM70 proteins contain transmembrane domains, and previous studies showed that endogenous tags at the C-termini of these subunits did not affect their physiology as cell retained functional mitochondria (Roberts et al., 2017; Wanet et al., 2015). In both hybrid proteins, the APEX2 proximity labeling enzyme (Lam et al., 2015) was thus fused to their cytoplasmic carboxyl (C-) terminus of the respective TOMM protein.

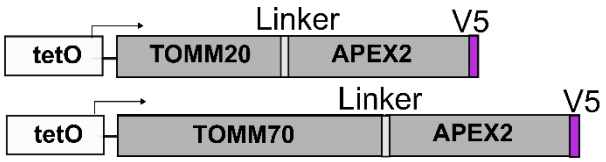

Figure 5. Constructs for expressing human TOMM20- and TOMM70 fusion proteins in HeLa cells.
Schematic representation of the cassette, stably intergraded into the genome of the HeLa-EM2-11ht master cell line for generating stable cell lines, expressing either TOMM20-APEX2-V5 or TOMM70-APEX2-V5. The expression of each transgene was controlled by the Tet-system, allowing inducible activation of the transcription. Tetracycline response elements (tetO) were bound by the transcriptional activator rtTA2S-M2, in the presence of doxycycline (DOX), thus allowing transcription of the corresponding transgene. Both transgenes contained a flexible linker consisting of 10 aa (GGSGDPPVAT), and an additional V5 epitope tag for detection.

Each transgene was stably integrated into the genome of the master HeLa-EM11ht cell line (**Figure 5).** This cell line (Weidenfeld et al., 2009), contains a specified locus with recombination sites, and stably expresses the transcription activator component, rtTA2S-M2 that is required for the Tet-system. The Flp recombinase-mediated cassette exchange system (RMCE system; Schlake & Bode, 1994) was utilized to integrate the corresponding transgene at the defined chromosomal locus into the genome of the HeLa-EM2-11ht cells in the same way. This ensured the stable, tunable, and uniform expression of each fusion protein across the cell lines, and thus allowed comparability. A short intervening flexible linker consisting of 10 aa (GGSGDPPVAT) was also introduced between tag and protein to facilitate the flexibility in the structure (**Figure 5**). The orientation displayed was chosen to biotinylate the potential cytosolic interactors, promiscuous to the resident TOM receptor subunits. Both fusion proteins contained an additional V5 epitope tag for detection (McLean et al., 2001), and were expressed by addition of doxycycline (**Figure 5**).

3.2. Co-localization of TOMM fusion proteins with the endogenous TOM complex

I initially used the V5 tag to test if the fusion proteins are targeted to mitochondria (**Figure 6**). After induction of the fusion protein expression by doxycycline (DOX) for 24 h, immunofluorescence microscopy revealed co-localization of TOMM20-APEX2-V5 and TOMM70-APEX2-V5 with the mitochondrial marker TOMM22, which indicated correct targeting of the fusion proteins. Furthermore, mitochondrial morphology remained unchanged, suggesting that the fusion proteins have no negative impact on mitochondrial function. We then analyzed the integration of both fusion proteins into mitochondria by subcellular fractionation (**Figure 7**). HeLa TOMM20-APEX2 cells were induced with doxycycline (DOX) for 24 h and subsequently lysed. Mitochondrial and cytosolic fractions were isolated, and mitochondria were solubilized by the addition of digitonin (see methods, chapter 4.4.1). Solubilized mitochondria and cytosolic fractions were subjected to SDS-PAGE and immunodecorated with antibodies against TOMM20, TOMM40, and glyceraldehyde-3-phosphate dehydrogenase (GAPDH). Like endogenous TOMM40 and TOMM20, TOMM20-APEX2, detected by an anti-TOMM20 antibody, was highly enriched in the mitochondrial fraction,

whereas GAPDH was primarily detected in the cytoplasmic fraction (**Figure 7A**).

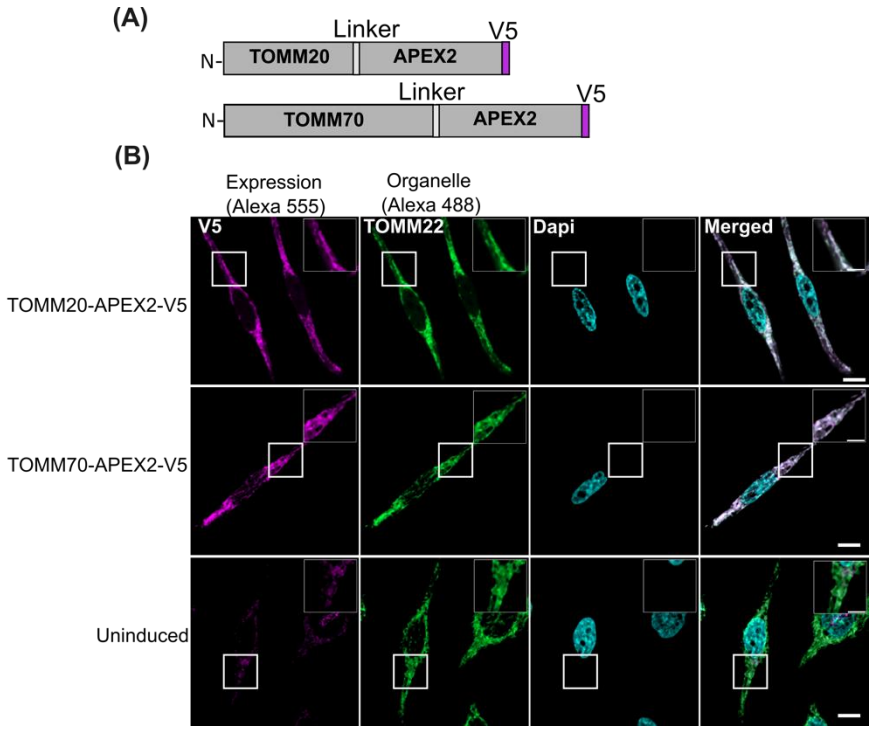

Figure 6. Fluorescence imaging confirming APEX2 localization in the cells stably expressing the indicated APEX2 fusion proteins.
After 24 h induction with DOX (doxycycline) and subsequent fixation, the fusion proteins were immunolabeled with antibodies directed against V5 (Magenta). The endogenous TOM complex was visualized using anti-TOM22 antibody (green; Scale bar: 10 µm). Nuclei were stained with DAPI (cyan). Uninduced cells were mock treated. Insets are the magnified portion of the cell shown on the uppermost right of each panel (Scale bar, 5 µm).

Subcellular co-fractionation was also used to assess the distribution of TOMM70-APEX2. Detection of the fusion protein and the endogenous TOMM70 via an anti-TOMM70 antibody revealed similar distribution patterns of both proteins in mitochondrial versus cytosolic fractions, indicative of the correct targeting of the fusion protein to mitochondria (**Figure 7B**). Importantly, these experiments also revealed similar expression levels of endogenous TOMM20 or TOMM70 and the corresponding fusion proteins TOMM20- or TOMM70-APEX2, respectively.

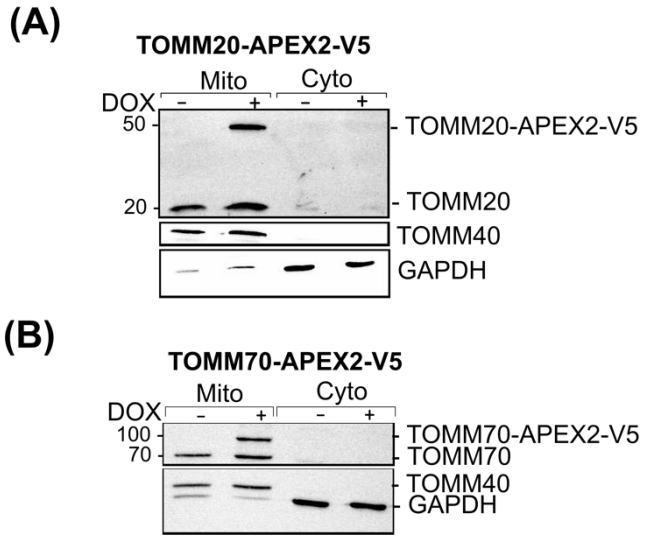

Figure 7. Western blot analysis of mitochondrial and cytosolic fractions of the TOM bait proteins.
(A) TOMM20-APEX2 expressing cell were either not induced or induced with doxycycline (DOX) for 24 hours, mitochondria were isolated and solubilized with digitonin-containing buffer and isolated fractions were analyzed with TOM20 and TOMM40 antibody. GAPDH was used as cytosolic marker. Endogenous (~20kDa) and APEX2 containing TOMM20 (~50 kDa) subunits were confirmed by TOMM20 antibody. **(B)** Western blot analysis of mitochondrial and cytosolic fractions of TOMM70-APEX2 expressing cells. Endogenous (70kDA) and APEX2 containing TOMM70 (~100 kDa) subunits were detected by TOMM70 antibody. The cytosolic fraction was validated by GAPDH.

To test for correct association of TOMM20-APEX2 with the TOM complex, I performed co-immunoprecipitation with endogenous TOM complex subunits. TOMM20-APEX2 expressing cells were induced with DOX 24 hours prior to lysis, mitochondria were isolated and solubilized with digitonin-containing buffer. Detergent extracts were subjected to co-immunoprecipitation where the TOM complex was pulled down by TOMM22 (**Figure 8A**) or TOMM40 antibodies (**Figure 8B**). Samples were further analyzed by SDS-PAGE and immunodecorated with V5 antibody. The 49 kDA TOMM20-APEX2 protein detected by the V5 antibody was found in both immunoprecipitates (**Figure 8A, B**).

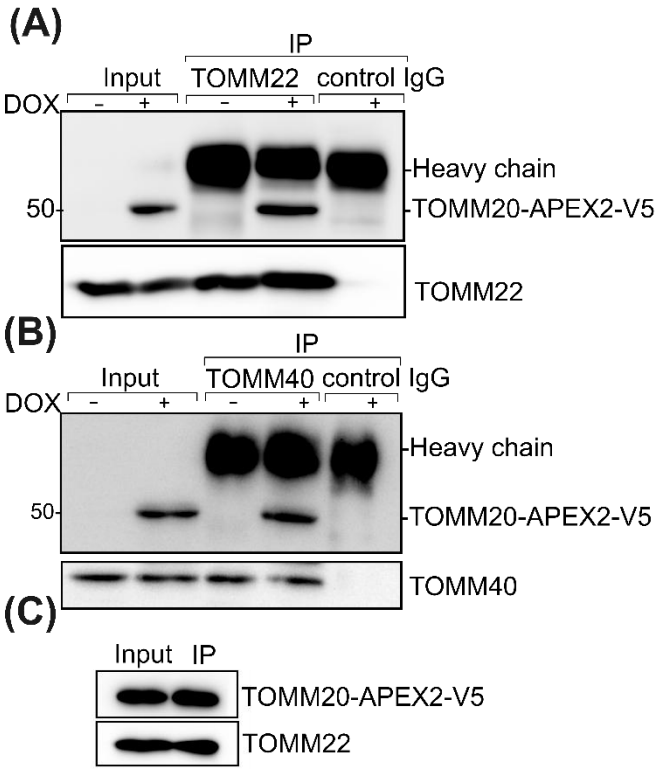

Figure 8. Immunoprecipitation of TOMM20-APEX2 cells.
Western blots show the interaction of the Tomm20-APEX2 fusion protein with the endogenous TOM complex subunits analyzed after immunoprecipitation. HeLa cells were either not induced or induced with doxycycline (DOX) for 24 hours to stably express the TOMM20-APEX2 fusion protein prior to lysis. Mitochondria were isolated, solubilized with digitonin-containing buffer, and further subjected to immunoprecipitation. The TOM complex was specifically pulled down either with TOMM22 IgG **(A)** or TOMM40 IgG **(B)**. Immunoprecipitates from uninduced cells (-DOX) were loaded in parallel. **(C)** Western blot showing the immunoprecipitation analysis of TOMM20-APEX2 fusion protein in isolated mitochondria using V5 beads.

In a reciprocal co-immunoprecipitation experiment using anti-V5 beads, I co-purified TOMM22, as shown by Western blotting using an anti-TOMM22 antibody (**Figure 8C**). These experiments confirmed that TOMM20-APEX2 associates with both members of the endogenous TOM core complex.

3.3. Specific biotinylation activity of TOMM20-APEX2 and TOMM70-APEX2 fusion proteins

After analyzing the correct localization of TOMM20- and TOMM70-APEX2 fusion proteins to mitochondria, I tested for biotinylation activity of the fusion proteins. After 24 h induction with doxycycline (DOX), cells were subjected to live-cell biotinylation, treated first with biotin-phenol (BP) for 30 minutes at 37 °C, followed

by hydrogen peroxide (H_2O_2) for 1 minute at room temperature. Cells were thoroughly washed in the quencher solution, lysed, and subjected to Western blot analysis. Biotinylated proteins were detected by using a streptavidin conjugate. Besides the expected endogenous biotinylated proteins like biotin-dependent carboxylases including pyruvate carboxylase, β-methylcrotonyl-CoA carboxylase, and propionyl-CoA-carboxylase (Grant et al., 2019; Pacheco-Alvarez et al., 2004), which were detected under all conditions, additional biotinylation in cells with integrated TOMM20- or TOMM70-APEX2 was detected after expression of the corresponding fusion protein (**Figure 9**, 'DOX'), addition of biotin-phenol ('BP'), and of H_2O_2 ('H_2O_2'). Both TOMM20- and TOMM70-APEX2 fusion proteins biotinylated the endogenous proteins efficiently showing distinct band patterns.

I also verified biotinylation by *in situ* labeling of biotinylated proteins, using biotin-binding neutravidin coupled to Alexa647 (neutravidin-Alexa647). Even under conditions that did not allow APEX2 activity - i.e. no expression, no BP, no H_2O_2 -, a neutravidin-Alexa647 signal was detectable that overlapped with the mitochondrial location of the APEX2 fusion proteins (**Figure 10 A,B**; left column). This most likely reflects the detection of endogenous biotinylated proteins, probably mitochondrial CoA-carboxylases (Grant et al., 2019; Pacheco-Alvarez et al., 2004). Only HeLa cells expressing the TOMM20- and TOMM70-APEX2 fusion proteins showed an additional and much stronger biotin-dependent fluorescence (**Figure 10 A,B**; left column), indicating an active APEX2 enzyme. Surprisingly, the biotinylation pattern seen in TOMM20-APEX and TOMM70-APEX expressing cells was not restricted to the mitochondrial location. However, this has been observed before for TOMM20-APEX2 (Lee et al., 2016), and has been assumed to depend on the cytosolic orientation of the APEX2 part of the fusion protein, diffusion of the activated biotin-phenoxyl radicals into the cytoplasm, and labeling of the cytosolic components.

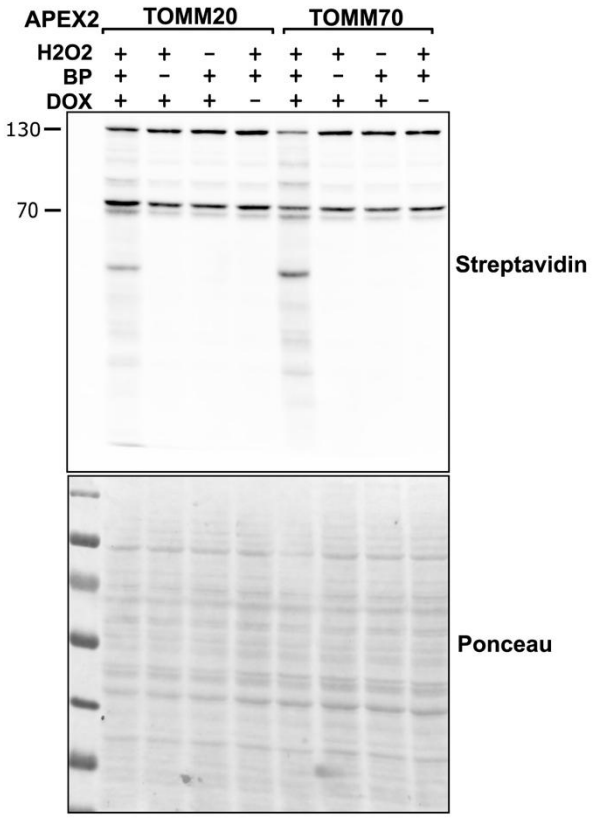

Figure 9. Target protein biotinylation is mediated by TOMM20- or TOMM70-APEX2 fusion proteins.
Following 24-hour DOX induction, cells were subjected to live-cell biotinylation with BP and H_2O_2 for one minute, and subsequently lysed. The blot was stained either with Streptavidin-HRP conjugate to detect biotinylated proteins (upper portion) or with Ponceau (lower portion). Biotinylation depended on the presence of both, biotin phenol (BP) and H_2O_2. Either omission of substrate or lack of APEX2 fusion protein expression resulted in detection of endogenous biotin-containing proteins, β-methylcrotonyl-CoA carboxylase (~72 kDa), propionyl-CoA-carboxylase (~74 kDa), and pyruvate carboxylase (~130 kDa).

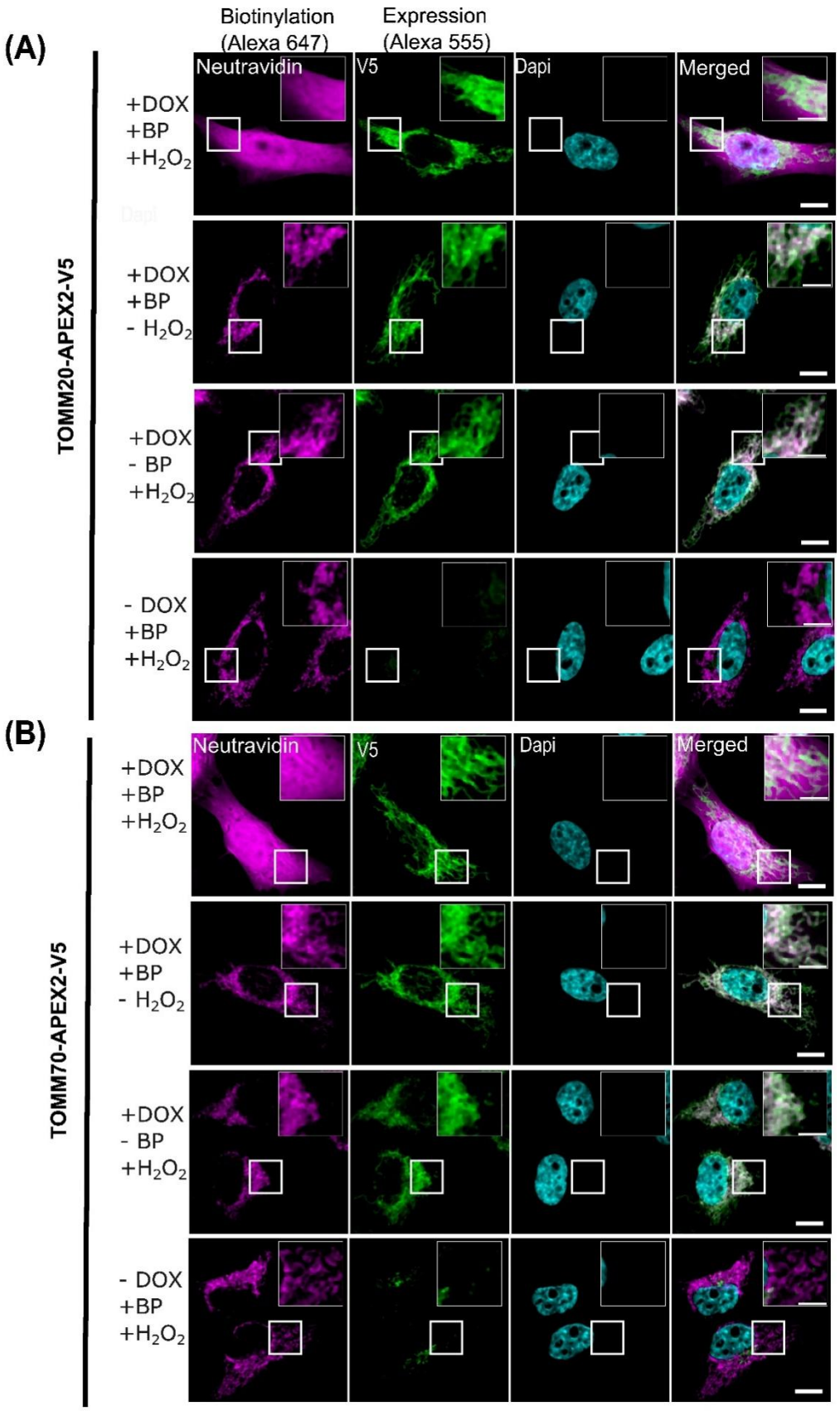

Figure 10. Local biotinylation at mitochondria by TOMM20- and TOMM70-APEX2. Fluorescence imaging of APEX2-mediated biotinylation in HeLa cells stably express the

indicated APEX2 fusion proteins, **(A)** TOMM20-APEX2-V5 **(B)** TOMM70-APEX2-V5. After 24 h of DOX induction, cells were exposed to live-cell biotinylation with biotin phenol (BP) and H_2O_2 for one minute and subsequently fixed. Cells were stained with anti-V5 tag antibody, coupled with a secondary antibody conjugated to Alexa555, to check the expression of indicated APEX2 fusion proteins (green), and 'Neutravidin-Alexa647' to stain the biotinylated species (magenta). When either H_2O_2 or BP is omitted, or when the cells are not induced, the endogenous mitochondrial biotinylated proteins become apparent. Nuclei are stained with DAPI (cyan). Insets are the magnified portion of the cell shown on the uppermost right of each panel (Scale bar: 10 µm; incent: 5 µm).

3.4. Designing and testing of control fusion proteins

To analyze and compare organelle specific interactions, I generated stable cell lines by expressing three additional APEX2 fusion proteins as controls into HeLa-EM2-11ht cells (**Figure 11A;** Lam et al., 2015; Rhee et al., 2013**)**. These include Mito-APEX2, which harnesses a 1-24 amino-acid sequence from the mitochondrial matrix resident protein, COX4, to localize APEX2 to the mitochondrial matrix **(Figure 11A)**. The second APEX2 fusion protein, ERM-APEX2, is directed to the endoplasmic reticulum membrane (ERM). It utilizes the first 27 amino acids derived from the transmembrane domain of the endoplasmic reticulum (ER) localized protein, P450 oxidase 2C1, to direct APEX2 to the ERM **(Figure 11A)**. APEX2-NES targets the APEX2 to the cytoplasm by a nuclear export signal **(**NES; **Figure 11A)**. Like the TOMM20- und TOMM70-APEX2 bait proteins, the expression of control fusion proteins was induced by addition of doxycycline ('DOX'; **Figure 11 B, C**). These fusion proteins were expressed at a similar level as validated by Western blotting (**Figure 11B**). As described before (Lam et al., 2015; Rhee et al., 2013), Mito-APEX2 and ERM-APEX2 were targeted to the corresponding organelle (**Figure 11C**), which is shown by co-localization with appropriate endogenous markers, calnexin for ER, and TOMM22 for mitochondria. The diffuse intracellular staining pattern and nuclear exclusion of APEX2-NES demonstrates its cytosolic location (**Figure 11C**). All three control APEX2 proteins were functional and increased detectable biotinylation only in the presence of biotin-phenol and H_2O_2 (**Figure 12**). In case of Mito-APEX2, neutravidin-Alexa647 staining of biotinlyated proteins *in situ* (**Figure 13**) showed a very similar distribution to that of the enzyme itself, most likely due to the confinement of the activated phenoxyl-biotin radical in the mitochondrial matrix. Staining of proteins biotinylated by ERM-APEX2 was more diffuse but overlapped with the ER staining of ERM-APEX2 (**Figure 13**). The more diffuse signal was

presumably due to the less restricted diffusion of the phenoxyl-biotin radicals before reacted with target (Rhee et al., 2013). As expected, the distribution of proteins biotinylated by APEX2-NES was more diffused and mimicked the distribution of cytoplasmic proteins.

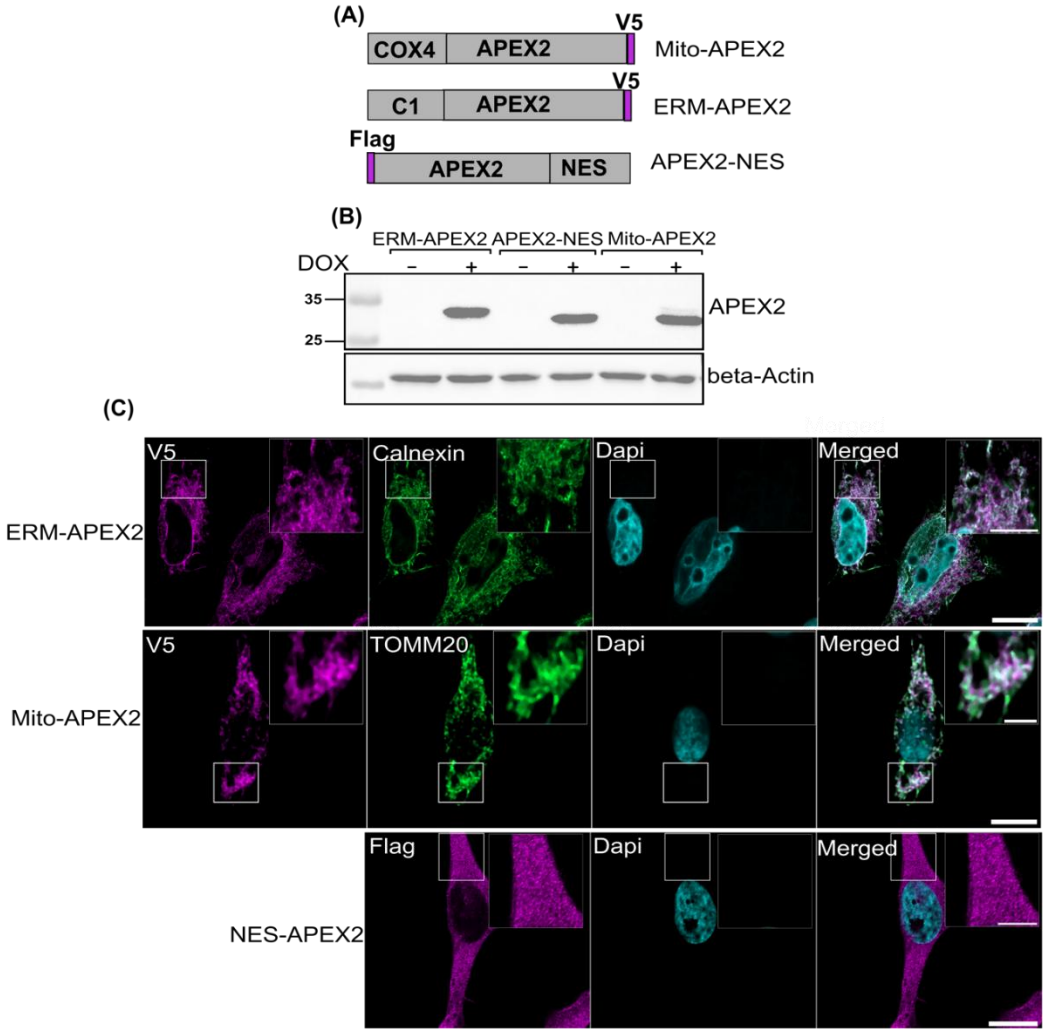

Figure 11. Expression and characterization of control bait proteins.
(A) Domain structures of the fusion proteins stably expressing APEX2 in various cellular compartments including mitochondrial matrix (Mito-APEX2), endoplasmic reticulum membrane (ERM-APEX2) and cytoplasm (APEX2-NES).
(B) Fluorescence imaging confirming the cellular localization of stably expressing ERM-APEX2, Mito-APEX2 and APEX2-NES fusion proteins. Cells were induced with DOX for 24 hours, immunolabeled with antibodies directed against V5 to detect ERM-APEX2, and Mito-APEX2 proteins (magenta) or flag to visualize APEX2-NES fusion protein (magenta). ER was visualized via anti-Calnexin antibody (green), and mitochondria were labeled with anti-Tom20 antibody (green). (Scale bar: 10 µm; inset: 5 µm). **C**. Western blot analysis of whole cell lysate of cells stably expressing ERM-APEX2, Mito-APEX2 or

APEX2-NES constructs. Cells induced with DOX for 24 hours prior to lysis; control lysates were prepared from non-induced cells. APEX2 containing fusion proteins are analyzed with APEX2 antibody. GAPDH is used as loading control.

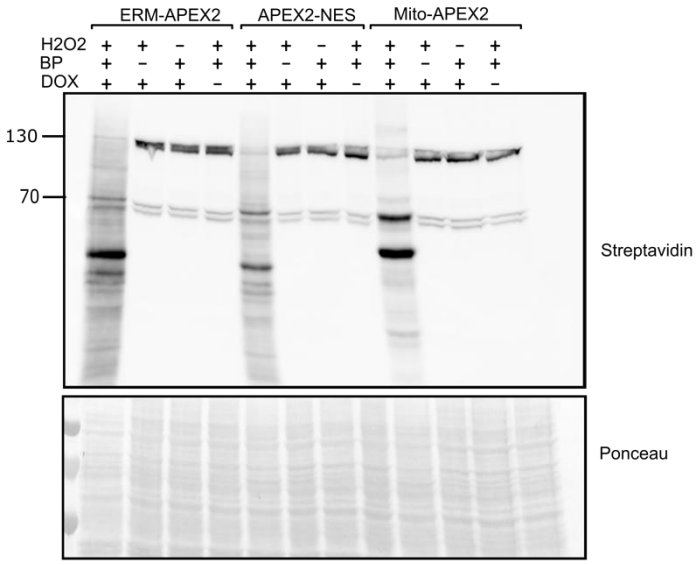

Figure 12. Biotinylation of control bait proteins in HeLa cells.
Western blot analysis of cell lysate to confirm the APEX2-mediated biotinylation in the cells stably expressing ERM-APEX2, Mito-APEX2, and APEX2-NES constructs. Biotinylated proteins were probed by Streptavidin-HRP conjugate (upper portion), ponceau staining is shown on the lower portion as loading control.

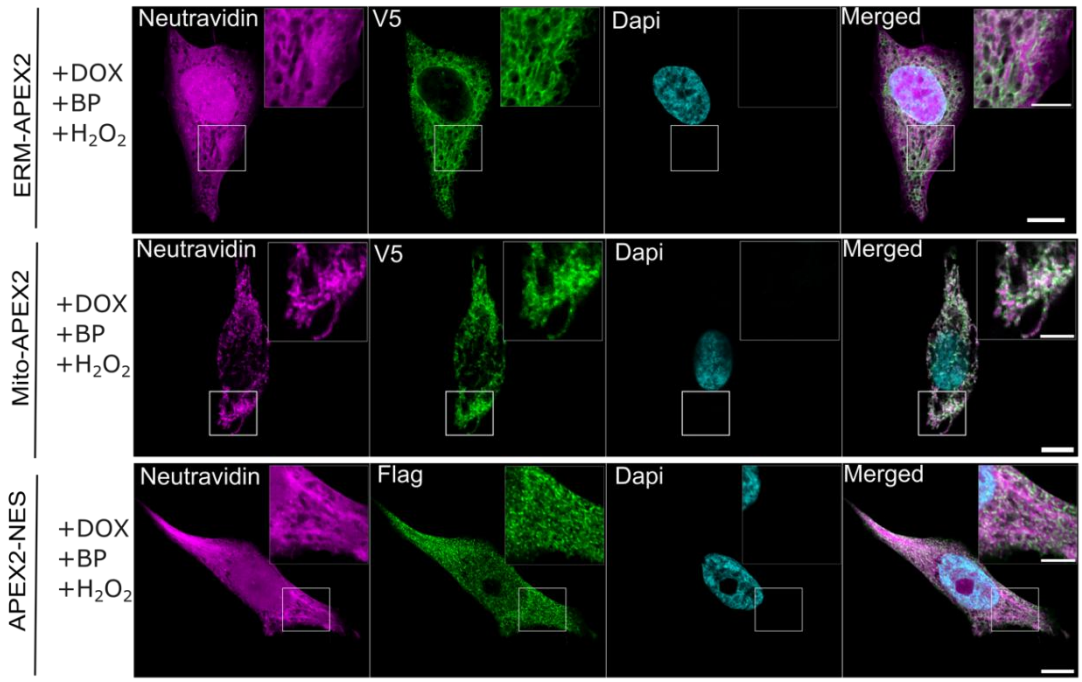

Figure 13. Fluorescence imaging of APEX2-mediated biotinylation of cells expressing control bait proteins
HeLa cells stably expressing the ERM-APEX2, Mito-APEX2, and APEX2-NES constructs after 24 hours of DOX induction, were subjected to live-cell biotinylation with

biotin phenol (BP) and H_2O_2 for one minute, then fixed. Cells were subsequently stained with either V5 or flag antibodies to confirm the expression of the indicated APEX2 fusion proteins (appearing in green), while 'Neutravidin' was utilized to stain the biotinylated species (appearing in magenta). Nuclei are stained with DAPI (cyan). (Scale bar: 10 µm; inset: 5 µm).

3.5 LFQ-based quantitative proteomics approach to study the TOMM20- and TOMM70 interactome

Six independent replicates for the interactomes of TOMM20-APEX2, and three for TOMM70-APEX2, APEX2-NES, Mito-APEX2, and ERM-APEX2 were analyzed by bottom-up proteomics. In addition, three replicates of control experiments performed with cells not expressing the corresponding TOM complex fusion proteins (‘-DOX’) were included. In each case, 1.5 million cells were used per experimental replicate. Biotinylation was performed with the addition of biotin-phenol and induced by a one-minute pulse of H_2O_2. Quenching, lysis and capturing by streptavidin beads were essentially done according to a published protocol (Hung et al., 2017). Captured proteins were analyzed by liquid chromatography-tandem mass spectrometer (LC-MS) after on-bead tryptic digestion. Downstream data processing was performed as label free quantification (LFQ; Cox et al., 2014), and imputation of missing values was applied during subsequent data analysis to increase the number of identifications (see method section 4.4.6.3). With this approach, we identified in total 2,177 protein groups of which 499 were annotated for mitochondrial localization by MitoCarta3.0 (Rath et al., 2021).

Except for -DOX controls, 1,300 to 1,700 protein groups were identified with the highest number of mitochondrially localized proteins for mito-APEX2, as expected (**Figure 14A**). Count of proteins was based on quantifying in minimum 3 out of 6 replicates for TOMM20-APEX2 and 2 out of 3 replicates for the remaining samples. This threshold, also referred to as 50% of replicates rule, is widely used in LFQ studies to balance stringency and data retention. It helps to identify biologically relevant proteins, which may not be captured in every run but are true candidates. Overall, excellent correlation was observed between the replicates (**Figure 14B**).

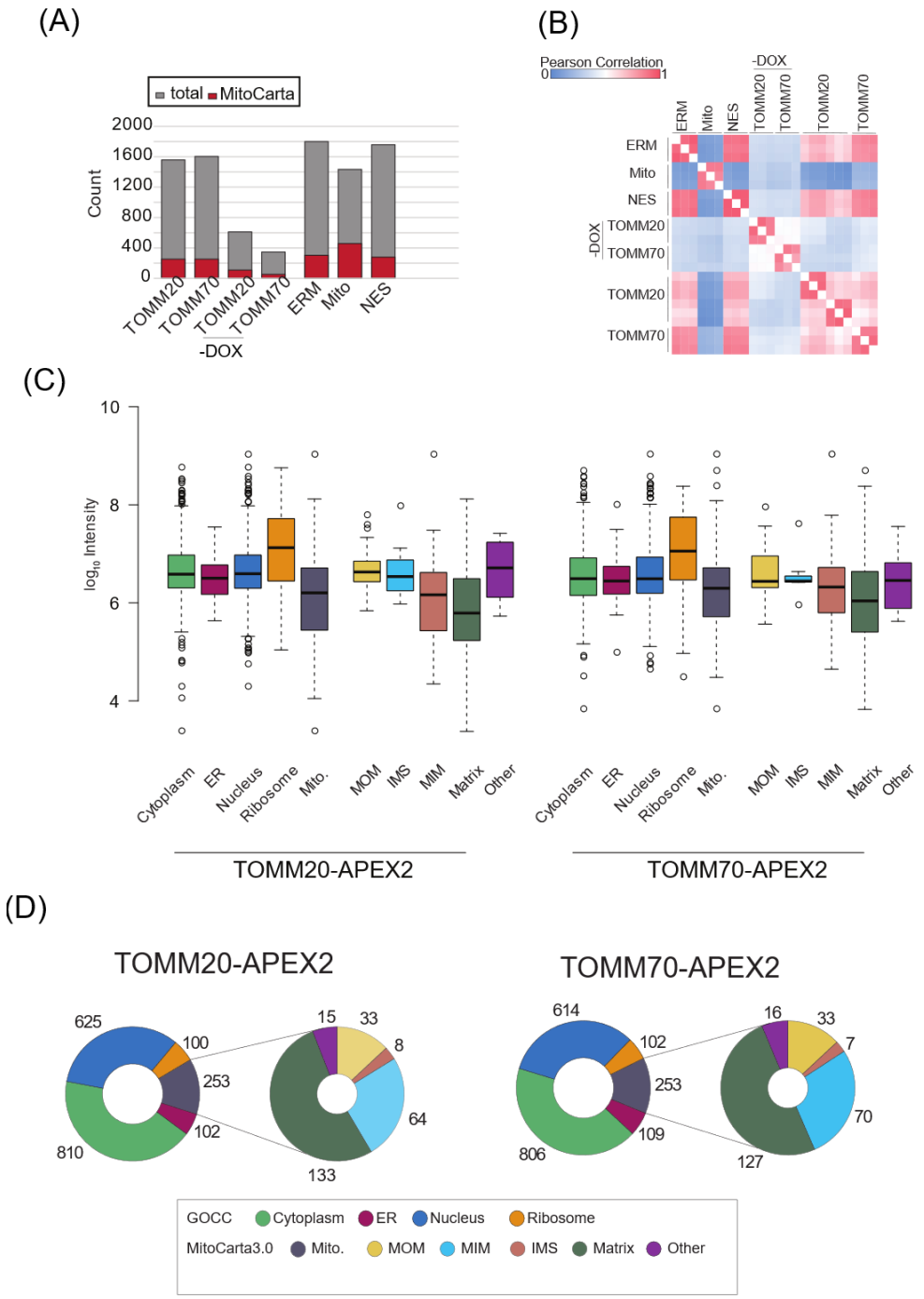

Figure 14. Quantitative analysis of TOMM20- and TOMM70-APEX2 interactomes. **(A)** Total identification of proteins (grey) and proteins annotated for mitochondrial localization (red) based on MitoCarta3.0. Count of proteins is based on quantification of minimum 3 out of 6 replicates for TOMM20-APEX and 2 out of 3 replicates for the remaining samples. (**B)** Correlation between replicates based on Pearson correlation. (**C)** Box plots showing the log-transformed intensity of organelle-annotated proteins identified in TOMM20-APEX2 (left) and TOMM70-APEX2 (right). (**D)** Donut plots showing the distribution of organelle-annotated proteins identified in TOMM20-APEX2 (left) and TOMM70-APEX2 (provided by Katharina Zittlau).

Next, the sub-organelle distribution of the proteins identified in TOMM20- and TOMM70-APEX2 interactomes was evaluated. Around 1700 proteins were

identified in TOMM20-APEX2 and TOMM70-APEX2, indicating a nearly identical number of proteins. Besides the expected mitochondrial proteins, surprisingly the enrichment of nuclear proteins, ribosomal, and cytosolic proteins in the interactomes of both fusion proteins was observed (**Figure 14C**). The appearance of nuclear proteins was unclear while cytoplasmic proteins in TOMM20- and TOMM70-APEX2 interactomes were presumably due to the relative positioning of the APEX2. In TOMM20-APEX2, 37.28% cytosolic, 36.29% nuclear, 5.81% ER, 14.7% mitochondrial, and 5.92% ribosomal proteins were identified (**Figure 14D, left)**, whereas TOMM70 shows a distribution of 37.9% cytosolic, 35.3% nuclear, 6.28% ER, 14.57% mitochondrial, and 5.87% ribosomal proteins (**Figure 14D, right).**

To validate that the TOMM20- and TOMM70-APEX2 fusion proteins allowed to study their interactomes, biotinylated proteomes generated by these two baits were compared with those from cells not induced for expression of the APEX2 constructs. The quantitative analysis of all replicates of TOMM20-APEX2 and TOMM70-APEX2 identified the highest number of proteins when cells were induced (+DOX). As expected, much fewer proteins were identified in the uninduced controls, making the imputation of especially low abundant proteins for these samples mandatory (**Figure 15).**

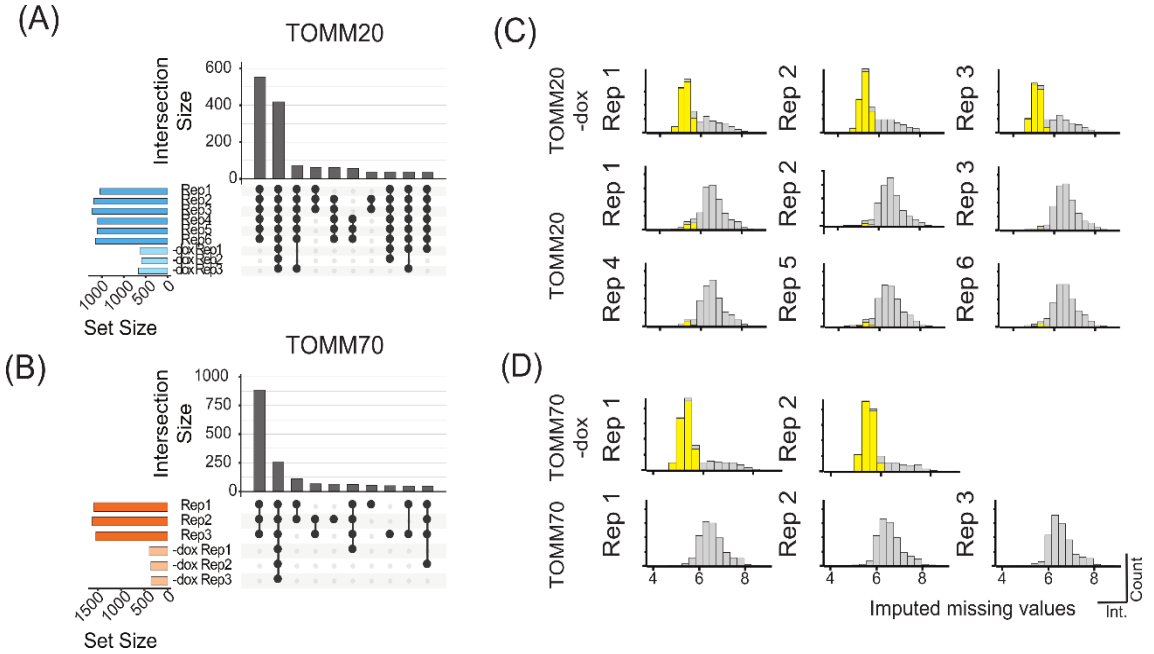

Figure 15. Quantitative analysis of TOMM20- and TOMM70-APEX2 interactomes. (**A)** Upset plot of overlapping proteins identified in six replicates of TOMM20-APEX2 and three replicates of controls (-DOX TOMM20-APEX2). (**B)** Upset plot of overlapping

proteins identified between replicates of TOMM70-APEX2 and controls (-DOX TOMM70-APEX2). Imputation of missing values (yellow bars) shows mostly unidentified low abundant proteins replaced from normal distribution for -DOX TOMM20-APEX **(C)** and -DOX TOMM70-APEX2 **(D)** (provided by Katharina Zittlau).

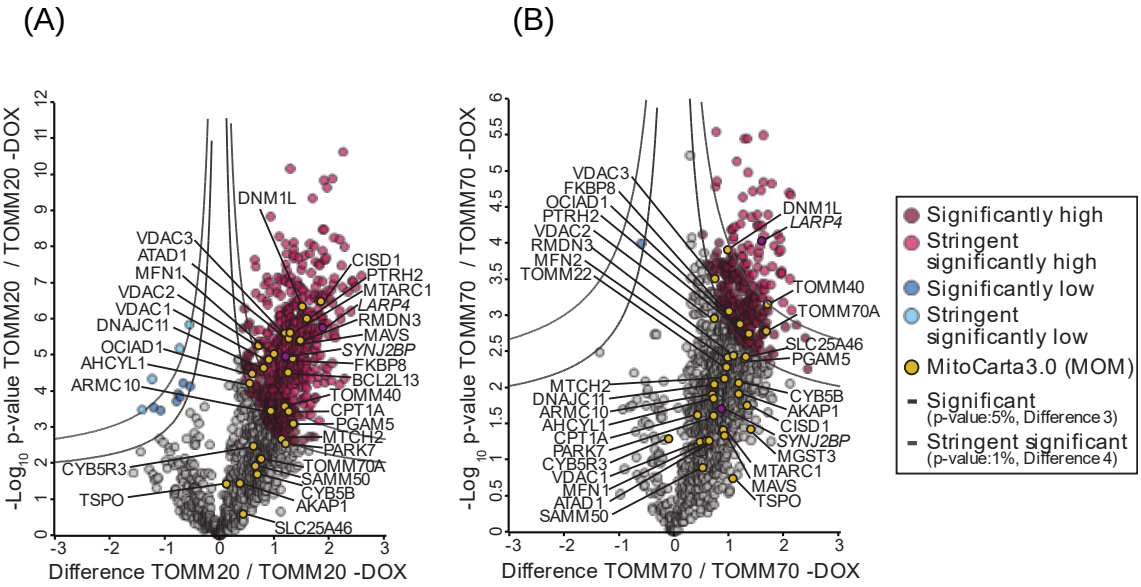

Figure 16. Interactomes of TOMM20-APEX2 and TOMM70-APEX2 at the mitochondrial outer membrane.
The interactome of TOMM20-APEX2 **(A)** and TOMM70-APEX2 **(B)** shows the enrichment of proteins including MOM proteins (annotated in yellow) compared to their uninduced (-DOX) controls. Difference was calculated by the two-sample Student's t-test (provided by Katharina Zittlau).

In the interactomes of TOMM20- or TOMM70-APEX2 versus their uninduced (-DOX) counterparts, many MOM proteins in their interactomes were identified (**Figure 16A, B**; Suppl. Table 1 and 2). Among the identified candidates, significantly abundant ones (p value ≤ 0.05) and stringently-significantly abundant ones (p ≤ 0.01) were further distinguished. The identification of several other subunits of the TOM complex (e.g. TOMM40) or other MOM proteins - 21 in case of TOMM20-APEX2, seven in case of TOMM70-APEX2; Table 1 and Table 2 - among the significantly and stringent significantly high abundant proteins demonstrates the effectiveness of our approach.

Table 1. MOM proteins enriched in the TOMM20 vs -DOX interactome

Gene names	Protein names
SYNJ2BP	Synaptojanin-2-binding protein
ARMC10	Armadillo repeat-containing protein 10
ATAD1	ATPase family AAA domain-containing protein 1

MTARC1	Mitochondrial amidoxime-reducing component 1
PTRH2	Peptidyl-tRNA hydrolase 2, mitochondrial
DNM1L	Dynamin-1-like protein
TOMM40	Mitochondrial import receptor subunit TOM40 homolog
VDAC1	Voltage-dependent anion-selective channel protein 1
VDAC2	Voltage-dependent anion-selective channel protein 2
CPT1A	Carnitine O-palmitoyltransferase 1, liver isoform
FKBP8	Peptidyl-prolyl cis-trans isomerase FKBP8
MAVS	Mitochondrial antiviral-signaling protein
MFN1	Mitofusin-1
PGAM5	Serine/threonine-protein phosphatase PGAM5, mitochondrial
RMDN3	Regulator of microtubule dynamics protein 3
BCL2L13	Bcl-2-like protein 13
OCIAD1	OCIA domain-containing protein 1
DNAJC11	DnaJ homolog subfamily C member 11
CISD1	CDGSH iron-sulfur domain-containing protein 1
VDAC3	Voltage-dependent anion-selective channel protein 3
AHCYL2	Putative adenosylhomocysteinase2

Table 2. MOM proteins enriched in TOMM70 vs -DOX interactome

Gene names	Protein names
PTRH2	Peptidyl-tRNA hydrolase 2, mitochondrial
DNM1L	Dynamin-1-like protein
TOMM70A	Mitochondrial import receptor subunit TOM70
TOMM40	Mitochondrial import receptor subunit TOM40 homolog
FKBP8	Peptidyl-prolyl cis-trans isomerase FKBP8
OCIAD1	OCIA domain-containing protein 1
VDAC3	Voltage-dependent anion-selective channel protein 3

Whereas TOMM70 was present in the dataset of potential interactors of TOMM20-APEX2 and identified as a biotinylated protein in TOMM70-APEX2 expressing cells, TOMM20 was not. Since it had been identified only by one peptide, due to the raw data processing settings it was not considered for further analysis. Potential reasons for the low number of TOMM20 peptides are the low number of the peptides generated from the miniature 20 kDa protein itself and

the limited accessibility to activated biotin of the rather small cytosol-facing domain of TOMM20 (Su et al., 2024). In addition, the cytoplasmic domain contains few aromatic amino acids available for reaction with the biotin-phenoxyl radical generated by APEX2 (Hung et al., 2017; Su et al., 2024).

3.6 TOMM20-/ TOMM70-APEX2 interactome at the MOM-cytoplasm interface

To validate that the interactome of TOMM20- and TOMM70-APEX2 indeed reflects proteins relevant for processes occurring at the MOM-cytoplasm interface, the patterns of the biotinylated proteins in these interactomes were compared with those of a cytosolically targeted APEX2 (APEX2-NES). Proteins were annotated for cytoplasmic and mitochondrial localization by utilizing Gene Ontology Cellular Component (GOCC; Ashburner et al., 2000) and MitoCarta3.0 (Rath et al., 2021) databases, respectively. Importantly, the first observation, when comparing the interactome of TOMM20- and TOMM70-APEX2 with that of APEX2-NES, was that MOM proteins were more abundant among the TOMM20- and TOMM70-APEX2 interactomes (**Figure 17 A-C**; Suppl. Table 3 and 4**).** However, cytoplasmic proteins were also enriched in both interactomes (TOMM20-APEX vs. APEX2-NES and TOMM70-APEX2 vs APEX2-NES).

The aim was to elucidate the complement of RBPs and translation related proteins associated with TOMM20 or TOMM70. For this purpose, the dataset was subsequently analyzed for the enrichment of proteins related to RNA function.

While no RBPs were identified as enriched in the TOMM70-APEX2 interactome when compared to that of a cytoplasmic APEX2, seven RBPs - i.e. 23% of all enriched proteins compared with APEX2-NES - were found in the TOMM20-APEX2 interactome, including synaptojanin 2 binding protein (SYNJ2BP), polyadenylate-binding protein-interacting protein 1 **(**PAIP1), mitochondrial antiviral-signaling protein (MAVS), polyadenylate-binding protein 4-like (PABPC4L), eukaryotic translation initiation factor 5 (eIF5), regulator of chromosome condensation 2 (RCC2), and partner of Y14 and mago protein (WIBG; Suppl. Table 3).

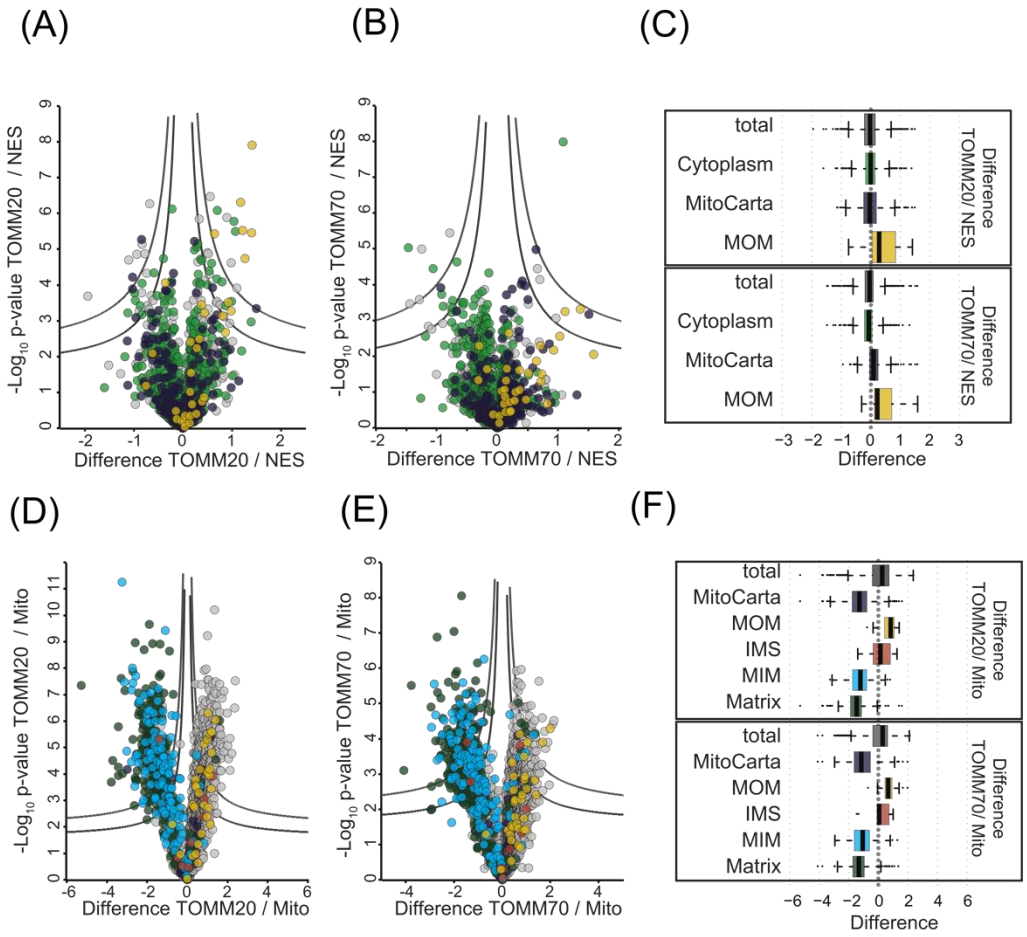

Figure 17. Interactomes of TOMM20-APEX2 and TOMM70-APEX2 at the mitochondrial outer membrane
Volcano plots for TOMM20-APEX2 **(A)** and TOMM70-APEX2 **(B)** against APEX2-NES interactome. Differences were calculated by a two-sample Student's t-test. Highlighted are proteins annotated for cytoplasmic localization (based on GOCC) and mitochondrial localization (MitoCarta3.0). The color code used to annotate the proteins in A and B is identical to C **(C)** Boxplot with distribution of total proteins compared to proteins annotated for mitochondrial or cytosolic localization for TOMM20- (above) and TOMM70-APEX2 (below) against APEX2-NES. Volcano plots for TOMM20-APEX2 **(D)** and TOMM70-APEX2 **(E)** against the Mito-APEX2 interactome. Highlighted are proteins annotated for their submitochondrial localization based on MitoCarta3.0. The color code used to annotate the proteins in F and G is identical to F. **(F)** Boxplot with distribution of total proteins compared to proteins annotated for mitochondrial and mitochondrial sublocalization for TOMM20- (above) and TOMM70-APEX2 (below) against Mito-APEX2. Indicated are thresholds for stringent significantly higher or lower abundant proteins (p-value 1%, Difference 4) and significantly abundant proteins (p-value 5%, Difference 3; provided by Katharina Zittlau).

The interactome of TOMM20- and TOMM70-APEX2 was also compared to that of matrix-targeted APEX2 (Mito-APEX2), to check if TOMM20- and TOMM70-APEX2 fusion proteins locally biotinylate the proteins, especially MOM proteins, and if this pattern is distinct from matrix localized APEX2 (**Figure 17 D-F**; Suppl. Table 5 and 6). In comparison to Mito-APEX2, both APEX2 fusion proteins

showed higher enrichment of annotated MOM proteins and low abundance of matrix or MIM proteins. This validated that this APEX2-based approach mainly identified proteins localized at MOM or the MOM-cytoplasm interface in close proximity to the TOM complex (**Figure 17**). Interestingly, in addition to several MOM proteins, additional mitochondrial proteins of the matrix, MIM or IMS were identified (**Figure 18)**. Compared to TOMM70-APEX2, for TOMM20-APEX2 we identified more MOM annotated proteins (14 compared to six). Besides the MOM proteins, additional interactors of TOMM70 belong to IMS, MIM, and matrix protein groups (**Figure 18)**. Overall, a comparison of significantly enriched candidates in TOMM20 or TOMM70 vs Mito-APEX2 revealed 17 proteins enriched only in TOMM20 vs Mito-APEX2, 12 proteins in TOMM70 vs Mito-APEX2, and five overlapping proteins in both interactomes (**Figure 18)**. Additionally, TOMM20 appears to interact with more MOM proteins compared to TOMM70, probably due to a more stable association with the MOM or the TOM complex (Morgenstern et al., 2021; Tucker & Park, 2019).

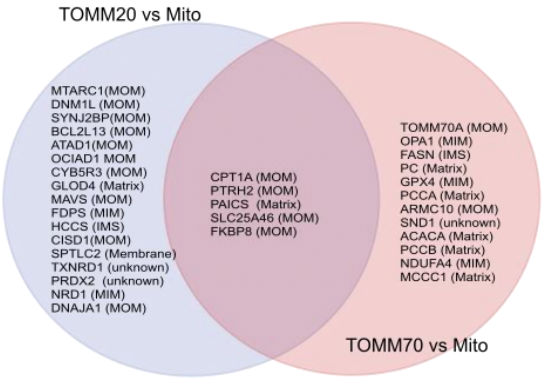

Figure 18. Venn diagram showing overlapping between the proteins enriched in TOMM20-APEX2 vs Mito-APEX2 and TOMM70-APEX2 vs Mito-APEX2.

However, when we compared the interactome of TOMM20- and TOMM70-APEX2 to that of an ERM-targeted APEX2, we did not identify the expected enrichment of MOM proteins, most probably due to contact sites shared with ER-mitochondria (**Figure 19;** Suppl. Table 7 and 8). These contact sites are formed when the apposing membranes of ER and mitochondria come into close proximity, within a distance ranging between 5 to 100 nm. This spatial arrangement can be discrete, or organelles can interact thoroughly in close juxtaposition and share proteins (Barazzuol et al., 2021; Ganji et al., 2023; Vance,

2014). These contact sites, due to the narrow distance between the apposing membranes of the nearby organelles, could cause cross-labeling of both MOM and ER proteins by APEX2, thereby differentiating the proteins that are truly localized to the MOM from those, belonging to ER becomes challenging, due to close association between both organelles.

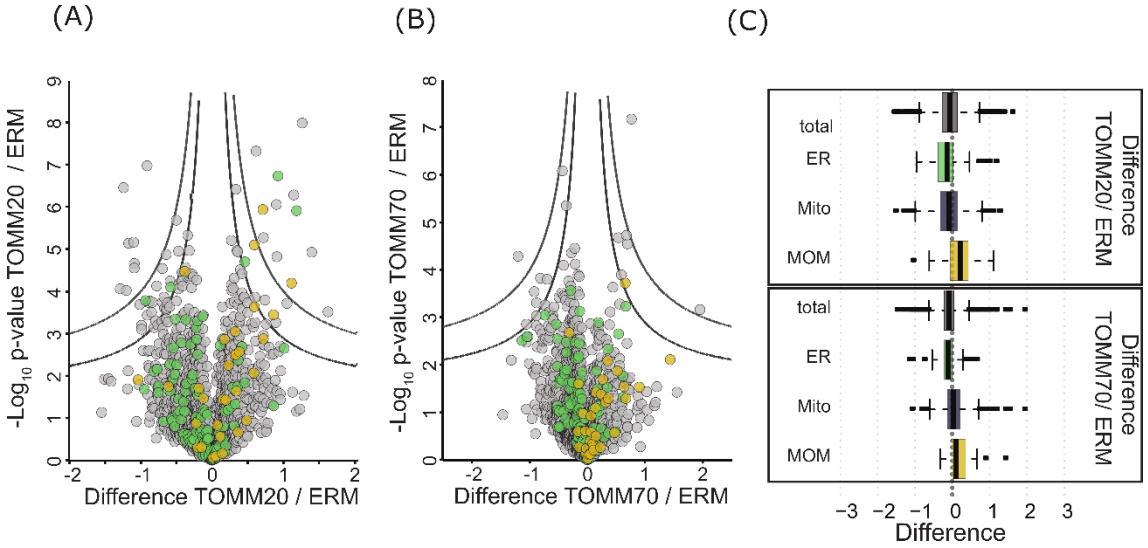

Figure 19. Interactomes of TOMM20-APEX2 and TOMM70-APEX2 versus ERM-APEX2
Volcano plots for the TOMM20-APEX2 **(A)** and TOMM70-APEX2 **(B)** against ERM-APEX2 interactome. Highlighted are proteins annotated for ER (based on GOCC) and mitochondrial localization (MitoCarta3.0). The color code used to annotate the proteins A and B is identical to C (provided by Katharina Zittlau).

3.7 Comparison of TOMM20-APEX2 vs TOMM70-APEX2 interactomes

In order to identify the receptor-specific interactions including their potential substrates, i.e. recruited RNA binding proteins (RBPs) and effectors of translation that associate with each receptor in their particular nano-environment, the interactome of TOMM20-APEX2 was directly compared with the TOMM70-APEX2 interactome (**Figure 20A**). While most mitochondrial proteins are similarly enriched between the two baits, 20 proteins were identified to be significantly overrepresented in the TOMM70-APEX2 interactome including three proteins annotated as exclusively mitochondrial, NDUFA4 (MIM; Balsa et al., 2012), PPA2 (matrix; Bezpalaya et al., 2024), TST (matrix; Bezpalaya et al., 2024), and seven proteins annotated as dual or multiple localized including pyruvate carboxylase (matrix, cytosol; Marin-Valencia et al., 2010), MCCC1 (matrix, cytosol; Cao et al., 2016), UQCRC2 (MIM, nucleoplasm; Han, Wu, et al., 2019), MFN2 (MOM, ER,

cytosol; Filadi et al., 2018), GPX4 (MIM, extracellular space, nuclear envelope, cytosol; Xie et al., 2023), MACROD1 (matrix, cytoplasm, nucleus; Žaja et al., 2020), and SPRYD4 (cytosol, matrix; Ma et al., 2023; Suppl. Table 9). A total of 35 proteins was found to be significantly overrepresented in the TOMM20-APEX2 interactome, among them four proteins annotated as mitochondrial including DLAT (matrix; Zhang et al., 2023), TST (matrix; Bezpalaya et al., 2024), TXNRD2 (matrix, cytosol; Sun et al., 1999), and DNAJA1 (MOM, ER, cytosol, nucleus, extracellular matrix; Rodríguez-González et al., 2020) (**Figure 20A**; Suppl. Table 9). There was doubt if these proteins were mature mitochondrial proteins or alternatively precursors that were caught, while interacting with the TOMM proteins. Likely due to the overall low coverage of peptides in the MTS regions, hardly any MTS containing peptides expected to be part of the precursors were identified. Thus, distinguishing between precursors in transit and mature proteins already at their destination site was not possible.

3.8 RNA-binding proteins and translation factors are part of the TOMM20-APEX2 interactome

A surprisingly large number of cytoplasmic RBPs including CHERP (De Maio et al., 2018), PAIP1 (Roy et al., 2002), KHSRP/FUBP2 (Zheng et al., 2020), PABPC4L (Aslam et al., 2019), TIAL1 (Osma-Garcia et al., 2023), PARN (Osma-Garcia et al., 2023), DDX46 (Yang et al., 2023), ANKRD17 (Wang et al., 2012), LRRC59 (Hannigan et al., 2020), as well as components of the translational machinery like RPL10A (Wenz et al., 2015) and eIF5 (Singh et al., 2006) were identified as significantly enriched in TOMM20-APEX2 compared to TOMM70-APEX2. To investigate this further and to identify how these proteins are functionally connected, we subjected the significantly enriched proteins in the differential TOMM20 vs TOMM70 interactome to a STRING-based network analysis (Szklarczyk et al., 2023).

The majority (43%) of proteins in the TOMM20-APEX2 interactome are overrepresented for cytoplasmic localization with multiple of them annotated as RBP (**Figure 20B; Up**). STRING analysis further reveals that most of the processes, the enriched RBPs are involved in, are interconnected, supporting our hypothesis that TOMM20-APEX2 specifically biotinylates a distinct and functionally related group of RBPs and translation factors that reside in close

proximity. We further checked, if these proteins were also abundant in other interactome comparisons (TOMM20-APEX2 vs -DOX, TOMM20-APEX2 vs APEX2-NES and TOMM20-APEX2 vs Mito-APEX2; Suppl. Table 10). These analyses revealed that many RBPs and translation factors including PAIP1, PABPCL and eIF5 were enriched in the TOMM20 interactome versus the other ones, providing additional support for our argument.

In contrast, the STRING analysis of TOMM70-APEX2 revealed that most proteins that are preferentially enriched in its interactome versus that of TOMM20-APEX2 are linked to membrane bound organelles, including one cluster consisting of mitochondrial proteins (PPA2, UQCRC2, MFN2 and NDUFA4; **Figure 20B; down**). We analyzed the interaction profile of the specific TOMM20 interactome derived from the comparison of TOMM20 vs. TOMM70 (35 proteins, see **Figure 20A**) with the enriched proteins in TOMM20-APEX2 vs APEX2-NES interactome (31 proteins: see **Figure 17A**). 36% of the higher abundant proteins are shared between these interactomes and are annotated as either RNA binding or translation-related (supplementary **Figure 1A,** see Appendix).

The identification of several RBPs or proteins involved in translation in our enriched proteomes tempted us to investigate, how the interactomes of TOMM20- and TOMM70-APEX2 change in the presence of the translation inhibitor puromycin. To this end, we included three replicates of puromycin-treated (+puro) samples for TOMM20- and TOMM70-APEX2 expressing cells. For treatment, I chose a 30 min window and 200 µM puromycin, since a similar treatment had revealed changes in the interactome of a MOM-located APEX2 with selected RBPs, which had already indicated an effect of translation on RBP presence at the MOM (Fazal et al., 2019; Qin et al., 2021). Puromycin treatment (+puro) of TOMM20-APEX2 expressing cells resulted in surprisingly little change in the associated proteome with only one protein in significantly higher (PRTEDC1) and three in lower abundance (FANC1, CHERP and FADS1) after treatment **(**see Appendix**; Suppl. Figure 1B;** Suppl. Table 11**)**. However, none of these proteins have obvious connections to each other, to RNA or to mitochondrial function. A similar observation was made after treatment of TOMM70-APEX2 cells with puromycin, although the number of lower or higher abundant proteins was slightly larger (**Suppl. Figure 1C,** see Appendix**;** Suppl. Table 12).

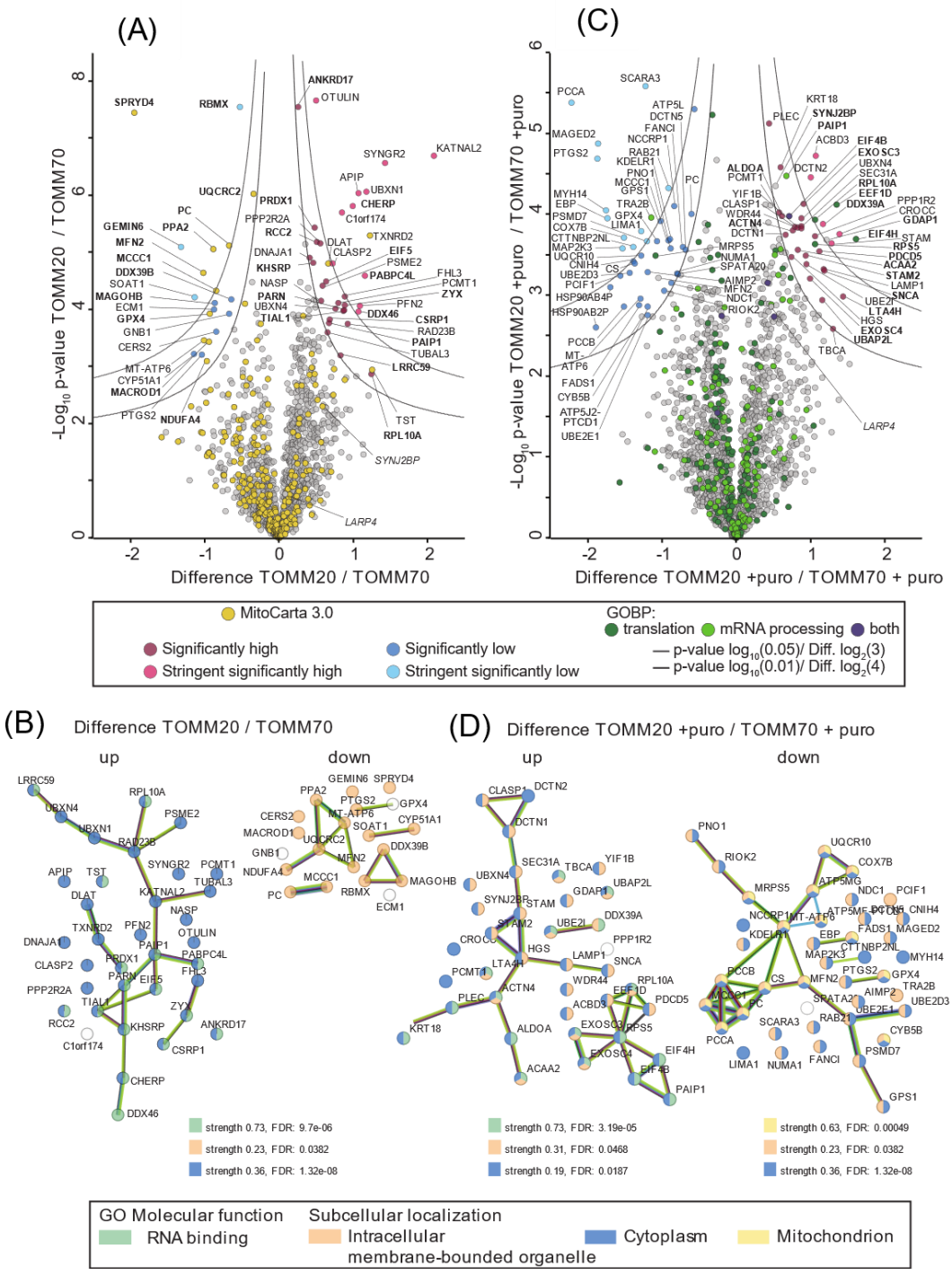

Figure 20. Differential interactome of TOMM20-APEX2 versus TOMM70-APEX2. **(A)** Volcano plot for the TOMM20-APEX2 interactome against the TOMM70-APEX2 interactome. Proteins highlighted in yellow are annotated for mitochondrial localization (MitoCarta3.0). Indicated are thresholds for stringent significantly higher or lower abundant proteins (p-value 1%, Difference 4) and significantly abundant proteins (p-value 5%, Difference 3). **(B)** STRING analysis of proteins abundant in the differential interactome of TOMM20-APEX2 vs TOMM70-APEX2 from volcano plot A, showing enriched candidates of TOMM20 (up), and TOMM70 (down). Proteins are annotated according to GO molecular function and subcellular localization. **(C)** Volcano plots for

TOMM20-APEX2 interactome under puromycin treatment (+puro) against TOMM70-APEX2 interactome (+puro). Highlighted are the proteins annotated (based on GOBP) for translation and mRNA processing **(D).** STRING analysis of proteins abundant in the differential interactome of TOMM20-APEX2 (+puro) vs TOMM70-APEX2 (+puro) from volcano plot C showing enriched candidates of TOMM20 (up), and TOMM70 (down). Proteins are highlighted according to GO molecular function and subcellular localization. Strength and False discovery rate (FDR) of each pathway are indicated (provided by Katharina Zittlau).

However, when we compared the differential interactome of TOMM20 vs TOMM70 (both after treatment with puromycin) and focused especially on proteins annotated by GOBP as being involved in translation and mRNA processing, we found in total 258 proteins, eleven of which were significantly more enriched in the TOMM20-APEX2 after puromycin treatment vs TOMM70-APEX after exposure to puromycin (**Figure 20C;** Suppl. Table 13).

These include the translation initiation and elongation factors (eIF4B, eIF4H, eEF1D; Marintchev et al., 2009; Negrutskii et al., 2023; Sen et al., 2016), ribosomal proteins (RPS5, RPL10A; Pollutri & Penzo, 2020; L. Qiu et al., 2023), and RBPs that are primarily involved in controlling mRNA stability. Among the latter proteins are PAIP1, a translational co-activator interacting with polyA-binding protein PABP (Roy et al., 2002); SYNJ2BP, a MOM-localized RBP that binds to mRNAs encoding mitochondrial proteins, mitigates the effects of translation stress, and has been linked to the local translation at the mitochondrial surface (Qin et al., 2021), and finally SNCA, an unconventional RBP that forms an amphipathic helix, similar to the MTS motifs (Davidson et al., 1998) and a known interactor of TOMM20 (De Miranda et al., 2020). The increased abundance of RBPs that are involved in the mRNA stability in the TOMM20-APEX2 dataset after translation inhibition suggests that TOMM20, via interacting with these proteins has a more mRNA-protective role than TOMM70. Though depletion of these candidates from TOMM70 differential interactome after puromycin treatment suggests that TOMM70 is also dynamically involved in their translation-dependent mitochondrial targeting.

In a similar analysis as before (**Figure 20B**), the significantly enriched proteins in the TOMM20-APEX2 (+puro) (**Figure 20D; up**) and TOMM70-APEX2 (+puro) (**Figure 20D; down**) datasets were subjected to STRING-based network analysis. For the TOMM20-APEX2 interactome, we identified a cluster of proteins annotated as translation regulators. This group of proteins includes a RBP

(PAIP1), translation factors (eIF4B, eIF4H, eEF1D), and ribosomal protein (RPS4), suggesting that components of the translation machinery are still proximal to TOMM20 upon puromycin inhibition.

Interestingly multiple proteins were enriched for their mitochondrial inner membrane and matrix localization among the significantly high enriched interactors of TOMM70-APEX2 after puromycin treatment (**Figure 20C;** Suppl. Table 13**)**. Specifically mitochondrial matrix proteins such as MCCC1 (encoding a subunit of the 3-methylcrotonyl-CoA carboxylase) and PC (pyruvate carboxylase) are similarly overrepresented even under non-translation inhibitory conditions, suggesting a translation-independent import of these proteins. In summary, our quantitative proteomic approach using differential interactomes supports the hypothesis that the TOMM20 and TOMM70 receptors interact with unique sets of proteins. More importantly, our analysis provides first evidence that both receptors remodel their proteome differentially in response to the translation stress.

3.9 Validation of co-localization of enriched candidates identified by MS

SYNJ2BP was one of the candidates that was identified in almost all interactomes of TOMM20. To verify that this protein is indeed be localized in the proximity of the TOM complex, I performed airyscan confocal super-resolution microscopy, using antibodies against TOMM20 and SYNJ2BP (**Figure 21**). Quantification of the signals by ImageJ revealed a high positional overlap of both proteins, supporting the proximity labeling data.

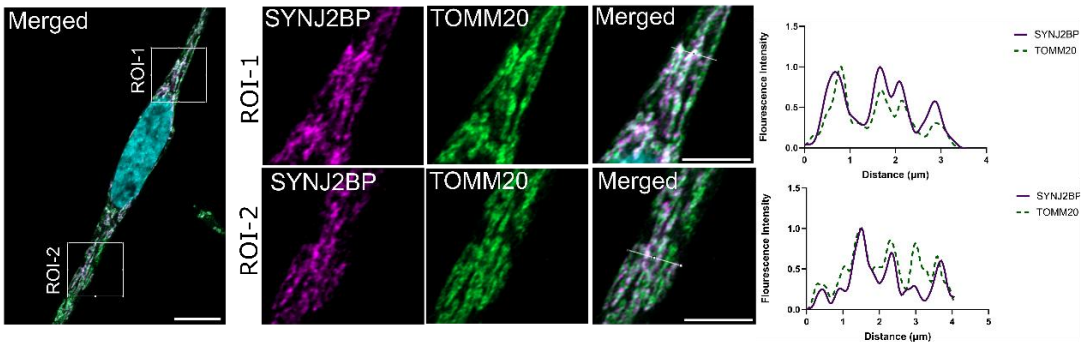

Figure 21. SYNJ2BP colocalizes with TOMM20 in HeLa cells.
Fluorescence images of HeLa cells showing co-localization of SYNJ2BP and TOMM20. Cells were fixed and immunolabeled with antibodies directed against TOMM20 (green) and SYNJ2BP (magenta). Each representative confocal image represents a merged

image of green and magenta channels and two ROI were selected for each candidate in the cell. Nuclei were stained with DAPI (cyan) (Scale bar: 10 µm). Each ROI is a zoomed-in portion of the cell showing in the middle (Scale bars, 5 µm). Scan intensity profiles along the indicated lines in the ROIs represent the overlapping fluorescence signals of SYNJ2BP and TOMM20.

3.10 APEX2-fusion proteins biotinylate proximal RNA

Previous studies reported that biotin-phenoxyl radicals do not only react with aromatic amino acids in proteins but also with guanosine nucleotides in RNA (Fazal et al., 2019; Padrón et al., 2019). In order to identify the localization of nuclear-encoded mitochondrial transcripts to the MOM, particularly to the TOMM20 and TOMM70 receptors of the TOM complex, I first validated if APEX2-TOMM fusion proteins biotinylatd efficiently nearby RNAs present within their labeling radius in the HeLa cells. For that, the cells were subjected to live-cell biotinylation after 24 h induction with doxycycline (DOX), treated first with biotin-phenol (BP) for 30 minutes at 37 °C, and afterwards with hydrogen peroxide (H_2O_2) for 1 minute at room temperature. Cells were thoroughly washed in quencher solution, and subsequently lysed. RNA was freshly isolated, subjected to UV- cross-linking, and subsequently blotted on a nitrocellulose membrane. Biotinylated RNA was detected by using a streptavidin conjugate. Dot blot RNA analysis revealed that the biotin signals in the dot blot were only detected when TOMM20- or TOMM70-APEX2 fusion proteins were expressed after doxycycline induction, and only in the presence of biotin-phenol (BP), and H_2O_2 (**Figure 22**).

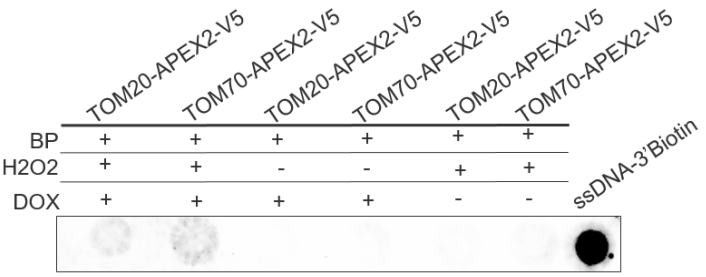

Figure 22. RNA dot-blot analysis to validate APEX2-mediated RNA biotinylation in HeLa cells stably expressing the fusion proteins.
Cells expressing TOMM20-APEX2 and TOMM70-APEX2 constructs were either or not induced with DOX for 24 hours. Cells were subjected to biotinylation with biotin phenol (BP) and H_2O_2 for one minute. Cells were quenched, RNA was isolated and blotted on nitrocellulose membrane. Only when cells were induced and expressed APEX2-fusion proteins, and in the presence of BP and H_2O_2, the biotinylated signal was observed. A ssDNA probe, labeled with biotin at its 3´ end was used as positive control.

3.11 RNA-seq analysis of TOMM-proximal mRNAs

After validating that TOMM fusion proteins also biotinylate RNA, I tried to harness the full potential of this approach by integrating it with RNA-seq for identifying the localized RNAs at the TOM complex. A previous study identified targeting of nuclear-encoded mitochondrial transcripts to MOM, by utilizing a similar APEX2-based approach, where APEX2 was targeted to the MOM but not specifically to the TOM complex. The authors reported the enrichment of nuclear-encoded mitochondrial mRNAs over non-mitochondrial or secretory transcripts in their dataset (Fazal et al., 2019). I initially performed a preliminary analysis to identify the enriched mRNAs at MOM biotinylated by the TOMM-APEX2 fusion protein. For control, mock treated cells were biotinylated and harvested in parallel. Cells were thoroughly washed, RNA was isolated, and the biotinylated RNA fraction was subsequently pulled down by streptavidin beads (see method section 4.4.9). Further library preparation and RNA sequencing was done by Novogene. When I compared the transcripts enriched in TOMM20- versus ERM-APEX2, I did not observe an obvious enrichment of nuclear-encoded mitochondrial transcripts over non-mitochondrial ones (**Figure 23, A**). This might be from the consequence of the low RNA yield during enrichment, which did not allow library preparation in optimal quality. The yield of RNA following streptavidin pulldown was low and ranged between 50 ng to 100 ng. However, other authors considered this amount enough to generate a good RNA-seq library (Fazal et al., 2019). Since the large number of transcripts was also identified in mock samples (**Figure 23**, **B, C**), further optimization of the protocol, including additional washing steps, will probably be helpful.

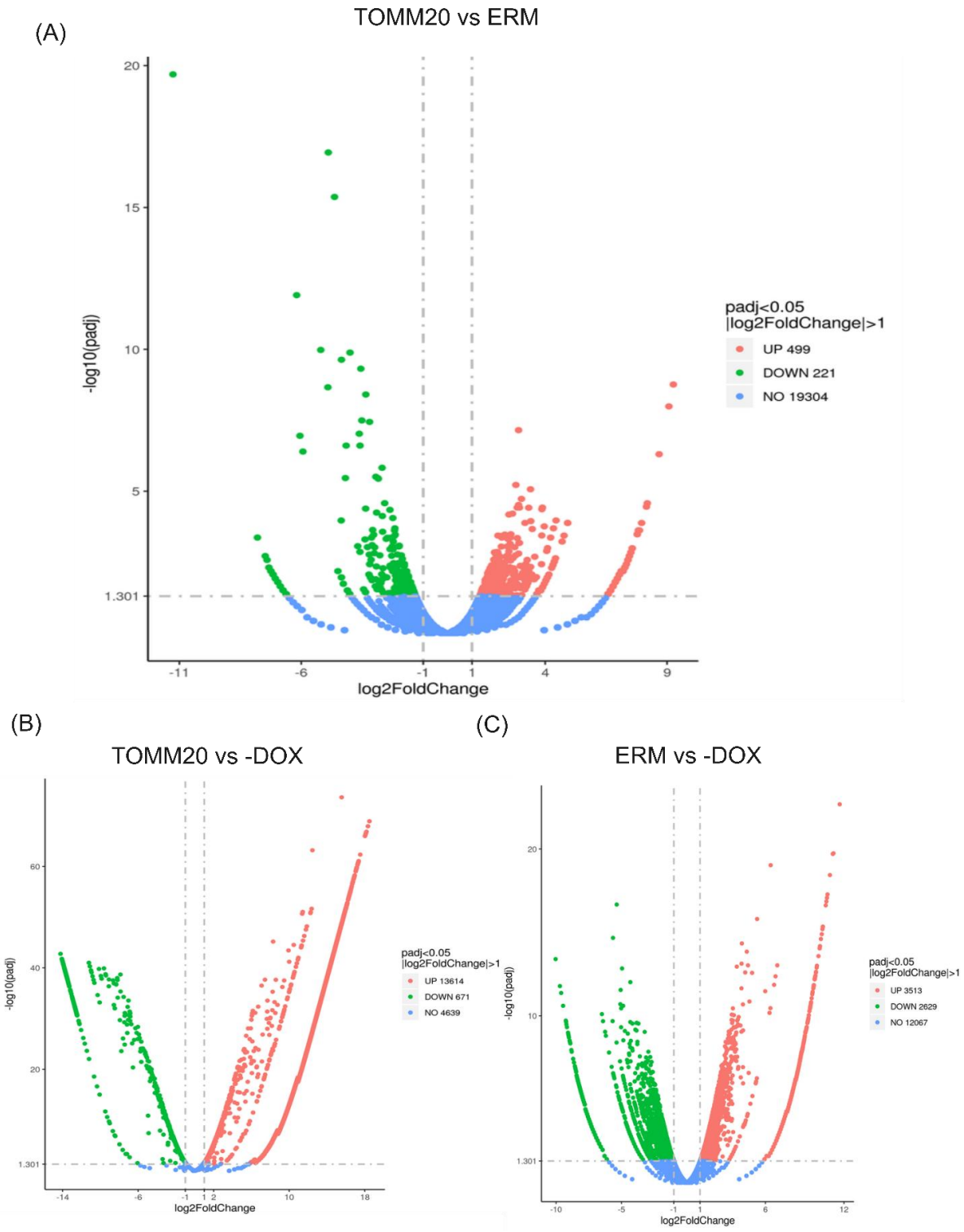

Figure 23. Enrichment of transcripts identified by RNA-seq.
(A). Volcano plot for TOMM20-APEX2 showing enrichment of transcripts compared to ERM-APEX2. UP shows the number of transcripts enriched in TOMM20 vs ERM, DOWN shows the number of transcripts enriched in ERM, while NO shows the number of transcripts having no effect **(B).** Volcano plot for TOMM20-APEX2 showing enrichment of transcripts compared to mock (-DOX) **(C).** Volcano plot for ERM-APEX2 showing enrichment of transcripts compared to mock (-DOX) (plots are provided by Novogene).

Chapter 3: Discussion

Proximity labeling (PL) approaches have been extensively used in the past to investigate the mitochondrial proteome and transcriptome (Cho, Branon, Udeshi, et al., 2020; Fazal et al., 2019; Qin et al., 2021; Rhee et al., 2013). These approaches mainly employ modified engineered enzymes, e.g. engineered APEX2 or biotin ligases). Biotin ligases- based approaches (e.g. BioID, TurboID, miniTurbo, transitID) are implemented to analyze the sub-mitochondrial compartment specific proteome (Antonicka et al., 2020; Cho, Branon, Udeshi, et al., 2020; Hung et al., 2017; Qin et al., 2023; Williams et al., 2014). The split versions of the promiscuous biotin ligases are also useful for studying the proteome of mitochondria-associated membranes (MAMs) after improving off-target labeling effects (Cho, Branon, Rajeev, et al., 2020; Qin et al., 2023; Schopp et al., 2017).

APEX2-based PL approaches have become more popular in recent years, as APEX2 offers higher temporal resolution and better catalytic function than the biotin ligase enzymes TurboID or BioID (Cho, Branon, Udeshi, et al., 2020; Fazal et al., 2019; Lam et al., 2015; Meurant et al., 2023; Roux et al., 2012). APEX2 was efficiently employed for short-term labeling of sub-mitochondrial compartments including MOM, IMM, and matrix to analyze the local interactome and transcriptome. MOM labeling was achieved by fusing APEX2 to the mitochondrial targeting peptide, derived from the MAVS protein (Fazal et al., 2019; Hung et al., 2017; Qin et al., 2021). Although this peptide-fused, recombinant APEX2 was efficiently targeted to MOM in live cells, as confirmed by corresponding immunofluorescence and Western blot analysis, it was believed to integrate randomly into the MOM. It did not reveal whether the identified associated proteins had a functional relation to other components of the MOM, particularly with the TOM complex, that controls mitochondrial protein import. To address this question more directly, I applied an APEX2-based protein profiling methodology to investigate the association profiles of human TOMM20 and TOMM70 receptors of the TOM complex in their cellular environment and identified their interactomes. An excellent correlation was observed between all technical replicates in the study, which underlined experimental efficiency and high data quality. The number of identified proteins (around 1700) and their sub-

organelle distribution pattern were almost identical. Besides the expected mitochondrial proteins, an enrichment of the nuclear, ribosomal, and cytosolic proteins was also observed (**Figure 13C**). While the appearance of nuclear proteins is unclear, though it has already been observed in the interactome revealed by a TOMM20-TurboID protein fusion approach (Meurant et al., 2023). The cytoplasmic proteins in TOMM20- and TOMM70-APEX2 interactomes might be due to the relative positioning of APEX2. Since the APEX2 parts of the two fusion proteins are facing the cytosol, I expected them to not only biotinylate MOM proteins but also in addition, due to the release and diffusion of phenoxyl-biotin radicals, proteins in the surrounding cytoplasm. The approach demonstrated an enrichment of MOM proteins in proximity to the TOM complex, especially when comparing TOMM-APEX2 interactomes with that of cytoplasmic or mitochondrial matrix localized APEX2. Particularly in case of TOMM20-APEX2, besides expected MOM components like MTARC1 (a MOM-localized oxidoreductase), OCIAD1 (OCIA domain-containing protein 1), CISD1 (a redox active mitochondrial protein with an iron–sulfur domain), RMDN3 (a regulator of microtubule dynamics), BCL2L13 (a BCL2-like protein), and CYB5R3 (NADH-cytochrome b5 reductase 3), seven RNA-binding proteins (RBPs) were also enriched. These include SYNJ2BP and MAVS that had already previously been located at the MOM (Hanada et al., 2020; Qin et al., 2021). In an independent but related study, the interactome of human TOMM20 was recently captured in HCT116 cells by tagging it with the miniTurbo biotin ligase (Meurant et al., 2023). For negative control, the authors targeted APEX2 to carnitine palmitoyl transferase 1A (CPT1A) protein. Though CPT1A is a MOM protein, authors chose it based on string analysis, showing that none of its interactors belong to TOM complex. Around 22% of proteins significantly enriched in our TOMM20- versus APEX2-NES interactome were also enriched in their dataset. These proteins include the MOM proteins like CISD1, RMDN3, MTARC1, OCIAD1, and MAVS. The low overlap of enriched proteins between the studies is presumably due to the difference in proximity labeling enzymes, expression setups, and labeling time. They labeled the cells with biotin for 24 hours, and then captured the interactome of TOMM20, whereas I used APEX2, which needs only 1 minute, thus capturing also the transient interactions. Since transient interactions at the MOM are crucial for modulating mitochondrial quality control and function, our

approach is helpful in capturing the one-minute snapshot of such transient and spatial interactions of both TOM receptors.

To rigorously investigate the receptor specific, reciprocal interactions, a direct comparative analysis between TOMM20- and TOMM70-APEX2 was necessary. The comparison of TOMM20- versus TOMM70-APEX2 interactome showed that both receptors are in proximity of a unique set of proteins in their nano-environment at MOM. TOMM20- and TOMM70-APEX2 associate with different substrates of mitochondrial preproteins destined for various sub-mitochondrial compartments as seen with their yeast homologs. Mitochondrial proteins labeled by TOMM20-APEX2 mainly belong to the matrix protein group while those proteins enriched in the TOMM70-APEX2 interactome represent matrix and mitochondrial inner membrane (MIM) proteins. This supports previous studies showing that MTS-containing matrix precursor proteins are mainly imported by yeast Tom20 (Omura, 1998), or that the loss of Tom70/71 in yeast in particular affects import of matrix and MIM proteins (Sayyed & Mahalakshmi, 2022).

There was uncertainty whether the enriched proteins were mature mitochondrial proteins or precursors that were captured while interacting with the TOMM proteins. Likely due to the overall low coverage of peptides in the MTS regions, hardly any MTS-containing peptides were identified, which are expected to be part of the precursors. Thus, distinguishing between precursors in transit and mature proteins already at their destination site was not possible. Previous studies showed that biotin-phenoxyl radicals generated by APEX2 at the cytoplasmic face of mitochondria may occasionally traverse the MOM through porins and can biotinylate MIM and IMS proteins. This may also explain the identification of such proteins in my approach. However, these radicals cannot penetrate the matrix due to the selective permeability of MIM (Hung et al., 2017; Rhee et al., 2013). This suggests that the biotinylated matrix proteins in the TOMM20-APEX2 interactome were captured rather during transit than after processing in the matrix. Our results thus support the idea that mammalian TOMM20 and TOMM70 receptors, similar to their yeast counterparts (Abe et al., 2000; Yamamoto et al., 2011), might interact with distinct but overlapping sets of precursor proteins.

In addition to MOM-associated RBPs like SYNJ2BP, TOMM20- in contrast to TOMM70-APEX2, appears to associate with cytoplasmic RBPs like PAIP1,

KSHRP, and PABPC4L, as well as the components of the translation machinery, like ribosomal proteins or the translation initiation factor eIF5. This enrichment of cytoplasmic RBPs and components of the translation machinery not only corroborates the hypothesis of localized translation at the MOM (Cohen et al., 2024; Eliyahu et al., 2010; Sharma & Fazal, 2024), but also suggests that TOMM20 rather than TOMM70 might play a role in localized translation of nuclear encoded mitochondrial mRNAs or co-translational import of their encoded proteins. This study captured the local interactomes of the TOMM20 and TOMM70 receptors in their nano-environment at MOM. A local interactome refers to a set of proteins, that is enriched temporally around a certain bait protein. Interactome encompasses not only the direct interactors of that bait protein but also those spatially close to it, even if not physically interacting with the bait protein. Hence, all the interactors of TOMM receptors identified in this study still need to be further validated through additional orthogonal experiments such as co-immunoprecipitation (Co-IP) or import assays.

When cells were treated with puromycin, the comparison of the differential interactome of TOMM20- vs TOMM70-APEX2 identified an enrichment of proteins involved in translation and mRNA processing in TOMM20 (Figure 18C). Remodeling of its interactome during translation inhibition suggests that TOMM20 may play a role in preserving cellular homeostasis during translation stress by retaining translation-related proteins at the MOM. It specifically interacts with certain RPBs involved in mRNA stability such as SYNJ2BP, PAIP1, or SNCA. SYNJ2BP has previously been identified as a key regulator that safeguards specific nuclear-encoded mitochondrial transcripts during translation stress (Qin et al., 2021). It anchors these transcripts at MOM under translation stress, and stabilizes them, which might facilitate their local translation and import of corresponding protein products, thereby maintaining OXPHOS activity and mitochondrial function. I captured not only this RBP in the TOMM20 interactome under translation arrest but also other components of the translation machinery, such as eiF4B, eiF4H, eEF1D, or ribosomal proteins, providing further evidence for a SYNJ2BP- mediated localized translation at the MOM, in proximity of the TOMM20 receptor. When these components and SYNJ2BP are localized simultaneously at MOM, they likely act in concert, presumably facilitating the local translation of mRNAs encoding mitochondrial proteins. SYNJ2BP stabilizes

mRNAs under translation stress by anchoring and escorting them. The nearby initiation factors (eiF4B, eiF4H) facilitate the unwinding of secondary structures, typically present in the 5′- untranslated regions of mRNAs, promoting ribosomes recruitment during translation initiation. eEF1D mediates the delivery of aminoacyl-tRNAs to the ribosomes. Its localization, together with other components of translation machinery, ensures that the elongation phase proceeds efficiently once translation is initiated (Negrutskii et al., 2023; Sen et al., 2016). PAIP1 interacts with key translation factors, including eIF4A and eIF3, and facilitates translation initiation (He et al., 2019; Roy et al., 2002; Xue et al., 2023). Another candidate, α-Synuclein (SNCA) was identified, that associates with P-bodies and stabilizes mRNAs by slowing their degradation (Hallacli et al., 2022). Its pathological form, after aggregation, sequesters RNA (Rupert et al., 2023). SNCA is an unconventional RBP that forms amphipathic helices, similar to the MTS motifs (Davidson et al., 1998). It is a known interactor of TOMM20 (Di Maio et al., 2016), and TOMM20 overexpression was reported to rescued SNCA induced dopaminergic neurodegeneration in Parkinson's disease patients (De Miranda et al., 2020). However, how all these enriched RBPs, identified in the TOMM20 interactome interact with TOMM20 and modulate mRNA localization and local translation, particularly under translation stress, still needs to be investigated.

Hence, I successfully implemented the APEX2-methodology in HeLa cells for the first time to study the local proteome at the TOM complex and identified interaction profiles of the human TOMM20 and TOMM70 receptors. One of the challenges encountered was the overall low coverage of peptides acquired by MS data acquisition in bottom-up proteomics using a label free quantification method. This drawback could be attributed to several factors, including sample complexity, insufficient protein digestion, and the inherent bias of the data-dependent acquisition (DDA) method, which usually prioritizes abundant peptides. Future studies could employ alternative MS quantification methods, such as Stable Isotope Labeling by Amino Acids in Cell Culture (SILAC) or Tandem Mass Tags (TMT) labeling, which offer better peptide coverage, improved labeling efficiency, and enhanced quantification. Alternatively, cellular fractionation could also enrich corresponding peptides, particularly those belonging to mitochondrial precursors, and reduce sample complexity.

Additionally, recently developed advanced label-free quantification methods could offer better proteome coverage and could be implemented for the future studies (Guzman et al., 2024).

Since one of my aims was to support previous findings for mRNA localization to the MOM, I harnessed the potential of the APEX2-mediated labeling of nearby RNAs, and combined it with RNA-seq (APEX-Seq; Fazal et al., 2019; Padrón et al., 2019). I enriched the mRNAs localized to the MOM that were biotinylated there by TOMM20-APEX2, and compared them with the mRNAs biotinylated by ERM tagged APEX2. In the RNA-Seq dataset comparing TOMM20- versus ERM-APEX2, I did not observe any enrichment of nuclear-encoded mitochondrial transcripts over non-mitochondrial ones. One possible reason could be the low yield of enriched RNA after streptavidin pull down. Generally, the phenoxyl radicals generated by APEX2 react more efficiently with electron-dense aromatic amino acid side chains in proteins than with electron deficient nucleobases in RNA (Li et al., 2022). Among the latter, guanosine is considered the best reactant but in contrast to aromatic acids much weaker, hence the labeling of RNA is generally low. However, recent improvements of the method have been made to use APEX2-Seq to selectively profile a sub-cellular nascent transcriptome (Li et al., 2022). Here, the authors selectively profiled newly transcribed mRNAs at subcellular organelles including the mitochondrial matrix by first metabolically incorporating electron-rich ribonucleosides (e.g. 4-thiouridine, and 6-thioguanosine), followed by combining this approach with APEX2-Seq. This method resulted in a 20-fold increase in labeling efficiency compared to the standard APEX2-Seq. Further optimization of APEX2-seq methodology through this approach could be beneficial to identify the local transcriptome at TOM complex.

In the future, the APEX2 based methodology could be extended to other cell types, such as neurons for studying mitochondrial specific local protein and RNA interactome at the TOM complex. Integrating similar APEX2-based proximity labeling approaches for other TOM complex subunits or TOM-associated proteins, such as the SAM complex, with the presented data could provide a more detailed view of the complex interactions, localized translation at the MOM and its contribution to mitochondrial import. Importantly, I identified a potential differential recruitment of RBPs and other components of the translation

apparatus to TOMM20 rather than TOMM70. These identified interactors require further validations based on additional pull-down assays. Future studies are required to further validate whether and how the TOM complex, particularly TOMM20 dynamically regulates mRNA localization at the MOM by recruiting RBPs and effectors, and how it mediates localized translation at the MOM. Additionally, it also necessary to analyze the role of the identified RBPs in targeting, translation, and stabilizing their putative mRNA targets. Addressing these research questions in future could potentially provide insights into the association of RBPs with TOMM20.

Chapter 4: Material and Methods

4.1 Materials

4.1.1 Equipment

Table 3. List of equipment and software used

Equipment	Supplier
ChemiDoc MP MyCycler Thermo Cycler Mini-PROTEAN Tetra Electrophoresis System PowerPac HC Power Supply	Bio-Rad
Pipettes P1000, P200, P20, P10 Centrifuge 5702 Centrifuge 5810R Centrifuge 5415R	Eppendorf
ThermoCell Mixing Block MB-102	BIO ER
Nanodrop	Thermo
Ultracentrifuge TLA-120.2 Ultracentrifuge rotor SW 40 Ti CytoFLEX Flow Cytometer	Beckman Coulter
ZEISS Axio Examiner	Zeiss
Magnetic rack	Sigma
Cx-2000 UV Crosslinker	Stratalinker
Odyssey Infrared Imaging System used (HNO, Tuebingen)	LI-COR Biosciences
LSM980 laser scanning confocal microscope	Carl Zeiss, Germany
Fiji/ImageJ software	-
Perseus software version 1.6.7.0	-
MaxQuant software suite version 2.2.0.0	-
Snapgene software	-

4.1.2 Enzymes

Table 4. List of enzymes used

Enzyme	Supplier
Restriction digestion enzymes	New England Biolabs
Fast-Digest Restriction Enzymes RNse Inhibitor (RNAse A) Proteinase K RNase Inhibitor T4 DNA Ligase PageRuler Prestained Protein Ladder PageRuler Unstained Protein Ladder PageRuler DNA ladder (100 bp, 1 Kb)	Thermo Scientific/Fermentas/ Ambion
KOD polymerase	Sigma Aldrich

4.1.3. Commercial Kits

Table 5. List of kits used

Kits	Supplier
NucleoSpin Plasmid NucleoSpin Gel and PCR clean up	Macherey and Nagel
RNeasy Plus Mini Kit Endotoxin free plasmid extraction kit QIAquick PCR Purification Kit	Qiagen
RNA Clean and Concentrator−5 kit	Zymoresearch

4.1.4. Consumables

Table 6. List of consumables used

Consumable	Supplier
10-cm glass-bottomed Petri dishes	Corning
Carl Roth Cover slips	Carl Roth Cover slips
Nitrocellulose Membranes PVDF Membranes	LI-COR Biosciences
High quality pipette tips High quality serological pipettes 15 ml CryoPure Storage Systems	SARSTEDT AG & Co

1.5 ml PCR reaction tubes Semi-micro cuvette Centrifuge tube 50 ml TC dish 100, Standard Sarstedt TC dish 150, Standard Sarstedt TC plate, 6 Well, Standard F Sarstedt TC plate, 12 Well, Standard F Sarstedt TC plate, 24 Well, Standard F Sarstedt TC plate, 96 Well, Standard F Sarstedt	
DMEM, low glucose	Sigma
Lipofectamine 3000	Thermo
PBS	Thermo
Pierce™ streptavidin magnetic beads	Pierce
Whatman paper, 3 mm	Whatman
Dounce homogenizer	Sigma-Aldrich
Competent *E. coli* cells DH5α strain	New England Biolabs
3,3'-Dithiodipropionic acid bis(N-succinimidyl ester (DSP crosslinker)	Thermo
Chemiluminescent substrate solution	Thermo
Dynabeads MyOne Streptavidin C1 magnetic beads	Thermo
Pierce™ streptavidin beads	Thermo
V5-Traps beads	Chromo Tek
Invitrogen™ Dynabeads™ Protein A	Invitrogen
Amicon® ultra centrifugal filter, 3 kDa MWCO	Sigma

Table 7. List of chemicals used

Chemical	Supplier
4-(2-hydroxyethyl)-1-piperazineethanesulfonic acid (HEPES)	Sigma-Aldrich
Acetic acid	Carl Roth
30% Acrylamide/Bis Solution (37.5:1)	Carl Roth
Agarose, electrophorese grade	Carl Roth
Ammonium persulfate (APS)	Carl Roth

Ampicillin	AppliChem
Bromophenol blue	Carl Roth
cOmpleteTM Protease Inhibitor, EDTA-free	Roche
Dimethyl sulfoxide (DMSO)	Carl Roth
Dithiothreitol (DTT)	Carl Roth
Dulbecco's Modified Eagle Medium (DMEM)	Sigma Merck
Ethanol	Carl Roth
Ethylene glycol tetraacetic acid (EGTA)	Carl Roth
Ethylenediaminetetraacetic acid (EDTA)	Carl Roth
Fetal bovine serum (FBS)	Gibco, Life Technologies
Glycerol	Sigma-Aldrich
Glycine	Sigma-Aldrich
Hydrochloric acid	Carl Roth
Hygromycin B	Thermo Scientific
Isopropanol	AppliChem
Kanamycin sulfate	AppliChem
Magnesium Chloride Hexahydrate	Carl Roth
Methanol	AppliChem
N,N,N',N'-tetramethylethylendiamine (TEMED)	Carl Roth
Nonfat dried milk powder	AppliChem
Opti-Minimal Essential Medium (MEM)®	Gibco, Life Technologies
Paraformaldehyde	Carl Roth
Penicillin-Streptomycin	Gibco, Life Technologies
Potassium chloride (KCl)	Carl Roth
Potassium hydroxide (KOH)	AppliChem
Triton X-100	Carl Roth
Sodium carbonate (Na_2CO_3)	AppliChem
Sodium chloride (NaCl)	Carl Roth
Sodium dihydrogen phosphate (NaH_2PO_4)	AppliChem
Sodium dodecyl sulfate (SDS)	Carl Roth

Sodium hydroxide (NaOH)	AppliChem
Sodium pyruvate	Gibco, Life Technologies
D-Sucrose	Carl Roth
Trichloroacetic acid (TCA)	AppliChem
Tris Base	Carl Roth
Fetal Bovine Serum	Thermo Scientific
Doxycycline	Sigma-Aldrich
Glycerin	Carl Roth
2-Mercaptoethanol	Carl Roth
Deoxynucleotide triphosphate Mix (dNTPs)	Fermentas
Ponceau S powder	Carl Roth
Gibson Assembly master mix	New England Biolabs
Ganciclovir powder	Sigma-Aldrich
Gelatin Powder	Carl Roth
Mannitol	Sigma-Aldrich
Sodium azide	Sigma-Aldrich
Sodium ascorbate	Sigma-Aldrich
Trolox	Sigma-Aldrich
20% N-Lauryl sarcosine sodium solution	Sigma Aldrich
List of reagents used for Mass Spectrometry	
Urea	Thermo
Thiourea	Thermo
Lysyl endopeptidase	Wako chemicals
Iodoacetamide	Promega
75 µm ID PicoTip fused silica emitter	New Objective
ReproSil-Pur C18-AQ 1.9 µm resin	Dr Maisch GmbH Ltd
Trypsin	Promega
Trifluoroacetic acid (TFA)	Thermo
PreOmics® Phoenix kit	PreOmics
Formic acid (FA)	Thermo

Acetonitrile (ACN)	Sigma

Table 8. List of antibodies

Antibodies	Host	Source	Identifier/catalog no.
Anti-TOM20	Mouse	Santa Cruz Biotechnology	sc-17764
Anti-TOM40	Mouse	Santa Cruz Biotechnology	sc-365467
Anti-TOM70	Mouse	Santa Cruz Biotechnology	sc-390545
Anti-GAPDH	Mouse	Proteintech	60004-1-Ig
Anti-TOM22	Rabbit	Abcam	ab246862
Anti-APEX2	Rabbit	AG Jansen	-
Rabbit IgG Isotype Control	Rabbit	Invitrogen	02-6102
Anti-TOM40	Rabbit	Proteintech	18409-1-AP
Anti-V5	Mouse	Invitrogen	R96025
Anti-beta-actin	Mouse	Sigma Aldrich	A1978
Anti-flag	Rat	Agilent	200473
Neutravidin-Alexa647	-	Invitrogen	A2666
Anti-SYNJ2BP	Rabbit	Proteintech	15666-1-AP
Anti-TOM20	Rabbit	Proteintech	11802-1-AP
Streptavidin IRDye 800CW	-	LI-COR	926-32230

Table 9. List of secondary antibodies

Secondary Antibody	Host	Dilution	Supplier
Anti-Mouse (HRP)	Sheep	1:10000	Amersham ECL
Anti-Rabbit (HRP)	Donkey	1:10000	Amersham ECL
Anti-Rat (HRP)	Goat	1:10000	Amersham ECL
Donkey anti-Rabbit IgG (H+L) Highly Cross-Adsorbed Secondary Antibody, Alexa Fluor™ Plus 488	Donkey	1:1000	Invitrogen, Thermo
Goat anti-Mouse IgG (H+L) Highly Cross-Adsorbed Secondary Antibody, Alexa Fluor™ Plus 555	Goat	1:1000	Invitrogen, Thermo

Goat anti-Rat IgG (H+L) Cross-Adsorbed Secondary Antibody, Alexa Fluor™ 568	Rat	1:1000	Invitrogen, Thermo

4.2 Molecular biology methods

4.2.1 Polymerase chain reaction (PCR)

All PCR reactions were carried out using a KOD Hot start DNA Polymerase (Sigma). The gene fragments were amplified by PCR under the conditions mentioned in Table 10 and 11. The annealing temperatures were adjusted to the primers' Tm and extension time according to the fragment length.

Table 10. Reaction mixture of a standard PCR reaction

Component	Volume (µl)
Template	1
90 x KOD buffer	5
2mM dNTP	5
forward primer	2
reverse primer	2
25mM $MgSO_4$	3
DMSO	1
KOD polymerase	1
distilled water	30
Total volume	50

Table 11. Thermocycling conditions

Cycle step	Temperature	Time	Repeats
Initial Denaturation	95 °C	2 min	1x
Denaturation	95 °C	20 sec	40x
Annealing	[Lowest Primer Tm] °C	30 sec	
Extension	70 °C	20 sec/ kb	
Final Extension	72 °C	10 min	1x
hold	4 °C	∞	

After the PCR reaction, 1 µl of DpnI and 5 µl Tango buffer were added to digest the template. The PCR products were separated by agarose gel electrophoresis (1%) and further purified using the QIAquick PCR Purification Kit following manufacturer's instructions.

4.2.2 Restriction endonuclease digestion

The standard conditions for a restriction digestion reaction are mentioned in the Table 12. The digestion was carried out at 37°C for 1 hour. Successful digestion was further assayed by (1%) agarose gel electrophoresis. The linearized fragments were purified using the QIAquick Gel Extraction Kit following manufacturer's instructions

Table 12. Restriction digestion reaction

Components	Volume (µl)
Plasmid	3 (1µg/µl)
Enzyme 1	1
Enzyme 2	1
CutSmart buffer	5
distilled water	40
Total volume	50

4.2.3 Gibson assembly

80-120 ng of linearized plasmid DNA was mixed with up to 3 to 9 - fold molar excess of insert fragments together with the NEBuilder HiFi DNA Assembly Master Mix (NEB). The reaction mixture was prepared according to the following table and incubated at 50° for 1 hour.

Table 13. Gibson assembly reaction mixture

Components	Volume (µl)
Total Amount of Fragments	~0.2 pmol
NEBuilder HiFi DNA Assembly Master Mix	10
Deionized H_2O	~ 8
Total volume	20

4.2.4. Bacterial transformation

For transformation, 2 µl of the Gibson mixture was gently mixed with 50 µL NEB 5-alpha competent *E. coli* cells DH5α, and the reaction mixture was placed on the ice for 30 minutes. The mixture was heat shocked for 45 seconds at 42 °C followed by 5 minutes incubation on ice. 500 µl antibiotic-free LB was added to the bacteria. After agitation for 1h at 37°C, 50 µl to 100 µl LB mixture was streaked on LB agar plates with ampicillin. Colonies were grown at 37 °C. After overnight incubation, 4-6 colonies were selected for each construct and further inoculated in a small-scale culture. Plasmid was extracted and sequencing was performed by Eurofins.

4.2.5. Agarose gel electrophoresis

Agarose gels were prepared with 1-2 % (w/v) agarose dissolved in TAE buffer (40 mM Tris,1 mM EDTA pH 8.6) depending on the product size, with the addition of 2-3 of 10000 x Gelred dye. The samples were mixed with 6x loading dye before loading. The required bands were excised from the gel using 70% intensity of the UV illuminator at 365 nm and further purified using a QIAquick Gel Extraction Kit, following manufacturer's instructions.

4.2.6. Plasmid construction

All plasmids were generated following the Gibson method (Gibson et al., 2009). As a backbone for all constructs, plasmid RJP 2051, a pSF3 backbone vector containing the gene for GFP, was digested with restriction endonucleases BglII and PacI to excise the GFP gene. The linearized vector was used as a template to generate all plasmids by the Gibson method (mentioned in section 4.2.3; Table 14; Suppl. Figure 2). Each corresponding fragment of the insert contained overlapping ends, amplified by the suitable primers (Table 14,15) to facilitate the seamless joining of adjacent fragments.

Table 14. List of plasmids generated in this study and corresponding primers to amplify the targeted gene

Number	Plasmid name	Source	Primers used	
			Fwd primer	Reverse primer
RJP 2303	pSF3-TOMM20-APEX2-V5 (Suppl. Figure 3)	This study	CCTCCGCGGAATTTCTTAATGAT TGTACTGAGAGTTTGG (RPO 7758)	GGAATAGGAACTTCGCGGCAGT GAGTTAGCTCACTCATTAG (RPO 7759)
RJP 2307	pSF3-TOMM70-APEX2-V5 (Suppl. Figure 4)	This study	CCTCCGCGGAATTTCTTAATGCC ACCTGACGTCTAAGAAAC (RPO 7760)	ACCTCTATCCAGATCTTGCTTCCA CTGAAG (RPO 7761)
			AGCAAGATCTGGATAGAGGTTT GGAACTTATC (RPO 7762)	GGAATAGGAACTTCGCGGCAAGA ATTCGCTAGCTCTAG (RPO 7763)
RJP 2358	pSF3-FLAG-APEX2-NES (Suppl. Figure 5	This study	CCTCCGCGGAATTTCTTAATATG GACTACAAGGATGACGAC (RPO 7764)	GGAATAGGAACTTCGCGGCATTA GTCCAGGGTCAGGCG (RPO 7765)
RJP 2359	pSF3-mito-V5-APEX2 (Suppl. Figure 6)	This study	GCCTCCGCGGAATTCTTAATCAC TATAGGGAGACCCAAG (RPO 7766)	GAATAGGAACTTCGCGGCCACAT TAGGCATCAGCAAAC (RPO 7767)
RJP 2297	pSF3-ERM-APEX2-V5 (Suppl. Figure 7)	This study	GCCTCCGCGGAATTCTTAATTTC GAAGGAGATAGAACC (RPO 7768)	GAATAGGAACTTCGCGGCCATTA TCAGGTGCTGTCCAG (RPO 7769)

The fragments encoding TOMM20-APEX2-V5 and TOMM20-APEX2-V5 were synthesized via Genewiz, and ligated in the template plasmid (RJP 2051) following the Gibson method, to generate plasmids RJP 2303 (Suppl. Figure 3) and RJP 2307 (Suppl. Figure 4). Plasmids encoding APEX2-NES (RJP 2358; Suppl. Figure 5), Mito-APEX2 (RJP 2359; Suppl. Figure 6), and ERM-APEX2 (RJP 2297; Suppl. Figure 7) were also generated in a similar way by the Gibson method. Primers, template plasmids, and PCR conditions are listed in Table 14-16.

Table 15. PCR conditions to generate overlapping fragments of transgenes

PCR product (inserts)	Template	Primers	Tm (°C)	Extension time (sec)
TOMM20-APEX2-V5	RJP 2251	RPO 7758 + RPO 7759	53	30
TOMM70-APEX2-V5 (fragment 1)	RJP 2252	RPO 7760 + RPO 7761	50	45
TOMM70-APEX2-V5 (fragment 2)	RJP 2253	RPO 7762 + RPO 7763	55	30
APEX2-NES	RJP 2148	RPO 7764 + RPO 7765	50	30
Mito-APEX2	RJP 2308	RPO 7766 + RPO 7767	50	30
ERM-APEX2	RJP 2255	RPO 7768 + RPO 7769	50	30

Table 16. Generation of plasmids for doxycycline inducible cell lines expressing APEX2 fusion proteins using the Gibson method

Plasmid vector	inserts		Constructed plasmid	Hela Cell line
	Fragment #1	Fragment #2		
pSF3	TOMM20-APEX2-V5	-	PSF3-TOMM20-APEX2-V5 (RJP 2303)	TOM20-APEX2-V5
pSF3	TOMM70-APEX2-V5 (fragment 1)	TOMM70-APEX2-V5 (fragment 2)	PSF3-TOMM70-APEX2-V5 (RPJ 2307)	TOMM70-APEX2-V5
pSF3	APEX2-NES	-	PSF3-APEX2-NES (RJP 2358)	APEX2-NES
pSF3	Mito-APEX2	-	PSF3-Mito-APEX2 (RJP 2359)	Mito-APEX2
pSF3	ERM-APEX2	-	PSF3-ERM-APEX2 (RJP 2397)	ERM-APEX2

4.3 Cell biology methods

4.3.1 Cell culture

Each APEX2 fusion protein expressing cell line was generated by using a low passage HeLa 11ht parental cell line obtained from Dr. Kai Schönig (Central Institute of Mental Health in Mannheim Germany; Weidenfeld et al., 2009). Cells were always cultured in low glucose DMEM (Sigma) supplemented with 10% fetal bovine serum (FBS), 110 mg ml^{-1} sodium pyruvate, and 1x penicillin/streptomycin at 37°C with 5% CO2, and maintained by 200 µg ml^{-1} hygromycinB (Sigma) and 200 µg ml^{-1} G418 (Sigma).

4.3.2. Generation of stable cell lines

To enable tunable doxycycline (DOX) induced expression, the fusion protein expression cassettes, that were placed in the pSF3 plasmid backbone, were stably integrated in the genome of the HeLa 11ht cells via recombinase-mediated cassette exchange (RMCE). The host cell line was transfected with the target vector expressing corresponding fusion proteins together with a vector encoding the Flp-recombinase. Each doxycycline inducible cell line expressing APEX2 containing fusion protein was obtained by selection with 50 µM ganciclovir. The integration of the transgene was confirmed by checking corresponding protein expression via Western blot.

4.4. Biochemical methods

4.4.1 Cell fractionation

For each cell fractionation experiment, cells were induced with 500 ng ml^{-1} doxycycline for 24 hours or mock treated. Following induction, media was discarded from the around 85% confluent cell culture dishes, and cells were washed with PBS twice and then collected in 15 ml centrifuge tubes. Cells were pelleted at 500 × *g*, for 3 min at 4°C, the supernatant discarded, and the cell pellet resuspended in HMS-A buffer (0.22 M mannitol, 0.02 M HEPES-KOH, pH 7.6, 1 mM EDTA, 0.075 M sucrose, 0.1% BSA, 1X cOmplete™protease inhibitor cocktail; Becker et al., 2012). The suspension was incubated for 10 minutes on ice, transferred to a homogenizer (Sigma) and lysed with 30 cycles on ice. The lysates were centrifuged at 900 × *g*, 5 min at 4 °C. The supernatant was collected and centrifuged again for 9000 × *g*, 15 min at 4 °C, resulting in a crude mitochondrial fraction in the pellet and a cytosolic fraction in the supernatant. The mitochondrial pellet was further washed with HMS-B buffer (HMS-A buffer without BSA) and mitochondria was pelleted again at 10,000 × g, 10 min, 4 °C. Pellet was resuspended in HMS-B buffer and protein concentration was estimated using Bradford method (Bradford, 1976). To solubilize mitochondria, the pellet was resuspended again in HMS-B buffer with digitonin (4:1 (w/w) ratio of detergent to the protein) and incubated for 30 minutes at 4°C. Non-solubilized material was removed by centrifugation (13,000 × *g*, for 10 min, 4 °C). The solubilized mitochondrial fraction was collected and denatured for Western blot analysis. For each sample, around 100 µg protein was separated either on a 12% SDS-PAGE gel (for TOMM20-APEX2 detection) or a 10% SDS-PAGE gel (for TOMM70-APEX2 detection). For expression validation check in Western blots, blots were incubated with primary antibodies for 1 hour at room temperature or overnight at 4°C. Primary antibodies include mouse anti-TOM20 (1: 250 dilution), rabbit anti-TOM40 (1: 500 dilution), mouse anti-TOM70 (1:500 dilution), and mouse anti-GAPDH (1:1000 dilution).

4.4.2 SDS-PAGE and Western blotting

4.4.2.1 SDS-PAGE

The protein samples were separated by the sodium dodecyl sulfate polyacrylamide gel electrophoresis (SDS-PAGE; (Laemmli, 1970)), using the

Mini-Protean® Tetra System (BIO-RAD). Either 10% or 12% separating gels (Table17) were used together with 4% stacking gel. The samples were first boiled in Laemmli buffer (31.5 mM Tris-HCl, pH 6.8, 1% SDS, 10% glycerol, 0.005% bromophenol blue) at 95ºC for 10 min, then shortly centrifuged before loading. The SDS-gels were first run at 60V for 20-30 minutes, then at 100 V for around 90 min until the bromophenol blue front reached the bottom of the gel.

Table 17. SDS-PAGE gel composition

Components	Separating Gel		Stacking gel (4%)
	10%	12%	
2 M Tris-HCl, pH 8.8	1.8 ml	1.8 ml	-
0.5 M Tris-HCl, pH 6.8	-	-	0.3 ml
30% Acrylamide solution	3 ml	3.6 ml	0.5 ml
20% (v/v) SDS	45 µl	45 µl	15 µl
10% (V/V) APS	80 µl	80 µl	50 µl
TEMED	8 µl	8 µl	5 ul
H_2O	4.2 ml	3.5 ml	2.15 ml

4.4.2.2 Western Blotting

The wet immunoblotting method was used for protein transfer onto nitrocellulose or methanol-activated PVDF membranes using a transfer cell (BIO-RAD). Both SDS-gel and slices of the Whatman-paper were put in the blotting buffer (0.25 M Tris, 1.92 M glycine, pH 8.6 ± 0.2) for 5 min. A transfer assembly sandwich was prepared consisting of 3 thin sheets of the Whatman-paper, a nitrocellulose or PVDF membrane, the gel, 3 thin Whatman paper slices, and proteins were subsequently transferred at 0.32 A for 90 minutes. After transfer, the sandwich was disassembled, and the membrane was either immersed in Ponceau S staining solution (method section 4.4.2.3) or directly incubated in the blocking solution (5% w/v milk in TBS-T; 0.01 M Tis HCl, pH 7.4, 0.15 M NaCl, 0.1% (v/v) Tween 20) for 45 minutes. Subsequently, the membrane was first immersed in the corresponding primary antibody solution diluted in TBS-T (Table 8), followed by overnight incubation at 4°C. Next day, the membrane was washed three times for 10 min in TBS-T under constant agitation and followed by incubation with the appropriate secondary antibody (Table 9) in TBS-T for 1 hour at room temperature. Afterwards, the membrane was washed twice for 10 min with TBS-

T and finally rinsed for 10 min in TBS. The protein bands were visualized with chemiluminescent substrate solution (Thermo) by imaging with the ChemiDoc (Bio-Rad) chemiluminescence imaging system.

4.4.2.3 Ponceau S staining

The membrane was immersed in the Ponceau staining solution (0.1% (w/v) Ponceau S; 5% (v/v) acetic acid) for 2 to 3 minutes under constant agitation. Then the stain was removed by rinsing with water until the bands were clearly visible without background.

4.4.3 Co-immunoprecipitation

Mitochondria were isolated and solubilized in digitonin as described above in section 4.4.1. Around 250 µg of solubilized mitochondria (~150 µl volume) were used for each co-purification and incubated with 10 µg of anti-TOM22 (Abcam) or 20 µg of anti-TOM40 (Proteintech) antibodies for 2 h at 4°C. Normal rabbit IgG was used as an isotype control. After incubation, prewashed protein A agarose beads were added and incubated for another hour at room temperature. Beads were washed three times with HMS-B buffer and proteins eluted with 2x Laemmli buffer at 95°C for 10 min. For V5 co-immunoprecipitation, V5 beads (ChromoTek) were pre-washed with HMS-B buffer three times. Solubilized mitochondria were crosslinked first with 1 mM DSP for 1 h at 4°C followed by quenching with 1 M Tris-HCl, pH 7.5. The crosslinked solubilized mitochondria were purified on a filter column (Amicon® ultra centrifugal filter, 3 kDa MWCO; sigma), and incubated with 50 µl of V5 beads in HMS-B for 1h at room temperature. Beads were washed three times with HMS-B buffer, eluted in 2x Laemmli buffer with 0.1 M DTT at 95°C for 10 min, and further analyzed by Western blot. After boiling the beads in Laemmli buffer, the eluate was collected, separated on a 12% SDS-PAGE gel before detection of proteins by Western blotting. The primary antibodies used were rabbit anti-APEX2 (1:3000 dilution), rabbit anti-TOM22 (1:500 dilution), rabbit anti-TOM40 (1:500 dilution), and mouse anti-V5 (1:1000 dilution).

4.4.4 Proximity labeling

For biotin labeling via APEX2, expression of the corresponding fusion proteins was induced with doxycycline (DOX) or cells were mock treated as described above. After 24 h, cells at around 85% confluency were incubated with fresh DMEM containing 0.5 mM biotin-phenol (BP; Iris Biotech GMBH) for 30 min at 37°C. Biotinylation was initiated by adding H_2O_2 for one minute at room

temperature to the final concentration of 1 mM under constant agitation for each cell line (Hung et al., 2017). Control samples omitted either BP or H_2O_2 or uninduced cells were included for each APEX2-fusion protein expressing cell lines. Labeling reactions were quenched by removing media and immediate washing of the cells with an equal volume of quenching DPBS solution that was prepared freshly after mixing DPBS with 10 mM sodium azide, 10 mM sodium ascorbate, and 5mM Trolox. Cells were washed twice two times with quenching DBPS solution, and once with PBS before trypsinization, then pelleted at 500 × *g*. The pellet was washed with PBS and cells were immediately lysed in RIPA buffer (50 mM Tris, pH 7.5, 150 mM NaCl, 0.1% SDS, 1% Triton X-100, 0.5% sodium deoxycholate and 1x cOmplete™protease inhibitor cocktail) supplemented with 10 mM sodium azide, 10 mM sodium ascorbate, and 5 mM Trolox. The lysates were incubated on ice for 15 minutes, sonicated briefly, then centrifuged at 15,000 × *g* for 10 min at 4°C. Protein concentration of the clarified lysates was determined with a Pierce™ 660-nm protein assay (Thermo, catalog no. 22660). 20 µg of whole cell lysate was combined with Laemmli buffer and boiled for 10 min. Lysates were separated on a 9% SDS-PAGE gel and transferred to nitrocellulose membrane. Membranes were stained by Ponceau S (0.1% w/v Ponceau S in 5% acetic acid (v/v), afterwards incubated in 3% BSA in TBST (0.1% Tween-20 in Tris-buffered saline) overnight. On the next day, the blot was incubated with 0.3 µg ml^{-1} streptavidin-HRP (Thermo) in TBS-T for 1 hour at room temperature and further developed using the Pierce™ ECL Western Blotting-Substrate (Thermo).

4.4.5 Immunofluorescence microscopy and image acquisition

Around 25,000 cells were seeded on the coverslips coated with 0.2% gelatin and placed in 12-well plates. Cells were incubated either with or without 500 ng ml^{-1} doxycycline for 24 hours. The samples were then thoroughly washed three times with PBS to remove media, fixed and permeabilized with ice-cold methanol for 10 minutes at −20°C. The samples were washed twice with PBS containing 5 mM $MgCl_2$ (PBSM) and once with 50 mM glycine in PBSM. Cells were further incubated in 3% bovine serum albumin (BSA) diluted in PBSM (blocking solution) for 1 h. This was followed by incubation with the corresponding primary antibodies (mouse anti-V5 antibody, 1:1000 dilution; rabbit anti-TOM22 antibody, 1:200 dilution; mouse anti-TOM20 antibody,1:200 dilution; rat anti-flag antibody,1:500

dilution; rabbit anti-TOM20 antibody, 1:200 dilution; table 8) in the blocking solution for 1 h at room temperature or overnight at 4 °C. After washing three times with PBS, cells were incubated with Alexa Fluor coupled secondary antibodies (Invitrogen) at 1:1000 dilution in the same blocking buffer for 1 h. The cells were washed two times with PBS first and then incubated for 5 minutes with DAPI (0.1 µg ml^{-1}) diluted in PBS. Cells were thoroughly washed again with PBS and mounted with ProLong™ Glass Antifade Mountant (Thermo). After overnight incubation at room temperature, the slides were stored at 4 °C until imaging. To analyze biotinylated proteins, biotinylation was performed directly on the cells seeded on the cover slips as described before, treatment with the corresponding antibodies and mounted as explained before. All images were captured using a Zeiss LSM980 laser scanning confocal microscope (Carl Zeiss, Germany) equipped with an Airyscan 2 detector with a 60x oil objective and further processed with ImageJ/Fiji.

4.4.6 Mass spectrometry (MS) sample preparation

Around 1.5 million cells for each replicate were induced with doxycycline (DOX) for 24 hours. Controls for mock treated and puromycin treated cells were seeded at the same time, having similar number and confluency. Next day, cells having 85% confluency were biotinylated and further lysed in the RIPA buffer as described above. For puromycin treatment, cells were treated with 200 µM puromycin and 0.5 mM BP for 30 min at 37°C (Fazal et al., 2019; Qin et al., 2021). APEX2 labeling was induced by H_2O_2 treatment for one minute as described above.

4.4.6.1 Streptavidin pulldown to enrich biotinylated proteins

For capturing biotinylated proteins, we followed a published protocol (Hung et al., 2017). 50 µl streptavidin-coated magnetic beads (Pierce) were used for each replicate and washed three times with RIPA buffer with end-to-end rotation. Pre-washed beads were incubated with 120 µg of lysate for each replicate for 2 hours at room temperature under constant end-to-end rotation. After capturing, beads were washed twice with 1 ml of RIPA lysis buffer for 2 min, once with 1 M KCl for 2 min, once with 0.1 M Na_2CO_3 for around 10 seconds, once with 2 M urea in 10 mM Tris-HCl (pH 8.0) for around 10 seconds, and again twice with 1 ml RIPA lysis buffer for 2 minutes at room temperature. The beads were subsequently transferred to fresh tubes and washed briefly first with RIPA buffer, once with 1ml

wash buffer (75 mM NaCl in 50mM Tris-HCL pH 7.5), and then processed for LC-MS/MS analysis as follows.

4.4.6.2 Downstream sample preparation for MS (performed by Katharina Zittlau)

Subsequent sample preparation for LC-MS/MS analysis including data processing and analysis was done at the Proteome Center Tuebingen (PCT), University of Tuebingen. Samples were processed by Silke Wahl and Katharina Zittlau. Data analysis was performed by Katharina Zittlau under the supervision of Boris Macek. On bead captured interaction partners of TOMM20, TOMM70, or otherwise tagged by NES-, and Mito-APEX2, and ERM markers including mock treated ones were resuspended in 30 µl of denaturation buffer (6 M urea, 2 M thiourea, 10 mM Tris, pH 8). Disulfide bonds were reduced with 10 mM of DTT for 1h and further alkylated with 55 mM of iodoacetamide for 1h in the dark. Proteins were predigested with 2 µl of LysC (Lysyl endopeptidase; Wako Chemicals) for 3h. For overnight digestion with 2 µl of trypsin (Promega Corporation) samples were diluted fourfold with 50 mM ammonium bicarbonate. On the next day, beads were pelleted, the supernatant was transferred to a new tube and the digestion was stopped by adding 1% of trifluoroacetic acid (TFA) the next day. Contaminants were removed by the PreOmics®' Phoenix kit prior their submission to the MS.

4.4.6.3 LC-MS measurement and data analysis (performed by Katharina Zittlau)

All proximity labeled samples were analyzed on a Q Exactive HF mass spectrometer (Thermo Fisher Scientific) online-coupled to an Easy-nLC 1200 UHPLC (Thermo Fisher Scientific) at the Proteome Center Tuebingen (PCT), University of Tuebingen. Prior to MS-based analysis peptides were separated on an in-house packed (ReproSil-Pur C18-AQ 1.9 µm resin [Dr Maisch GmbH Ltd]) 20 cm analytical column (75 µm ID PicoTip fused silica emitter [New Objective]). For gradient elution of the peptides solvent A (0.1% formic acid (FA)) and solvent B (0.1% FA in 80% acetonitrile (ACN)) were used across a 60 min gradient with a flow rate of 200 nl/min at 40 °C. The mass spectrometer was operated in positive ion and in data-dependent acquisition mode. MS1 spectra were acquired over a scan range from 300 to 1650 m/z at resolution 60k. The top 7 most abundant peptides were selected for isolation within an isolation window of 1.4

m/z, higher-energy collisional dissociation (HCD) fragmentation with normalized collision energy (NCE) set to 27 and a maximum injection time of 110 ms/ AGC target 1e5. MS2 spectra were acquired at resolution 60k. Peptides were excluded from re-analyzing for 30 s.

Generated raw files were further processed with the MaxQuant software suite, version 2.2.0.0 (Cox et al., 2014). All parameters were kept as default with trypsin specific digestion mode selected and two missed cleavages allowed. As quantification method, label-free quantification was selected with minimal ratio count of 1. Cysteine carbamidomethylation was selected as fixed as well as methionine oxidation and protein N-terminal acetylation as variable modifications. Match between runs was allowed across all raw files. All spectra were searched against the UniProt Homo sapiens database (downloaded on December 16, 2022, 103 830 entries) and commonly observed contaminants.

For downstream data analysis only protein groups were considered that had not been identified as contaminant. Data were analyzed using Perseus software (Tyanova et al., 2016), version 1.6.7.0 with annotation for cellular compartment and biological function based on gene ontology and MitoCarta3.0 (Rath et al., 2021) Within biological replicates only proteins quantified in two out of three replicates or if more replicates were performed 75% were used further. To decrease the number of missing values these were replaced from normal distribution with standard settings. To identify significantly higher or lower abundant proteins, a Student’s two-sample t-test was performed. Candidates were classified as significant (p-value: 5%, Difference: 3) and stringent significant (p-value: 1%, Difference: 4). Additional data visualization was performed within the R environment. The mass spectrometry proteomics data have been deposited to the ProteomeXchange Consortium via the PRIDE partner repository (Perez-Riverol et al., 2022) with the dataset identifier PXD057097 and 10.6019/PXD057097.

4.4.7 RNA Extraction

All RNA experiments were performed following standard protocols and utmost priority was given to minimizing RNase contamination. Lab bench surfaces were wiped thoroughly with a solution that eliminates RNase on the surfaces, and RNAse free consumables including filtered pipette tips were utilized. The cells were cultured, harvested and centrifuged as described before in section 4.4.4.

RNA was extracted using RNeasy plus mini kit (QIAGEN) utilizing all kit reagents supplied with the kit and the recommended protocol. The cells were lysed first in the lysis buffer supplemented with β-mercaptoethanol. The lysate was poured in a genomic DNA eliminator column that was supplied with the kit and centrifuged. After the subsequent washing steps following RNA extraction, the RNA was finally eluted with RNase-free water, and RNA concentration was checked with a Nanodrop instrument. Extracted RNA sample showed an A260/A280 ratio of ~2.0, corresponding to highly purified RNA, was saved for down-stream applications. Extracted RNA was further digested with Turbo DNase (Thermo) to remove the remaining genomic DNA contaminants at 37 °C for 30 minutes, and RNA was again purified via the RNA Clean and Concentrator −5 kit (Zymo Research). The purified RNA was saved at -80 °C for downstream experiments.

4.4.8 RNA dot blot assay

The extracted RNA was heated first at 95°C for 3 min to disrupt secondary structures and chilled immediately. Around ~2.5 µg RNA was blotted on a nitrocellulose membrane for each sample and the membrane was air dried for 10 minutes. RNA was crosslinked twice in a Cx-2000 UV Crosslinker (Stratalinker) using the auto crosslink mode (1,200 microjoules). Subsequently the membrane was immersed in TBS blocking buffer with 0.1 %Tween for one hour, followed by incubating in 15 mL PBST solution supplemented with 1µl Streptavidin IRDye 800CW for another hour. The membrane was further washed with TBST three times for 10 minutes and visualized on Odyssey Infrared Imaging System (HNO clinic, Tuebingen). ssDNA oligotides with a 3′-biotin modification were used as a positive control.

4.4.9 Enrichment of biotinylated RNA

To enrich the biotinylated RNA, a previously published protocol was followed (Fazal et al., 2019). For each sample, around 100 µg RNA was utilized and further enriched by using dynabeads MyOne streptavidin C1 magnetic beads (Thermo Fischer). The 40 µl beads slurry was taken per sample and first washed three times using 500 µl bead washing buffer (1 M NaCl, 0.5 mM EDTA, 5 mM Tris-HCl, pH = 7.5, 0.1% TWEEN 20). The beads were subsequently washed two times using 500 µl of Solution A (0.05 M NaCl, 0.1 M NaOH), and finally once with Solution B (0.1 M NaCl). Afterwards, the prewashed beads were re-suspended in ~150 µl 0.05 M NaCl and mixed with ~150 µl of 100µg RNA

(diluted in RNAse free water). 1µl Ribolock RNase Inhibitor was added in ~300µl RNA beads mixed and the whole mixture was incubated on a rotator for 2 hours at 4°C. After incubation, the beads were washed three times in washing buffer and resuspended again in 54 µl water. Afterwards the beads were mixed with 3 µl of Ribolock RNase inhibitor, 10 µl Proteinase K (20 mg/ml), and 33 µl of 3X proteinase digestion buffer (330 µl of 10x PBS pH 7.4, 66 µl 0.5M EDTA, 330 µl of solution B (20% N-Lauryl sarcosine sodium solution, 16.5 µl 1M DTT, and 357.5 µl water; total volume 1.1 mL). This mixture was first incubated under constant agitation at 42°C for one hour, then the temperature increased to 55°C and the beads were incubated for another hour. Afterwards, the supernatant was collected, and the enriched RNA was further purified utilizing the RNA clean and concentrator−5 kit (Zymo Research). The enriched (pulled-down) samples were sent to Novogene for RNA sequencing where all the further steps from library preparation to data analysis were performed.

References

Abdul, K. Md., Terada, K., Yano, M., Ryan, M. T., Streimann, I., Hoogenraad, N. J., & Mori, M. (2000). Functional Analysis of Human Metaxin in Mitochondrial Protein Import in Cultured Cells and Its Relationship with the Tom Complex. *Biochemical and Biophysical Research Communications*, *276*(3), 1028–1034. https://doi.org/10.1006/bbrc.2000.3589

Abe, Y., Shodai, T., Muto, T., Mihara, K., Torii, H., Nishikawa, S., Endo, T., & Kohda, D. (2000). Structural Basis of Presequence Recognition by the Mitochondrial Protein Import Receptor Tom20. *Cell*, *100*(5), 551–560. https://doi.org/10.1016/S0092-8674(00)80691-1

Ahting, U., Waizenegger, T., Neupert, W., & Rapaport, D. (2005). Signal-anchored Proteins Follow a Unique Insertion Pathway into the Outer Membrane of Mitochondria. *Journal of Biological Chemistry*, *280*(1), 48–53. https://doi.org/10.1074/jbc.M410905200

Albrecht, R., Rehling, P., Chacinska, A., Brix, J., Cadamuro, S. A., Volkmer, R., Guiard, B., Pfanner, N., & Zeth, K. (2006). The Tim21 binding domain connects the preprotein translocases of both mitochondrial membranes. *EMBO Reports*, *7*(12), 1233–1238. https://doi.org/10.1038/sj.embor.7400828

Altman, T., Ionescu, A., Ibraheem, A., Priesmann, D., Gradus-Pery, T., Farberov, L., Alexandra, G., Shelestovich, N., Dafinca, R., Shomron, N., Rage, F., Talbot, K., Ward, M. E., Dori, A., Krüger, M., & Perlson, E. (2021). Axonal TDP-43 condensates drive neuromuscular junction disruption through inhibition of local synthesis of nuclear encoded mitochondrial proteins. *Nature Communications*, *12*(1), 6914–6914. https://doi.org/10.1038/s41467-021-27221-8

Antonicka, H., Lin, Z.-Y., Janer, A., Aaltonen, M. J., Weraarpachai, W., Gingras, A.-C., & Shoubridge, E. A. (2020). A High-Density Human Mitochondrial Proximity Interaction Network. *Cell Metabolism*, *32*(3), 479-497.e9. https://doi.org/10.1016/j.cmet.2020.07.017

Araiso, Y., Tsutsumi, A., Qiu, J., Imai, K., Shiota, T., Song, J., Lindau, C., Wenz, L.-S., Sakaue, H., Yunoki, K., Kawano, S., Suzuki, J., Wischnewski, M., Schütze, C., Ariyama, H., Ando, T., Becker, T., Lithgow, T., Wiedemann, N., … Endo, T. (2019). Structure of the mitochondrial import gate reveals distinct preprotein paths. *Nature*, *575*(7782), 395–401. https://doi.org/10.1038/s41586-019-1680-7

Arceo, X. G., Koslover, E. F., Zid, B. M., & Brown, A. I. (2022). Mitochondrial mRNA localization is governed by translation kinetics and spatial transport. *PLOS Computational Biology*, *18*(8), e1010413.

Ashburner, M., Ball, C. A., Blake, J. A., Botstein, D., Butler, H., Cherry, J. M., Davis, A. P., Dolinski, K., Dwight, S. S., Eppig, J. T., Harris, M. A., Hill, D. P., Issel-Tarver, L., Kasarskis, A., Lewis, S., Matese, J. C., Richardson,

J. E., Ringwald, M., Rubin, G. M., & Sherlock, G. (2000). Gene Ontology: Tool for the unification of biology. *Nature Genetics*, *25*(1), 25–29. https://doi.org/10.1038/75556

Aslam, M., Ullah, A., Paramasivam, N., Kandasamy, N., Naureen, S., Badshah, M., Khan, K., Wajid, M., Abbasi, R., Eils, R., Brockmann, M. A., Schlesner, M., Ahmad, N., & Von Engelhardt, J. (2019). Segregation and potential functional impact of a rare stop-gain PABPC4L variant in familial atypical Parkinsonism. *Scientific Reports*, *9*(1), 13576. https://doi.org/10.1038/s41598-019-50102-6

Backes, S., Bykov, Y. S., Flohr, T., Räschle, M., Zhou, J., Lenhard, S., Krämer, L., Mühlhaus, T., Bibi, C., Jann, C., Smith, J. D., Steinmetz, L. M., Rapaport, D., Storchová, Z., Schuldiner, M., Boos, F., & Herrmann, J. M. (2021). The chaperone-binding activity of the mitochondrial surface receptor Tom70 protects the cytosol against mitoprotein-induced stress. *Cell Reports*, *35*(1). https://doi.org/10.1016/j.celrep.2021.108936

Backes, S., Hess, S., Boos, F., Woellhaf, M. W., Gödel, S., Jung, M., Mühlhaus, T., & Herrmann, J. M. (2018). Tom70 enhances mitochondrial preprotein import efficiency by binding to internal targeting sequences. *Journal of Cell Biology*, *217*(4), 1369–1382. https://doi.org/10.1083/jcb.201708044

Balsa, E., Marco, R., Perales-Clemente, E., Szklarczyk, R., Calvo, E., Landázuri, M. O., & Enríquez, J. A. (2012). NDUFA4 Is a Subunit of Complex IV of the Mammalian Electron Transport Chain. *Cell Metabolism*, *16*(3), 378–386. https://doi.org/10.1016/j.cmet.2012.07.015

Barazzuol, L., Giamogante, F., & Calì, T. (2021). Mitochondria Associated Membranes (MAMs): Architecture and physiopathological role. *Cell Calcium*, *94*, 102343. https://doi.org/10.1016/j.ceca.2020.102343

Bausewein, T., Mills, D. J., Langer, J. D., Nitschke, B., Nussberger, S., & Kühlbrandt, W. (2017). Cryo-EM Structure of the TOM Core Complex from Neurospora crassa. *Cell*, *170*(4), 693-700.e7. https://doi.org/10.1016/j.cell.2017.07.012

Becker, D., Richter, J., Tocilescu, M. A., Przedborski, S., & Voos, W. (2012). Pink1 Kinase and Its Membrane Potential (Δψ)-dependent Cleavage Product Both Localize to Outer Mitochondrial Membrane by Unique Targeting Mode. *Journal of Biological Chemistry*, *287*(27), 22969–22987. https://doi.org/10.1074/jbc.M112.365700

Becker, T., Böttinger, L., & Pfanner, N. (2012a). Mitochondrial protein import: From transport pathways to an integrated network. *Trends in Biochemical Sciences*, *37*(3), 85–91. https://doi.org/10.1016/j.tibs.2011.11.004

Becker, T., Böttinger, L., & Pfanner, N. (2012b). Mitochondrial protein import: From transport pathways to an integrated network. *Trends in Biochemical Sciences*, *37*(3), 85–91. https://doi.org/10.1016/j.tibs.2011.11.004

Becker, T., Pfannschmidt, S., Guiard, B., Stojanovski, D., Milenkovic, D., Kutik,

S., Pfanner, N., Meisinger, C., & Wiedemann, N. (2008). Biogenesis of the Mitochondrial TOM Complex: Mim1 PROMOTES INSERTION AND ASSEMBLY OF SIGNAL-ANCHORED RECEPTORS*. *Journal of Biological Chemistry*, *283*(1), 120–127. https://doi.org/10.1074/jbc.M706997200

Becker, T., Wenz, L.-S., Krüger, V., Lehmann, W., Müller, J. M., Goroncy, L., Zufall, N., Lithgow, T., Guiard, B., Chacinska, A., Wagner, R., Meisinger, C., & Pfanner, N. (2011). The mitochondrial import protein Mim1 promotes biogenesis of multispanning outer membrane proteins. *Journal of Cell Biology*, *194*(3), 387–395. https://doi.org/10.1083/jcb.201102044

Bezpalaya, E. Y., Matyuta, I. O., Vorobyeva, N. N., Kurilova, S. A., Oreshkov, S. D., Minyaev, M. E., Boyko, K. M., & Rodina, E. V. (2024). The crystal structure of yeast mitochondrial type pyrophosphatase provides a model to study pathological mutations in its human ortholog. *Biochemical and Biophysical Research Communications*, *738*, 150563. https://doi.org/10.1016/j.bbrc.2024.150563

Bolender, N., Sickmann, A., Wagner, R., Meisinger, C., & Pfanner, N. (2008). Multiple pathways for sorting mitochondrial precursor proteins. *EMBO Reports*, *9*(1), 42–49. https://doi.org/10.1038/sj.embor.7401126

Bolliger, L., Junne, T., Schatz, G., & Lithgow, T. (1995). Acidic receptor domains on both sides of the outer membrane mediate translocation of precursor proteins into yeast mitochondria. *The EMBO Journal*, *14*(24), 6318–6326. https://doi.org/10.1002/j.1460-2075.1995.tb00322.x

Bradford, M. M. (1976). A rapid and sensitive method for the quantitation of microgram quantities of protein utilizing the principle of protein-dye binding. *Analytical Biochemistry*, *72*(1–2), 248–254. https://doi.org/10.1016/0003-2697(76)90527-3

Branon, T. C., Bosch, J. A., Sanchez, A. D., Udeshi, N. D., Svinkina, T., Carr, S. A., Feldman, J. L., Perrimon, N., & Ting, A. Y. (2018). Efficient proximity labeling in living cells and organisms with TurboID. *Nature Biotechnology*, *36*(9), 880–887. https://doi.org/10.1038/nbt.4201

Brix, J., Dietmeier, K., & Pfanner, N. (1997). Differential Recognition of Preproteins by the Purified Cytosolic Domains of the Mitochondrial Import Receptors Tom20, Tom22, and Tom70 *. *Journal of Biological Chemistry*, *272*(33), 20730–20735. https://doi.org/10.1074/jbc.272.33.20730

Cao, Z., Xia, Z., Zhou, Y., Yang, X., Hao, H., Peng, N., Liu, S., & Zhu, Y. (2016). Methylcrotonoyl-CoA carboxylase 1 potentiates RLR-induced NF-κB signaling by targeting MAVS complex. *Scientific Reports*, *6*(1), 33557. https://doi.org/10.1038/srep33557

Chacinska, A., Koehler, C. M., Milenkovic, D., Lithgow, T., & Pfanner, N. (2009). Importing Mitochondrial Proteins: Machineries and Mechanisms. *Cell*, *138*(4), 628–644. https://doi.org/10.1016/j.cell.2009.08.005

Chacinska, A., Lind, M., Frazier, A. E., Dudek, J., Meisinger, C., Geissler, A.,

Sickmann, A., Meyer, H. E., Truscott, K. N., Guiard, B., Pfanner, N., & Rehling, P. (2005). Mitochondrial Presequence Translocase: Switching between TOM Tethering and Motor Recruitment Involves Tim21 and Tim17. *Cell*, *120*(6), 817–829. https://doi.org/10.1016/j.cell.2005.01.011

Chan, N. C., Likić, V. A., Waller, R. F., Mulhern, T. D., & Lithgow, T. (2006). The C-terminal TPR Domain of Tom70 Defines a Family of Mitochondrial Protein Import Receptors Found only in Animals and Fungi. *Journal of Molecular Biology*, *358*(4), 1010–1022. https://doi.org/10.1016/j.jmb.2006.02.062

Chatzi, A., Manganas, P., & Tokatlidis, K. (2016). Oxidative folding in the mitochondrial intermembrane space: A regulated process important for cell physiology and disease. *Biochimica et Biophysica Acta (BBA) - Molecular Cell Research*, *1863*(6, Part A), 1298–1306. https://doi.org/10.1016/j.bbamcr.2016.03.023

Chen, S., & Collart, M. A. (2024). Membrane-associated mRNAs: A Post-transcriptional Pathway for Fine-turning Gene Expression. *Journal of Molecular Biology*, *436*(11), 168579. https://doi.org/10.1016/j.jmb.2024.168579

Cho, K. F., Branon, T. C., Rajeev, S., Svinkina, T., Udeshi, N. D., Thoudam, T., Kwak, C., Rhee, H.-W., Lee, I.-K., Carr, S. A., & Ting, A. Y. (2020). Split-TurboID enables contact-dependent proximity labeling in cells. *Proceedings of the National Academy of Sciences*, *117*(22), 12143–12154. https://doi.org/10.1073/pnas.1919528117

Cho, K. F., Branon, T. C., Udeshi, N. D., Myers, S. A., Carr, S. A., & Ting, A. Y. (2020). Proximity labeling in mammalian cells with TurboID and split-TurboID. *Nature Protocols*, *15*(12), 3971–3999. https://doi.org/10.1038/s41596-020-0399-0

Cohen, B., Golani-Armon, A., & Arava, Y. S. (2024). Emerging implications for ribosomes in proximity to mitochondria. *Seminars in Cell & Developmental Biology*, *154*, 123–130. https://doi.org/10.1016/j.semcdb.2023.01.003

Cox, J., Hein, M. Y., Luber, C. A., Paron, I., Nagaraj, N., & Mann, M. (2014). Accurate Proteome-wide Label-free Quantification by Delayed Normalization and Maximal Peptide Ratio Extraction, Termed MaxLFQ *. *Molecular & Cellular Proteomics*, *13*(9), 2513–2526. https://doi.org/10.1074/mcp.M113.031591

Davidson, W. S., Jonas, A., Clayton, D. F., & George, J. M. (1998). Stabilization of α-Synuclein Secondary Structure upon Binding to Synthetic Membranes. *Journal of Biological Chemistry*, *273*(16), 9443–9449. https://doi.org/10.1074/jbc.273.16.9443

De Maio, A., Yalamanchili, H. K., Adamski, C. J., Gennarino, V. A., Liu, Z., Qin, J., Jung, S. Y., Richman, R., Orr, H., & Zoghbi, H. Y. (2018). RBM17 Interacts with U2SURP and CHERP to Regulate Expression and Splicing of RNA-Processing Proteins. *Cell Reports*, *25*(3), 726-736.e7.

https://doi.org/10.1016/j.celrep.2018.09.041
De Miranda, B. R., Rocha, E. M., Castro, S. L., & Greenamyre, J. T. (2020). Protection from α-Synuclein induced dopaminergic neurodegeneration by overexpression of the mitochondrial import receptor TOM20. *Npj Parkinson's Disease*, *6*(1), 38–38. https://doi.org/10.1038/s41531-020-00139-6
Dekker, P. J. T., Martin, F., Maarse, A. C., Bömer, U., Müller, H., Guiard, B., Meijer, M., Rassow, J., & Pfanner, N. (1997). The Tim core complex defines the number of mitochondrial translocation contact sites and can hold arrested preproteins in the absence of matrix Hsp70–Tim44. *The EMBO Journal*, *16*(17), 5408–5419. https://doi.org/10.1093/emboj/16.17.5408
Dembowski, M., Künkele, K.-P., Nargang, F. E., Neupert, W., & Rapaport, D. (2001). Assembly of Tom6 and Tom7 into the TOM Core Complex ofNeurospora crassa. *Journal of Biological Chemistry*, *276*(21), 17679–17685. https://doi.org/10.1074/jbc.M009653200
Di Maio, R., Barrett, P. J., Hoffman, E. K., Barrett, C. W., Zharikov, A., Borah, A., Hu, X., McCoy, J., Chu, C. T., Burton, E. A., Hastings, T. G., & Greenamyre, J. T. (2016). α-Synuclein binds to TOM20 and inhibits mitochondrial protein import in Parkinson's disease. *Science Translational Medicine*, *8*(342), 342ra78-342ra78. https://doi.org/10.1126/scitranslmed.aaf3634
Diederichs, K. A., Ni, X., Rollauer, S. E., Botos, I., Tan, X., King, M. S., Kunji, E. R. S., Jiang, J., & Buchanan, S. K. (2020). Structural insight into mitochondrial β-barrel outer membrane protein biogenesis. *Nature Communications*, *11*(1), 3290–3290. https://doi.org/10.1038/s41467-020-17144-1
Diekmann, Y., & Pereira-Leal, J. B. (2012). Evolution of intracellular compartmentalization. *Biochemical Journal*, *449*(2), 319–331. https://doi.org/10.1042/BJ20120957
Dimmer, K. S., Papić, D., Schumann, B., Sperl, D., Krumpe, K., Walther, D. M., & Rapaport, D. (2012). A crucial role for Mim2 in the biogenesis of mitochondrial outer membrane proteins. *Journal of Cell Science*, *125*(14), 3464–3473. https://doi.org/10.1242/jcs.103804
Doan, K. N., Grevel, A., Mårtensson, C. U., Ellenrieder, L., Thornton, N., Wenz, L.-S., Opaliński, Ł., Guiard, B., Pfanner, N., & Becker, T. (2020). The Mitochondrial Import Complex MIM Functions as Main Translocase for α-Helical Outer Membrane Proteins. *Cell Reports*, *31*(4). https://doi.org/10.1016/j.celrep.2020.107567
Dudek, J., Rehling, P., & van der Laan, M. (2013). Mitochondrial protein import: Common principles and physiological networks. *Biochimica et Biophysica Acta (BBA) - Molecular Cell Research*, *1833*(2), 274–285. https://doi.org/10.1016/j.bbamcr.2012.05.028
Dyall, S. D., Brown, M. T., & Johnson, P. J. (2004). Ancient Invasions: From

Endosymbionts to Organelles. *Science*, *304*(5668), 253–257. https://doi.org/10.1126/science.1094884

Eliyahu, E., Pnueli, L., Melamed, D., Scherrer, T., Gerber, A. P., Pines, O., Rapaport, D., & Arava, Y. (2010). Tom20 Mediates Localization of mRNAs to Mitochondria in a Translation-Dependent Manner. *Molecular and Cellular Biology*, *30*(1), 284–294. https://doi.org/10.1128/MCB.00651-09

Endres, M., Neupert, W., & Brunner, M. (1999). Transport of the ADP/ATP carrier of mitochondria from the TOM complex to the TIM22·54 complex. *The EMBO Journal*, *18*(12), 3214–3221. https://doi.org/10.1093/emboj/18.12.3214

Engel, K. L., Arora, A., Goering, R., Lo, H.-Y. G., & Taliaferro, J. M. (2020). Mechanisms and consequences of subcellular RNA localization across diverse cell types. *Traffic*, *21*(6), 404–418. https://doi.org/10.1111/tra.12730

Fan, A. C. Y., Kozlov, G., Hoegl, A., Marcellus, R. C., Wong, M. J. H., Gehring, K., & Young, J. C. (2011). Interaction between the Human Mitochondrial Import Receptors Tom20 and Tom70 in Vitro Suggests a Chaperone Displacement Mechanism*. *Journal of Biological Chemistry*, *286*(37), 32208–32219. https://doi.org/10.1074/jbc.M111.280446

Fazal, F. M., Han, S., Parker, K. R., Kaewsapsak, P., Xu, J., Boettiger, A. N., Chang, H. Y., & Ting, A. Y. (2019). Atlas of Subcellular RNA Localization Revealed by APEX-Seq. *Cell*, *178*(2). https://doi.org/10.1016/j.cell.2019.05.027

Filadi, R., Pendin, D., & Pizzo, P. (2018). Mitofusin 2: From functions to disease. *Cell Death & Disease*, *9*(3), 330. https://doi.org/10.1038/s41419-017-0023-6

Gabrovsek, L., Collins, K. B., Aggarwal, S., Saunders, L. M., Lau, H.-T., Suh, D., Sancak, Y., Trapnell, C., Ong, S.-E., Smith, F. D., & Scott, J. D. (2020). A-kinase-anchoring protein 1 (dAKAP1)-based signaling complexes coordinate local protein synthesis at the mitochondrial surface. *Journal of Biological Chemistry*, *295*(31), 10749–10765. https://doi.org/10.1074/jbc.RA120.013454

Gadir, N., Haim-Vilmovsky, L., Kraut-Cohen, J., & Gerst, J. E. (2011). Localization of mRNAs coding for mitochondrial proteins in the yeast Saccharomyces cerevisiae. *RNA*, *17*(8). https://doi.org/10.1261/rna.2621111

Ganji, R., Paulo, J. A., Xi, Y., Kline, I., Zhu, J., Clemen, C. S., Weihl, C. C., Purdy, J. G., Gygi, S. P., & Raman, M. (2023). The p97-UBXD8 complex regulates ER-Mitochondria contact sites by altering membrane lipid saturation and composition. *Nature Communications*, *14*(1), 638. https://doi.org/10.1038/s41467-023-36298-2

Gao, J., Schatton, D., Martinelli, P., Hansen, H., Pla-Martin, D., Barth, E., Becker, C., Altmueller, J., Frommolt, P., Sardiello, M., & Rugarli, E. I.

(2014). CLUH regulates mitochondrial biogenesis by binding mRNAs of nuclear-encoded mitochondrial proteins. *Journal of Cell Biology*, *207*(2), 213–223. https://doi.org/10.1083/jcb.201403129

Gao, X., Zhu, K., Qin, B., Olieric, V., Wang, M., & Cui, S. (2021). Crystal structure of SARS-CoV-2 Orf9b in complex with human TOM70 suggests unusual virus-host interactions. *Nature Communications*, *12*(1), 2843. https://doi.org/10.1038/s41467-021-23118-8

Garcia, M., Delaveau, T., Goussard, S., & Jacq, C. (2010). Mitochondrial presequence and open reading frame mediate asymmetric localization of messenger RNA. *EMBO Reports*, *11*(4), 285–291. https://doi.org/10.1038/embor.2010.17

Gehrke, S., Wu, Z., Klinkenberg, M., Sun, Y., Auburger, G., Guo, S., & Lu, B. (2015). PINK1 and Parkin Control Localized Translation of Respiratory Chain Component mRNAs on Mitochondria Outer Membrane. *Cell Metabolism*, *21*(1), 95–108. https://doi.org/10.1016/j.cmet.2014.12.007

Gershoni-Emek, N., Altman, T., Ionescu, A., Costa, C. J., Gradus-Pery, T., Willis, D. E., & Perlson, E. (2018). Localization of RNAi Machinery to Axonal Branch Points and Growth Cones Is Facilitated by Mitochondria and Is Disrupted in ALS. *Frontiers in Molecular Neuroscience*, *11*.

Giacomello, M., Pyakurel, A., Glytsou, C., & Scorrano, L. (2020). The cell biology of mitochondrial membrane dynamics. *Nature Reviews Molecular Cell Biology*, *21*(4), 204–224. https://doi.org/10.1038/s41580-020-0210-7

Gibson, D. G., Young, L., Chuang, R.-Y., Venter, J. C., Hutchison, C. A., & Smith, H. O. (2009). Enzymatic assembly of DNA molecules up to several hundred kilobases. *Nature Methods*, *6*(5), 343–345. https://doi.org/10.1038/nmeth.1318

Golani-Armon, A., & Arava, Y. (2016). Localization of nuclear-encoded mRNAs to mitochondria outer surface. *Biochemistry (Moscow)*, *81*(10), 1038–1043. https://doi.org/10.1134/S0006297916100023

Gornicka, A., Bragoszewski, P., Chroscicki, P., Wenz, L.-S., Schulz, C., Rehling, P., & Chacinska, A. (2014). A discrete pathway for the transfer of intermembrane space proteins across the outer membrane of mitochondria. *Molecular Biology of the Cell*, *25*(25), 3999–4009. https://doi.org/10.1091/mbc.e14-06-1155

Grant, M. K. O., Shapiro, S. L., Ashe, K. H., Liu, P., & Zahs, K. R. (2019). A Cautionary Tale: Endogenous Biotinylated Proteins and Exogenously-Introduced Protein A Cause Antibody-Independent Artefacts in Western Blot Studies of Brain-Derived Proteins. *Biological Procedures Online*, *21*(1), 6. https://doi.org/10.1186/s12575-019-0095-z

Gray, M. W., Burger, G., & Lang, B. F. (1999). Mitochondrial Evolution. *Science*, *283*(5407), 1476–1481. https://doi.org/10.1126/science.283.5407.1476

Guan, Z., Yan, L., Wang, Q., Qi, L., Hong, S., Gong, Z., Yan, C., & Yin, P. (2021). Structural insights into assembly of human mitochondrial translocase TOM complex. *Cell Discovery*, *7*(1), 22–22.

https://doi.org/10.1038/s41421-021-00252-7
Gupta, A., & Becker, T. (2021). Mechanisms and pathways of mitochondrial outer membrane protein biogenesis. *Biochimica et Biophysica Acta (BBA) - Bioenergetics*, *1862*(1), 148323. https://doi.org/10.1016/j.bbabio.2020.148323
Haastrup, M. O., Vikramdeo, K. S., Singh, S., Singh, A. P., & Dasgupta, S. (2023). The Journey of Mitochondrial Protein Import and the Roadmap to Follow. *International Journal of Molecular Sciences*, *24*(3). https://doi.org/10.3390/ijms24032479
Hallacli, E., Kayatekin, C., Nazeen, S., Wang, X. H., Sheinkopf, Z., Sathyakumar, S., Sarkar, S., Jiang, X., Dong, X., Di Maio, R., Wang, W., Keeney, M. T., Felsky, D., Sandoe, J., Vahdatshoar, A., Udeshi, N. D., Mani, D. R., Carr, S. A., Lindquist, S., … Khurana, V. (2022). The Parkinson's disease protein alpha-synuclein is a modulator of processing bodies and mRNA stability. *Cell*, *185*(12), 2035-2056.e33. https://doi.org/10.1016/j.cell.2022.05.008
Han, X., Maita, N., Shimada, A., & Kohda, D. (2022). Effects of targeting signal mutations in a mitochondrial presequence on the spatial distribution of the conformational ensemble in the binding site of Tom20. *Protein Science*, *31*(10), e4433. https://doi.org/10.1002/pro.4433
Han, Y., Branon, T. C., Martell, J. D., Boassa, D., Shechner, D., Ellisman, M. H., & Ting, A. (2019). Directed Evolution of Split APEX2 Peroxidase. *ACS Chemical Biology*, *14*(4), 619–635. https://doi.org/10.1021/acschembio.8b00919
Han, Y., Wu, P., Wang, Z., Zhang, Z., Sun, S., Liu, J., Gong, S., Gao, P., Iwakuma, T., Molina-Vila, M. A., Chen, B. P.-C., Zhang, Y., Ji, T., Mo, Q., Chen, P., Hu, J., Wang, S., Zhou, J., Lu, H., & Gao, Q. (2019). Ubiquinol-cytochrome C reductase core protein II promotes tumorigenesis by facilitating p53 degradation. *EBioMedicine*, *40*, 92–105. https://doi.org/10.1016/j.ebiom.2019.01.002
Hanada, Y., Ishihara, N., Wang, L., Otera, H., Ishihara, T., Koshiba, T., Mihara, K., Ogawa, Y., & Nomura, M. (2020). MAVS is energized by Mff which senses mitochondrial metabolism via AMPK for acute antiviral immunity. *Nature Communications*, *11*(1), 5711–5711. https://doi.org/10.1038/s41467-020-19287-7
Hannigan, M. M., Hoffman, A. M., Thompson, J. W., Zheng, T., & Nicchitta, C. V. (2020). Quantitative Proteomics Links the LRRC59 Interactome to mRNA Translation on the ER Membrane. *Molecular & Cellular Proteomics*, *19*(11), 1826–1849. https://doi.org/10.1074/mcp.RA120.002228
Harbauer, A. B., Hees, J. T., Wanderoy, S., Segura, I., Gibbs, W., Cheng, Y., Ordonez, M., Cai, Z., Cartoni, R., Ashrafi, G., Wang, C., Perocchi, F., He, Z., & Schwarz, T. L. (2022). Neuronal mitochondria transport Pink1 mRNA via synaptojanin 2 to support local mitophagy. *Neuron*, *110*(9),

1516-1531.e9. https://doi.org/10.1016/j.neuron.2022.01.035
Harbauer, A. B., Zahedi, R. P., Sickmann, A., Pfanner, N., & Meisinger, C. (2014). The Protein Import Machinery of Mitochondria—A Regulatory Hub in Metabolism, Stress, and Disease. *Cell Metabolism*, *19*(3), 357–372. https://doi.org/10.1016/j.cmet.2014.01.010
He, Y., Lin, Y., Zhu, Y., Ping, P., Wang, G., & Sun, F. (2019). Murine PAIP1 stimulates translation of spermiogenic mRNAs stored by YBX2 via its interaction with YBX2†. *Biology of Reproduction*, *100*(2), 561–572. https://doi.org/10.1093/biolre/ioy213
Hémono, M., Haller, A., Chicher, J., Duchêne, A.-M., & Ngondo, R. P. (2022). The interactome of CLUH reveals its association to SPAG5 and its co-translational proximity to mitochondrial proteins. *BMC Biology*, *20*(1), 13. https://doi.org/10.1186/s12915-021-01213-y
Herrmann, J. M., & Riemer, J. (2010). The Intermembrane Space of Mitochondria. *Antioxidants & Redox Signaling*, *13*(9), 1341–1358. https://doi.org/10.1089/ars.2009.3063
Hoseini, H., Pandey, S., Jores, T., Schmitt, A., Franz-Wachtel, M., Macek, B., Buchner, J., Dimmer, K. S., & Rapaport, D. (2016). The cytosolic cochaperone Sti1 is relevant for mitochondrial biogenesis and morphology. *The FEBS Journal*, *283*(18), 3338–3352. https://doi.org/10.1111/febs.13813
Hulett, J. M., Lueder, F., Chan, N. C., Perry, A. J., Wolynec, P., Likić, V. A., Gooley, P. R., & Lithgow, T. (2008). The Transmembrane Segment of Tom20 Is Recognized by Mim1 for Docking to the Mitochondrial TOM Complex. *Journal of Molecular Biology*, *376*(3), 694–704. https://doi.org/10.1016/j.jmb.2007.12.021
Hung, V., Lam, S. S., Udeshi, N. D., Svinkina, T., Guzman, G., Mootha, V. K., Carr, S. A., & Ting, A. Y. (2017a). Proteomic mapping of cytosol-facing outer mitochondrial and ER membranes in living human cells by proximity biotinylation. *eLife*, *6*, e24463. https://doi.org/10.7554/eLife.24463
Imai, K., Fujita, N., Gromiha, M. M., & Horton, P. (2011). Eukaryote-wide sequence analysis of mitochondrial β-barrel outer membrane proteins. *BMC Genomics*, *12*(1), 79–79. https://doi.org/10.1186/1471-2164-12-79
Jores, T., Klinger, A., Groß, L. E., Kawano, S., Flinner, N., Duchardt-Ferner, E., Wöhnert, J., Kalbacher, H., Endo, T., Schleiff, E., & Rapaport, D. (2016). Characterization of the targeting signal in mitochondrial β-barrel proteins. *Nature Communications*, *7*(1), 12036–12036. https://doi.org/10.1038/ncomms12036
Kaltimbacher, V., Bonnet, C., Lecoeuvre, G., Forster, V., Sahel, J.-A., & Corral-Debrinski, M. (2006). mRNA localization to the mitochondrial surface allows the efficient translocation inside the organelle of a nuclear recoded ATP6 protein. *RNA (New York, N.Y.)*, *12*(7), 1408–1417. https://doi.org/10.1261/rna.18206

Kanaji, S., Iwahashi, J., Kida, Y., Sakaguchi, M., & Mihara, K. (2000). Characterization of the Signal That Directs Tom20 to the Mitochondrial Outer Membrane. *Journal of Cell Biology*, *151*(2), 277–288. https://doi.org/10.1083/jcb.151.2.277

Keil, P., & Pfanner, N. (1993). Insertion of MOM22 into the mitochondrial outer membrane strictly depends on surface receptors. *FEBS Letters*, *321*(2–3), 197–200. https://doi.org/10.1016/0014-5793(93)80107-6

Kemper, C., Habib, S. J., Engl, G., Heckmeyer, P., Dimmer, K. S., & Rapaport, D. (2008). Integration of tail-anchored proteins into the mitochondrial outer membrane does not require any known import components. *Journal of Cell Science*, *121*(12), 1990–1998. https://doi.org/10.1242/jcs.024034

Kim, D. I., Jensen, S. C., Noble, K. A., Kc, B., Roux, K. H., Motamedchaboki, K., & Roux, K. J. (2016). An improved smaller biotin ligase for BioID proximity labeling. *Molecular Biology of the Cell*, *27*(8), 1188–1196. https://doi.org/10.1091/mbc.E15-12-0844

Komiya, T., Rospert, S., Koehler, C., Looser, R., Schatz, G., & Mihara, K. (1998). Interaction of mitochondrial targeting signals with acidic receptor domains along the protein import pathway: Evidence for the 'acid chain' hypothesis. *The EMBO Journal*, *17*(14), 3886–3898. https://doi.org/10.1093/emboj/17.14.3886

Kreimendahl, S., & Rassow, J. (2020). The Mitochondrial Outer Membrane Protein Tom70-Mediator in Protein Traffic, Membrane Contact Sites and Innate Immunity. *International Journal of Molecular Sciences*, *21*(19). https://doi.org/10.3390/ijms21197262

Krimmer, T., Rapaport, D., Ryan, M. T., Meisinger, C., Kassenbrock, C. K., Blachly-Dyson, E., Forte, M., Douglas, M. G., Neupert, W., Nargang, F. E., & Pfanner, N. (2001). Biogenesis of Porin of the Outer Mitochondrial Membrane Involves an Import Pathway via Receptors and the General Import Pore of the Tom Complex. *Journal of Cell Biology*, *152*(2), 289–300. https://doi.org/10.1083/jcb.152.2.289

Kubitz, L., Bitsch, S., Zhao, X., Schmitt, K., Deweid, L., Roehrig, A., Barazzone, E. C., Valerius, O., Kolmar, H., & Béthune, J. (2022). Engineering of ultraID, a compact and hyperactive enzyme for proximity-dependent biotinylation in living cells. *Communications Biology*, *5*(1), 657. https://doi.org/10.1038/s42003-022-03604-5

Kühlbrandt, W. (2015). Structure and function of mitochondrial membrane protein complexes. *BMC Biology*, *13*(1), 89–89. https://doi.org/10.1186/s12915-015-0201-x

Kurz, M., Martin, H., Rassow, J., Pfanner, N., & Ryan, M. T. (1999). Biogenesis of Tim Proteins of the Mitochondrial Carrier Import Pathway: Differential Targeting Mechanisms and Crossing Over with the Main Import Pathway. *Molecular Biology of the Cell*, *10*(7), 2461–2474. https://doi.org/10.1091/mbc.10.7.2461

Kutik, S., Stojanovski, D., Becker, L., Becker, T., Meinecke, M., Krüger, V., Prinz, C., Meisinger, C., Guiard, B., Wagner, R., Pfanner, N., & Wiedemann, N. (2008). Dissecting Membrane Insertion of Mitochondrial β-Barrel Proteins. *Cell*, *132*(6), 1011–1024. https://doi.org/10.1016/j.cell.2008.01.028

Laemmli, U. K. (1970). Cleavage of Structural Proteins during the Assembly of the Head of Bacteriophage T4. *Nature*, *227*(5259), 680–685. https://doi.org/10.1038/227680a0

Lam, S. S., Martell, J. D., Kamer, K. J., Deerinck, T. J., Ellisman, M. H., Mootha, V. K., & Ting, A. Y. (2015). Directed evolution of APEX2 for electron microscopy and proximity labeling. *Nature Methods*, *12*(1), 51–54. https://doi.org/10.1038/nmeth.3179

Lapointe, C. P., Stefely, J. A., Jochem, A., Hutchins, P. D., Wilson, G. M., Kwiecien, N. W., Coon, J. J., Wickens, M., & Pagliarini, D. J. (2018). Multi-omics Reveal Specific Targets of the RNA-Binding Protein Puf3p and Its Orchestration of Mitochondrial Biogenesis. *Cell Systems*, *6*(1), 125-135.e6. https://doi.org/10.1016/j.cels.2017.11.012

Lee, S.-Y., Kang, M.-G., Park, J.-S., Lee, G., Ting, A. Y., & Rhee, H.-W. (2016). APEX Fingerprinting Reveals the Subcellular Localization of Proteins of Interest. *Cell Reports*, *15*(8), 1837–1847. https://doi.org/10.1016/j.celrep.2016.04.064

Lennicke, C., Rahn, J., Lichtenfels, R., Wessjohann, L. A., & Seliger, B. (2015). Hydrogen peroxide – production, fate and role in redox signaling of tumor cells. *Cell Communication and Signaling*, *13*(1), 39. https://doi.org/10.1186/s12964-015-0118-6

Lewis, B. M., Cho, C. Y., Her, H.-L., Mizrahi, O., Hunter, T., & Yeo, G. W. (2024). LARP4 is an RNA-binding protein that binds nuclear-encoded mitochondrial mRNAs to promote mitochondrial function. *RNA*, *30*(3), 223–239. https://doi.org/10.1261/rna.079799.123

Li, R., Zou, Z., Wang, W., & Zou, P. (2022). Metabolic incorporation of electron-rich ribonucleosides enhances APEX-seq for profiling spatially restricted nascent transcriptome. *Cell Chemical Biology*, *29*(7), 1218-1231.e8. https://doi.org/10.1016/j.chembiol.2022.02.005

Lin, W., & Kang, U. J. (2008). Characterization of PINK1 processing, stability, and subcellular localization. *Journal of Neurochemistry*, *106*(1), 464–474. https://doi.org/10.1111/j.1471-4159.2008.05398.x

Liu, Q., Chang, C. E., Wooldredge, A. C., Fong, B., Kennedy, B. K., & Zhou, C. (2022). Tom70-based transcriptional regulation of mitochondrial biogenesis and aging. *eLife*, *11*, e75658. https://doi.org/10.7554/eLife.75658

Longen, S., Woellhaf, M. W., Petrungaro, C., Riemer, J., & Herrmann, J. M. (2014). The Disulfide Relay of the Intermembrane Space Oxidizes the Ribosomal Subunit Mrp10 on Its Transit into the Mitochondrial Matrix. *Developmental Cell*, *28*(1), 30–42.

https://doi.org/10.1016/j.devcel.2013.11.007
Ma, Z., Xie, T., Sun, J., Yu, J., Huang, S., Zhou, Q., & Li, B. (2023). Identification of SPRYD4 as a tumour suppressor predicts prognosis and correlates with immune infiltration in cholangiocarcinoma. *BMC Cancer*, *23*(1), 404. https://doi.org/10.1186/s12885-023-10810-9
Marc, P., Margeot, A., Devaux, F., Blugeon, C., Corral-Debrinski, M., & Jacq, C. (2002). Genome-wide analysis of mRNAs targeted to yeast mitochondria. *EMBO Reports*, *3*(2), 159–164. https://doi.org/10.1093/embo-reports/kvf025
Marintchev, A., Edmonds, K. A., Marintcheva, B., Hendrickson, E., Oberer, M., Suzuki, C., Herdy, B., Sonenberg, N., & Wagner, G. (2009). Topology and Regulation of the Human eIF4A/4G/4H Helicase Complex in Translation Initiation. *Cell*, *136*(3), 447–460. https://doi.org/10.1016/j.cell.2009.01.014
Marin-Valencia, I., Roe, C. R., & Pascual, J. M. (2010). Pyruvate carboxylase deficiency: Mechanisms, mimics and anaplerosis. *Molecular Genetics and Metabolism*, *101*(1), 9–17. https://doi.org/10.1016/j.ymgme.2010.05.004
Martell, J. D., Deerinck, T. J., Sancak, Y., Poulos, T. L., Mootha, V. K., Sosinsky, G. E., Ellisman, M. H., & Ting, A. Y. (2012). Engineered ascorbate peroxidase as a genetically encoded reporter for electron microscopy. *Nature Biotechnology*, *30*(11), 1143–1148. https://doi.org/10.1038/nbt.2375
McLean, P. J., Kawamata, H., & Hyman, B. T. (2001). α-Synuclein–enhanced green fluorescent protein fusion proteins form proteasome sensitive inclusions in primary neurons. *Neuroscience*, *104*(3), 901–912. https://doi.org/10.1016/S0306-4522(01)00113-0
Meinecke, M., Wagner, R., Kovermann, P., Guiard, B., Mick, D. U., Hutu, D. P., Voos, W., Truscott, K. N., Chacinska, A., Pfanner, N., & Rehling, P. (2006). Tim50 Maintains the Permeability Barrier of the Mitochondrial Inner Membrane. *Science*, *312*(5779), 1523–1526. https://doi.org/10.1126/science.1127628
Meineke, B., Engl, G., Kemper, C., Vasiljev-Neumeyer, A., Paulitschke, H., & Rapaport, D. (2008). The outer membrane form of the mitochondrial protein Mcr1 follows a TOM-independent membrane insertion pathway. *FEBS Letters*, *582*(6), 855–860. https://doi.org/10.1016/j.febslet.2008.02.009
Meisinger, C., Ryan, M. T., Hill, K., Model, K., Lim, J. H., Sickmann, A., Müller, H., Meyer, H. E., Wagner, R., & Pfanner, N. (2001). Protein Import Channel of the Outer Mitochondrial Membrane: A Highly Stable Tom40-Tom22 Core Structure Differentially Interacts with Preproteins, Small Tom Proteins, and Import Receptors. *Molecular and Cellular Biology*, *21*(7), 2337–2348.
Meisinger, C., Sickmann, A., & Pfanner, N. (2008). The Mitochondrial

Proteome: From Inventory to Function. *Cell*, *134*(1), 22–24. https://doi.org/10.1016/j.cell.2008.06.043

Merrill, R. A., & Strack, S. (2014). Mitochondria: A kinase anchoring protein 1, a signaling platform for mitochondrial form and function. *The International Journal of Biochemistry & Cell Biology*, *48*, 92–96. https://doi.org/10.1016/j.biocel.2013.12.012

Meurant, S., Mauclet, L., Dieu, M., Arnould, T., Eyckerman, S., & Renard, P. (2023). Endogenous TOM20 Proximity Labeling: A Swiss-Knife for the Study of Mitochondrial Proteins in Human Cells. *International Journal of Molecular Sciences*, *24*(11). https://doi.org/10.3390/ijms24119604

Minde, D.-P., Ramakrishna, M., & Lilley, K. S. (2020). Biotin proximity tagging favours unfolded proteins and enables the study of intrinsically disordered regions. *Communications Biology*, *3*(1), 38. https://doi.org/10.1038/s42003-020-0758-y

Moczko, M., Bömer, U., Kübrich, M., Zufall, N., Hönlinger, A., & Pfanner, N. (1997). The Intermembrane Space Domain of Mitochondrial Tom22 Functions as a trans Binding Site for Preproteins with N-Terminal Targeting Sequences. *Molecular and Cellular Biology*, *17*(11), 6574–6584. https://doi.org/10.1128/MCB.17.11.6574

Morgenstern, M., Peikert, C. D., Lübbert, P., Suppanz, I., Klemm, C., Alka, O., Steiert, C., Naumenko, N., Schendzielorz, A., Melchionda, L., Mühlhäuser, W. W. D., Knapp, B., Busch, J. D., Stiller, S. B., Dannenmaier, S., Lindau, C., Licheva, M., Eickhorst, C., Galbusera, R., … Warscheid, B. (2021). Quantitative high-confidence human mitochondrial proteome and its dynamics in cellular context. *Cell Metabolism*, *33*(12), 2464-2483.e18. https://doi.org/10.1016/j.cmet.2021.11.001

Mossmann, D., Meisinger, C., & Vögtle, F.-N. (2012). Processing of mitochondrial presequences. *Biochimica et Biophysica Acta (BBA) - Gene Regulatory Mechanisms*, *1819*(9), 1098–1106. https://doi.org/10.1016/j.bbagrm.2011.11.007

Narendra, D. P., Jin, S. M., Tanaka, A., Suen, D.-F., Gautier, C. A., Shen, J., Cookson, M. R., & Youle, R. J. (2010). PINK1 Is Selectively Stabilized on Impaired Mitochondria to Activate Parkin. *PLoS Biology*, *8*(1), e1000298. https://doi.org/10.1371/journal.pbio.1000298

Negrutskii, B. S., Shalak, V. F., Novosylna, O. V., Porubleva, L. V., Lozhko, D. M., & El'skaya, A. V. (2023). The eEF1 family of mammalian translation elongation factors. *BBA Advances*, *3*, 100067. https://doi.org/10.1016/j.bbadva.2022.100067

Neupert, W., & Herrmann, J. M. (2007). Translocation of proteins into mitochondria. *Annual Review of Biochemistry*, *76*, 723–749. https://doi.org/10.1146/ANNUREV.BIOCHEM.76.052705.163409

Obita, T., Muto, T., Endo, T., & Kohda, D. (2003). Peptide Library Approach with a Disulfide Tether to Refine the Tom20 Recognition Motif in

Mitochondrial Presequences. *Journal of Molecular Biology*, *328*(2), 495–504. https://doi.org/10.1016/S0022-2836(03)00288-2

Omura, T. (1998). Mitochondria-Targeting Sequence, a Multi-Role Sorting Sequence Recognized at All Steps of Protein Import into Mitochondria. *The Journal of Biochemistry*, *123*(6), 1010–1016. https://doi.org/10.1093/oxfordjournals.jbchem.a022036

Osma-Garcia, I. C., Mouysset, M., Capitan-Sobrino, D., Aubert, Y., Turner, M., & Diaz-Muñoz, M. D. (2023). The RNA binding proteins TIA1 and TIAL1 promote Mcl1 mRNA translation to protect germinal center responses from apoptosis. *Cellular & Molecular Immunology*, *20*(9), 1063–1076. https://doi.org/10.1038/s41423-023-01063-4

Pacheco-Alvarez, D., Solórzano-Vargas, R. S., Gravel, R. A., Cervantes-Roldán, R., Velázquez, A., & León-Del-Río, A. (2004). Paradoxical Regulation of Biotin Utilization in Brain and Liver and Implications for Inherited Multiple Carboxylase Deficiency. *Journal of Biological Chemistry*, *279*(50), 52312–52318. https://doi.org/10.1074/jbc.M407056200

Padrón, A., Iwasaki, S., & Ingolia, N. T. (2019). Proximity RNA Labeling by APEX-Seq Reveals the Organization of Translation Initiation Complexes and Repressive RNA Granules. *Molecular Cell*, *75*(4), 875-887.e5. https://doi.org/10.1016/j.molcel.2019.07.030

Palade, G. E. (1953). AN ELECTRON MICROSCOPE STUDY OF THE MITOCHONDRIAL STRUCTURE. *Journal of Histochemistry & Cytochemistry*, *1*(4), 188–211. https://doi.org/10.1177/1.4.188

Papić, D., Elbaz-Alon, Y., Koerdt, S. N., Leopold, K., Worm, D., Jung, M., Schuldiner, M., & Rapaport, D. (2013). The Role of Djp1 in Import of the Mitochondrial Protein Mim1 Demonstrates Specificity between a Cochaperone and Its Substrate Protein. *Molecular and Cellular Biology*, *33*(20), 4083–4094. https://doi.org/10.1128/MCB.00227-13

Papić, D., Krumpe, K., Dukanovic, J., Dimmer, K. S., & Rapaport, D. (2011). Multispan mitochondrial outer membrane protein Ugo1 follows a unique Mim1-dependent import pathway. *Journal of Cell Biology*, *194*(3), 397–405. https://doi.org/10.1083/jcb.201102041

Perez-Riverol, Y., Bai, J., Bandla, C., García-Seisdedos, D., Hewapathirana, S., Kamatchinathan, S., Kundu, D. J., Prakash, A., Frericks-Zipper, A., Eisenacher, M., Walzer, M., Wang, S., Brazma, A., & Vizcaíno, J. A. (2022). The PRIDE database resources in 2022: A hub for mass spectrometry-based proteomics evidences. *Nucleic Acids Research*, *50*(D1), D543–D552. https://doi.org/10.1093/nar/gkab1038

Pla-Martín, D., Schatton, D., Wiederstein, J. L., Marx, M., Khiati, S., Krüger, M., & Rugarli, E. I. (2020). CLUH granules coordinate translation of mitochondrial proteins with mTORC1 signaling and mitophagy. *The EMBO Journal*, *39*(9), e102731. https://doi.org/10.15252/embj.2019102731

Pollutri, D., & Penzo, M. (2020). Ribosomal Protein L10: From Function to Dysfunction. *Cells*, *9*(11), 2503. https://doi.org/10.3390/cells9112503

Popov-Čeleketić, J., Waizenegger, T., & Rapaport, D. (2008). Mim1 Functions in an Oligomeric Form to Facilitate the Integration of Tom20 into the Mitochondrial Outer Membrane. *Journal of Molecular Biology*, *376*(3), 671–680. https://doi.org/10.1016/j.jmb.2007.12.006

Qin, W., Cheah, J. S., Xu, C., Messing, J., Freibaum, B. D., Boeynaems, S., Taylor, J. P., Udeshi, N. D., Carr, S. A., & Ting, A. Y. (2023). Dynamic mapping of proteome trafficking within and between living cells by TransitID. *Cell*, *186*(15), 3307-3324.e30. https://doi.org/10.1016/j.cell.2023.05.044

Qin, W., Myers, S. A., Carey, D. K., Carr, S. A., & Ting, A. Y. (2021). Spatiotemporally-resolved mapping of RNA binding proteins via functional proximity labeling reveals a mitochondrial mRNA anchor promoting stress recovery. *Nature Communications*, *12*(1), 4980–4980. https://doi.org/10.1038/s41467-021-25259-2

Qiu, J., Wenz, L.-S., Zerbes, R. M., Oeljeklaus, S., Bohnert, M., Stroud, D. A., Wirth, C., Ellenrieder, L., Thornton, N., Kutik, S., Wiese, S., Schulze-Specking, A., Zufall, N., Chacinska, A., Guiard, B., Hunte, C., Warscheid, B., van der Laan, M., Pfanner, N., … Becker, T. (2013). Coupling of Mitochondrial Import and Export Translocases by Receptor-Mediated Supercomplex Formation. *Cell*, *154*(3), 596–608. https://doi.org/10.1016/j.cell.2013.06.033

Qiu, L., Chao, W., Zhong, S., & Ren, A.-J. (2023). Eukaryotic Ribosomal Protein S5 of the 40S Subunit: Structure and Function. *International Journal of Molecular Sciences*, *24*(4), 3386. https://doi.org/10.3390/ijms24043386

Ramage, L., Junne, T., Hahne, K., Lithgow, T., & Schatz, G. (1993). Functional cooperation of mitochondrial protein import receptors in yeast. *The EMBO Journal*, *12*(11), 4115–4123. https://doi.org/10.1002/j.1460-2075.1993.tb06095.x

Rangaraju, V., Lauterbach, M., & Schuman, E. M. (2019). Spatially Stable Mitochondrial Compartments Fuel Local Translation during Plasticity. *Cell*, *176*(1), 73-84.e15. https://doi.org/10.1016/j.cell.2018.12.013

Rath, S., Sharma, R., Gupta, R., Ast, T., Chan, C., Durham, T. J., Goodman, R. P., Grabarek, Z., Haas, M. E., Hung, W. H. W., Joshi, P. R., Jourdain, A. A., Kim, S. H., Kotrys, A. V., Lam, S. S., McCoy, J. G., Meisel, J. D., Miranda, M., Panda, A., … Mootha, V. K. (2021). MitoCarta3.0: An updated mitochondrial proteome now with sub-organelle localization and pathway annotations. *Nucleic Acids Research*, *49*(D1), D1541–D1547. https://doi.org/10.1093/nar/gkaa1011

Rehling, P., Model, K., Brandner, K., Kovermann, P., Sickmann, A., Meyer, H. E., Kühlbrandt, W., Wagner, R., Truscott, K. N., & Pfanner, N. (2003). Protein Insertion into the Mitochondrial Inner Membrane by a Twin-Pore Translocase. *Science*, *299*(5613), 1747–1751.

https://doi.org/10.1126/science.1080945
Rhee, H.-W., Zou, P., Udeshi, N. D., Martell, J. D., Mootha, V. K., Carr, S. A., & Ting, A. Y. (2013). Proteomic Mapping of Mitochondria in Living Cells via Spatially Restricted Enzymatic Tagging. *Science*, *339*(6125), 1328–1331. https://doi.org/10.1126/science.1230593
Roberts, B., Haupt, A., Tucker, A., Grancharova, T., Arakaki, J., Fuqua, M. A., Nelson, A., Hookway, C., Ludmann, S. A., Mueller, I. A., Yang, R., Horwitz, R., Rafelski, S. M., & Gunawardane, R. N. (2017). Systematic gene tagging using CRISPR/Cas9 in human stem cells to illuminate cell organization. *Molecular Biology of the Cell*, *28*(21), 2854–2874. https://doi.org/10.1091/mbc.e17-03-0209
Rodríguez-González, C., Lin, S., Arkan, S., & Hansen, C. (2020). Co-chaperones DNAJA1 and DNAJB6 are critical for regulation of polyglutamine aggregation. *Scientific Reports*, *10*(1), 8130. https://doi.org/10.1038/s41598-020-65046-5
Roise, D., Horvath, S. J., Tomich, J. M., Richards, J. H., & Schatz, G. (1986). A chemically synthesized pre-sequence of an imported mitochondrial protein can form an amphiphilic helix and perturb natural and artificial phospholipid bilayers. *The EMBO Journal*, *5*(6), 1327–1334. https://doi.org/10.1002/j.1460-2075.1986.tb04363.x
Rosencrans, W. M., Rajendran, M., Bezrukov, S. M., & Rostovtseva, T. K. (2021). VDAC regulation of mitochondrial calcium flux: From channel biophysics to disease. *Cell Calcium*, *94*, 102356–102356. https://doi.org/10.1016/j.ceca.2021.102356
Roux, K. J., Kim, D. I., Raida, M., & Burke, B. (2012). A promiscuous biotin ligase fusion protein identifies proximal and interacting proteins in mammalian cells. *Journal of Cell Biology*, *196*(6), 801–810. https://doi.org/10.1083/jcb.201112098
Roy, G., De Crescenzo, G., Khaleghpour, K., Kahvejian, A., O'Connor-McCourt, M., & Sonenberg, N. (2002). Paip1 Interacts with Poly(A) Binding Protein through Two Independent Binding Motifs. *Molecular and Cellular Biology*, *22*(11), 3769–3782. https://doi.org/10.1128/MCB.22.11.3769-3782.2002
Rupert, J., Monti, M., Zacco, E., & Tartaglia, G. G. (2023). RNA sequestration driven by amyloid formation: The alpha synuclein case. *Nucleic Acids Research*, *51*(21), 11466–11478. https://doi.org/10.1093/nar/gkad857
Ryan, M. T., Müller, H., & Pfanner, N. (1999). Functional Staging of ADP/ATP Carrier Translocation across the Outer Mitochondrial Membrane *. *Journal of Biological Chemistry*, *274*(29), 20619–20627. https://doi.org/10.1074/jbc.274.29.20619
Sagan, L. (1967). On the origin of mitosing cells. *Journal of Theoretical Biology*, *14*(3), 225-IN6. https://doi.org/10.1016/0022-5193(67)90079-3
Saint-Georges, Y., Garcia, M., Delaveau, T., Jourdren, L., Le Crom, S., Lemoine, S., Tanty, V., Devaux, F., & Jacq, C. (2008). Yeast Mitochondrial Biogenesis: A Role for the PUF RNA-Binding Protein

Puf3p in mRNA Localization. *PLOS ONE*, *3*(6), e2293.
Saitoh, T., Igura, M., Obita, T., Ose, T., Kojima, R., Maenaka, K., Endo, T., & Kohda, D. (2007). Tom20 recognizes mitochondrial presequences through dynamic equilibrium among multiple bound states. *The EMBO Journal*, *26*(22), 4777–4787. https://doi.org/10.1038/sj.emboj.7601888
Sayyed, U. Mohd. H., & Mahalakshmi, R. (2022). Mitochondrial protein translocation machinery: From TOM structural biogenesis to functional regulation. *Journal of Biological Chemistry*, *298*(5). https://doi.org/10.1016/j.jbc.2022.101870
Schatton, D., Pla-Martin, D., Marx, M.-C., Hansen, H., Mourier, A., Nemazanyy, I., Pessia, A., Zentis, P., Corona, T., Kondylis, V., Barth, E., Schauss, A. C., Velagapudi, V., & Rugarli, E. I. (2017). CLUH regulates mitochondrial metabolism by controlling translation and decay of target mRNAs. *The Journal of Cell Biology*, *216*(3), 675–693. https://doi.org/10.1083/jcb.201607019
Schendzielorz, A. B., Schulz, C., Lytovchenko, O., Clancy, A., Guiard, B., Ieva, R., van der Laan, M., & Rehling, P. (2016). Two distinct membrane potential–dependent steps drive mitochondrial matrix protein translocation. *Journal of Cell Biology*, *216*(1), 83–92. https://doi.org/10.1083/jcb.201607066
Schlake, T., & Bode, J. (1994). Use of Mutated FLP Recognition Target (FRT) Sites for the Exchange of Expression Cassettes at Defined Chromosomal Loci. *Biochemistry*, *33*(43), 12746–12751. https://doi.org/10.1021/bi00209a003
Schlossmann, J., Lill, R., Neupert, W., & Court, D. A. (1996). Tom71, a Novel Homologue of the Mitochondrial Preprotein Receptor Tom70*. *Journal of Biological Chemistry*, *271*(30), 17890–17895. https://doi.org/10.1074/jbc.271.30.17890
Schopp, I. M., Amaya Ramirez, C. C., Debeljak, J., Kreibich, E., Skribbe, M., Wild, K., & Béthune, J. (2017). Split-BioID a conditional proteomics approach to monitor the composition of spatiotemporally defined protein complexes. *Nature Communications*, *8*(1), 15690–15690. https://doi.org/10.1038/ncomms15690
Sen, N. D., Zhou, F., Harris, M. S., Ingolia, N. T., & Hinnebusch, A. G. (2016). eIF4B stimulates translation of long mRNAs with structured 5′ UTRs and low closed-loop potential but weak dependence on eIF4G. *Proceedings of the National Academy of Sciences*, *113*(38), 10464–10472. https://doi.org/10.1073/pnas.1612398113
Setoguchi, K., Otera, H., & Mihara, K. (2006). Cytosolic factor- and TOM-independent import of C-tail-anchored mitochondrial outer membrane proteins. *The EMBO Journal*, *25*(24), 5635–5647. https://doi.org/10.1038/sj.emboj.7601438
Sharma, S., & Fazal, F. M. (2024). Localization of RNAs to the Mitochondria – Mechanisms and Functions. *RNA*, rna.079999.124.

https://doi.org/10.1261/rna.079999.124
Singh, C. R., Lee, B., Udagawa, T., Mohammad-Qureshi, S. S., Yamamoto, Y., Pavitt, G. D., & Asano, K. (2006). An eIF5/eIF2 complex antagonizes guanine nucleotide exchange by eIF2B during translation initiation. *The EMBO Journal*, *25*(19), 4537–4546. https://doi.org/10.1038/sj.emboj.7601339
Sinzel, M., Tan, T., Wendling, P., Kalbacher, H., Özbalci, C., Chelius, X., Westermann, B., Brügger, B., Rapaport, D., & Dimmer, K. S. (2016). Mcp3 is a novel mitochondrial outer membrane protein that follows a unique IMP-dependent biogenesis pathway. *EMBO Reports*, *17*(7), 965–981. https://doi.org/10.15252/embr.201541273
Sjöstrand, F. S. (1953). Electron Microscopy of Mitochondria and Cytoplasmic Double Membranes: Ultra-Structure of Rod-shaped Mitochondria. *Nature*, *171*(4340), 30–31. https://doi.org/10.1038/171030a0
Söllner, T., Griffiths, G., Pfaller, R., Pfanner, N., & Neupert, W. (1989). MOM19, an import receptor for mitochondrial precursor proteins. *Cell*, *59*(6), 1061–1070. https://doi.org/10.1016/0092-8674(89)90762-9
Spillane, M., Ketschek, A., Merianda, T. T., Twiss, J. L., & Gallo, G. (2013). Mitochondria Coordinate Sites of Axon Branching through Localized Intra-axonal Protein Synthesis. *Cell Reports*, *5*(6), 1564–1575. https://doi.org/10.1016/j.celrep.2013.11.022
Stojanovski, D., Guiard, B., Kozjak-Pavlovic, V., Pfanner, N., & Meisinger, C. (2007). Alternative function for the mitochondrial SAM complex in biogenesis of α-helical TOM proteins. *Journal of Cell Biology*, *179*(7), 1613–1613. https://doi.org/10.1083/jcb.20070604320071212c
Stojanovski, D., Müller, J. M., Milenkovic, D., Guiard, B., Pfanner, N., & Chacinska, A. (2008). The MIA system for protein import into the mitochondrial intermembrane space. *Biochimica et Biophysica Acta (BBA) - Molecular Cell Research*, *1783*(4), 610–617. https://doi.org/10.1016/j.bbamcr.2007.10.004
Su, J., Liu, D., Yang, F., Zuo, M.-Q., Li, C., Dong, M.-Q., Sun, S., & Sui, S.-F. (2022). Structural basis of Tom20 and Tom22 cytosolic domains as the human TOM complex receptors. *Proceedings of the National Academy of Sciences*, *119*(26), e2200158119–e2200158119. https://doi.org/10.1073/pnas.2200158119
Su, J., Tian, X., Wang, Z., Yang, J., Sun, S., & Sui, S.-F. (2024). Structure of the intact Tom20 receptor in the human translocase of the outer membrane complex. *PNAS Nexus*, *3*(7), pgae269–pgae269. https://doi.org/10.1093/pnasnexus/pgae269
Sun, Q.-A., Wu, Y., Zappacosta, F., Jeang, K.-T., Lee, B. J., Hatfield, D. L., & Gladyshev, V. N. (1999). Redox Regulation of Cell Signaling by Selenocysteine in Mammalian Thioredoxin Reductases. *Journal of Biological Chemistry*, *274*(35), 24522–24530. https://doi.org/10.1074/jbc.274.35.24522

Sylvestre, J., Margeot, A., Jacq, C., Dujardin, G., & Corral-Debrinski, M. (2003). The Role of the 3′ Untranslated Region in mRNA Sorting to the Vicinity of Mitochondria Is Conserved from Yeast to Human Cells. *Molecular Biology of the Cell*, *14*(9), 3848–3856. https://doi.org/10.1091/mbc.e03-02-0074

Szklarczyk, D., Kirsch, R., Koutrouli, M., Nastou, K., Mehryary, F., Hachilif, R., Gable, A. L., Fang, T., Doncheva, N. T., Pyysalo, S., Bork, P., Jensen, L. J., & von Mering, C. (2023). The STRING database in 2023: Protein–protein association networks and functional enrichment analyses for any sequenced genome of interest. *Nucleic Acids Research*, *51*(D1), D638–D646. https://doi.org/10.1093/nar/gkac1000

Taanman, J.-W. (1999). The mitochondrial genome: Structure, transcription, translation and replication. *Biochimica et Biophysica Acta (BBA) - Bioenergetics*, *1410*(2), 103–123. https://doi.org/10.1016/S0005-2728(98)00161-3

Takeda, H., Tsutsumi, A., Nishizawa, T., Lindau, C., Busto, J. V., Wenz, L.-S., Ellenrieder, L., Imai, K., Straub, S. P., Mossmann, W., Qiu, J., Yamamori, Y., Tomii, K., Suzuki, J., Murata, T., Ogasawara, S., Nureki, O., Becker, T., Pfanner, N., … Endo, T. (2021). Mitochondrial sorting and assembly machinery operates by β-barrel switching. *Nature*, *590*(7844), 163–169. https://doi.org/10.1038/s41586-020-03113-7

Toto, A., Camilloni, C., Giri, R., Brunori, M., Vendruscolo, M., & Gianni, S. (2016). Molecular Recognition by Templated Folding of an Intrinsically Disordered Protein. *Scientific Reports*, *6*(1), 21994. https://doi.org/10.1038/srep21994

Tsuboi, T., Viana, M. P., Xu, F., Yu, J., Chanchani, R., Arceo, X. G., Tutucci, E., Choi, J., Chen, Y. S., Singer, R. H., Rafelski, S. M., & Zid, B. M. (2020). Mitochondrial volume fraction and translation duration impact mitochondrial mRNA localization and protein synthesis. *eLife*, *9*, e57814–e57814. https://doi.org/10.7554/eLife.57814

Tucker, K., & Park, E. (2019). Cryo-EM structure of the mitochondrial protein-import channel TOM complex at near-atomic resolution. *Nature Structural & Molecular Biology*, *26*(12), 1158–1166. https://doi.org/10.1038/s41594-019-0339-2

Tyanova, S., Temu, T., & Cox, J. (2016). The MaxQuant computational platform for mass spectrometry-based shotgun proteomics. *Nature Protocols*, *11*(12), 2301–2319. https://doi.org/10.1038/nprot.2016.136

Uyhazi, K. E., Yang, Y., Liu, N., Qi, H., Huang, X. A., Mak, W., Weatherbee, S. D., de Prisco, N., Gennarino, V. A., Song, X., & Lin, H. (2020). Pumilio proteins utilize distinct regulatory mechanisms to achieve complementary functions required for pluripotency and embryogenesis. *Proceedings of the National Academy of Sciences*, *117*(14), 7851–7862. https://doi.org/10.1073/pnas.1916471117

Vance, J. E. (2014). MAM (mitochondria-associated membranes) in mammalian

cells: Lipids and beyond. *Biochimica et Biophysica Acta (BBA) - Molecular and Cell Biology of Lipids*, *1841*(4), 595–609. https://doi.org/10.1016/j.bbalip.2013.11.014

Vardi-Oknin, D., & Arava, Y. (2019). Characterization of Factors Involved in Localized Translation Near Mitochondria by Ribosome-Proximity Labeling. *Frontiers in Cell and Developmental Biology*, *7*. https://doi.org/10.3389/fcell.2019.00305

Vessey, J. P., Vaccani, A., Xie, Y., Dahm, R., Karra, D., Kiebler, M. A., & Macchi, P. (2006). Dendritic Localization of the Translational Repressor Pumilio 2 and Its Contribution to Dendritic Stress Granules. *The Journal of Neuroscience*, *26*(24), 6496–6496. https://doi.org/10.1523/JNEUROSCI.0649-06.2006

Vestweber, D., Brunner, J., Baker, A., & Schatz, G. (1989). A 42K outer-membrane protein is a component of the yeast mitochondrial protein import site. *Nature*, *341*(6239), 205–209. https://doi.org/10.1038/341205a0

Vogel, F., Bornhövd, C., Neupert, W., & Reichert, A. S. (2006). Dynamic subcompartmentalization of the mitochondrial inner membrane. *Journal of Cell Biology*, *175*(2), 237–247. https://doi.org/10.1083/jcb.200605138

Vögtle, F.-N., Wortelkamp, S., Zahedi, R. P., Becker, D., Leidhold, C., Gevaert, K., Kellermann, J., Voos, W., Sickmann, A., Pfanner, N., & Meisinger, C. (2009). Global Analysis of the Mitochondrial N-Proteome Identifies a Processing Peptidase Critical for Protein Stability. *Cell*, *139*(2), 428–439. https://doi.org/10.1016/j.cell.2009.07.045

Waizenegger, T., Stan, T., Neupert, W., & Rapaport, D. (2003). Signal-Anchor Domains of Proteins of the Outer Membrane of Mitochondria: STRUCTURAL AND FUNCTIONAL CHARACTERISTICS*. *Journal of Biological Chemistry*, *278*(43), 42064–42071. https://doi.org/10.1074/jbc.M305736200

Wakim, J., Goudenege, D., Perrot, R., Gueguen, N., Desquiret-Dumas, V., Chao De La Barca, J. M., Dalla Rosa, I., Manero, F., Le Mao, M., Chupin, S., Chevrollier, A., Procaccio, V., Bonneau, D., Logan, D. C., Reynier, P., Lenaers, G., & Khiati, S. (2017). CLUH couples mitochondrial distribution to the energetic and metabolic status. *Journal of Cell Science*, *130*(11), 1940–1951. https://doi.org/10.1242/jcs.201616

Walther, D. M., Rapaport, D., & Tommassen, J. (2009). Biogenesis of β-barrel membrane proteins in bacteria and eukaryotes: Evolutionary conservation and divergence. *Cellular and Molecular Life Sciences*, *66*(17), 2789–2804. https://doi.org/10.1007/s00018-009-0029-z

Wanet, A., Arnould, T., Najimi, M., & Renard, P. (2015). Connecting Mitochondria, Metabolism, and Stem Cell Fate. *Stem Cells and Development*, *24*(17), 1957–1971. https://doi.org/10.1089/scd.2015.0117

Wang, G., Moffitt, J. R., & Zhuang, X. (2018). Multiplexed imaging of high-density libraries of RNAs with MERFISH and expansion microscopy.

Scientific Reports, *8*(1), 4847–4847. https://doi.org/10.1038/s41598-018-22297-7

Wang, W., Chen, X., Zhang, L., Yi, J., Ma, Q., Yin, J., Zhuo, W., Gu, J., & Yang, M. (2020). Atomic structure of human TOM core complex. *Cell Discovery*, *6*(1), 67–67. https://doi.org/10.1038/s41421-020-00198-2

Wang, X., Qin, G., Yang, J., Zhao, C., Ren, J., & Qu, X. (2024). A subcellular selective APEX2-based proximity labeling used for identifying mitochondrial G-quadruplex DNA binding proteins. *Nucleic Acids Research*, gkae1259–gkae1259. https://doi.org/10.1093/nar/gkae1259

Wang, Y., Tong, X., Li, G., Li, J., Deng, M., & Ye, X. (2012). Ankrd17 positively regulates RIG-I -like receptor (RLR)-mediated immune signaling. *European Journal of Immunology*, *42*(5), 1304–1315. https://doi.org/10.1002/eji.201142125

Weidenfeld, I., Gossen, M., Löw, R., Kentner, D., Berger, S., Görlich, D., Bartsch, D., Bujard, H., & Schönig, K. (2009). Inducible expression of coding and inhibitory RNAs from retargetable genomic loci. *Nucleic Acids Research*, *37*(7), e50–e50. https://doi.org/10.1093/nar/gkp108

Wenz, L.-S., Ellenrieder, L., Qiu, J., Bohnert, M., Zufall, N., van der Laan, M., Pfanner, N., Wiedemann, N., & Becker, T. (2015). Sam37 is crucial for formation of the mitochondrial TOM–SAM supercomplex, thereby promoting β-barrel biogenesis. *Journal of Cell Biology*, *210*(7), 1047–1054. https://doi.org/10.1083/jcb.201504119

Wiedemann, N., & Pfanner, N. (2017). Mitochondrial Machineries for Protein Import and Assembly. *Annual Review of Biochemistry*, *86*(Volume 86, 2017), 685–714. https://doi.org/10.1146/annurev-biochem-060815-014352

Wiedemann, N., Pfanner, N., & Ryan, M. T. (2001). The three modules of ADP/ATP carrier cooperate in receptor recruitment and translocation into mitochondria. *The EMBO Journal*, *20*(5), 951–960. https://doi.org/10.1093/emboj/20.5.951

Williams, C. C., Jan, C. H., & Weissman, J. S. (2014). Targeting and plasticity of mitochondrial proteins revealed by proximity-specific ribosome profiling. *Science*, *346*(6210), 748–751. https://doi.org/10.1126/science.1257522

Wrobel, L., Sokol, A. M., Chojnacka, M., & Chacinska, A. (2016). The presence of disulfide bonds reveals an evolutionarily conserved mechanism involved in mitochondrial protein translocase assembly. *Scientific Reports*, *6*(1), 27484–27484. https://doi.org/10.1038/srep27484

Wrobel, L., Trojanowska, A., Sztolsztener, M. E., & Chacinska, A. (2013). Mitochondrial protein import: Mia40 facilitates Tim22 translocation into the inner membrane of mitochondria. *Molecular Biology of the Cell*, *24*(5), 543–554. https://doi.org/10.1091/mbc.e12-09-0649

Wu, Y., & Sha, B. (2006). Crystal structure of yeast mitochondrial outer membrane translocon member Tom70p. *Nature Structural & Molecular Biology*, *13*(7), 589–593. https://doi.org/10.1038/nsmb1106

Xie, Y., Kang, R., Klionsky, D. J., & Tang, D. (2023). GPX4 in cell death, autophagy, and disease. *Autophagy*, *19*(10), 2621–2638. https://doi.org/10.1080/15548627.2023.2218764

Xue, M., Cong, F., Zheng, W., Xu, R., Liu, X., Bao, H., Sung, Y. Y., Xi, Y., He, F., Ma, J., Yang, X., & Ge, W. (2023). Loss of Paip1 causes translation reduction and induces apoptotic cell death through ISR activation and Xrp1. *Cell Death Discovery*, *9*(1), 288–288. https://doi.org/10.1038/s41420-023-01587-8

Xue, M., Hou, J., Wang, L., Cheng, D., Lu, J., Zheng, L., & Xu, T. (2017). Optimizing the fragment complementation of APEX2 for detection of specific protein-protein interactions in live cells. *Scientific Reports*, *7*(1), 12039. https://doi.org/10.1038/s41598-017-12365-9

Xue, Q., Pei, H., Liu, Q., Zhao, M., Sun, J., Gao, E., Ma, X., & Tao, L. (2017). MICU1 protects against myocardial ischemia/reperfusion injury and its control by the importer receptor Tom70. *Cell Death & Disease*, *8*(7), e2923–e2923. https://doi.org/10.1038/cddis.2017.280

Yamamoto, H., Itoh, N., Kawano, S., Yatsukawa, Y.-I., Momose, T., Makio, T., Matsunaga, M., Yokota, M., Esaki, M., Shodai, T., Kohda, D., Aiken Hobbs, A. E., Jensen, R. E., & Endo, T. (2011). *Dual role of the receptor Tom20 in specificity and efficiency of protein import into mitochondria*. www.pnas.org/cgi/doi/10.1073/pnas.1014918108

Yamano, K., Yatsukawa, Y., Esaki, M., Hobbs, A. E. A., Jensen, R. E., & Endo, T. (2008). Tom20 and Tom22 Share the Common Signal Recognition Pathway in Mitochondrial Protein Import. *Journal of Biological Chemistry*, *283*(7), 3799–3807. https://doi.org/10.1074/jbc.M708339200

Yang, F., Bian, T., Zhan, X., Chen, Z., Xing, Z., Larsen, N. A., Zhang, X., & Shi, Y. (2023). Mechanisms of the RNA helicases DDX42 and DDX46 in human U2 snRNP assembly. *Nature Communications*, *14*(1), 897. https://doi.org/10.1038/s41467-023-36489-x

Yang, H., Sibilla, C., Liu, R., Yun, J., Hay, B. A., Blackstone, C., Chan, D. C., Harvey, R. J., & Guo, M. (2022). Clueless/CLUH regulates mitochondrial fission by promoting recruitment of Drp1 to mitochondria. *Nature Communications*, *13*(1), 1582. https://doi.org/10.1038/s41467-022-29071-4

Youle, R. J., & van der Bliek, A. M. (2012). Mitochondrial Fission, Fusion, and Stress. *Science*, *337*(6098), 1062–1065. https://doi.org/10.1126/science.1219855

Young, J. C., Hoogenraad, N. J., & Hartl, F. U. (2003). Molecular Chaperones Hsp90 and Hsp70 Deliver Preproteins to the Mitochondrial Import Receptor Tom70. *Cell*, *112*(1), 41–50. https://doi.org/10.1016/S0092-8674(02)01250-3

Zabezhinsky, D., Slobodin, B., Rapaport, D., & Gerst, J. E. (2016). An Essential Role for COPI in mRNA Localization to Mitochondria and Mitochondrial Function. *Cell Reports*, *15*(3), 540–549.

https://doi.org/10.1016/j.celrep.2016.03.053
Žaja, R., Aydin, G., Lippok, B. E., Feederle, R., Lüscher, B., & Feijs, K. L. H. (2020). Comparative analysis of MACROD1, MACROD2 and TARG1 expression, localisation and interactome. *Scientific Reports*, *10*(1), 8286. https://doi.org/10.1038/s41598-020-64623-y
Zaninello, M., Schlegel, T., Nolte, H., Pirzada, M., Savino, E., Barth, E., Klein, I., Wüstenberg, H., Uddin, T., Wolff, L., Wirth, B., Lehmann, H. C., Cioni, J.-M., Langer, T., & Rugarli, E. I. (2024). CLUH maintains functional mitochondria and translation in motoneuronal axons and prevents peripheral neuropathy. *Science Advances*, *10*(22), eadn2050. https://doi.org/10.1126/sciadv.adn2050
Zanphorlin, L. M., Lima, T. B., Wong, M. J., Balbuena, T. S., Minetti, C. A. S. A., Remeta, D. P., Young, J. C., Barbosa, L. R. S., Gozzo, F. C., & Ramos, C. H. I. (2016). Heat Shock Protein 90 kDa (Hsp90) Has a Second Functional Interaction Site with the Mitochondrial Import Receptor Tom70*. *Journal of Biological Chemistry*, *291*(36), 18620–18631. https://doi.org/10.1074/jbc.M115.710137
Zhang, P., Zhao, J.-H., Yuan, L.-X., Ju, L.-L., Wang, H.-X., Wang, F., Chen, L., & Cai, W.-H. (2023). DLAT is a promising prognostic marker and therapeutic target for hepatocellular carcinoma: A comprehensive study based on public databases. *Scientific Reports*, *13*(1), 17295. https://doi.org/10.1038/s41598-023-43835-y
Zhang, Y., Wang, Z.-H., Liu, Y., Chen, Y., Sun, N., Gucek, M., Zhang, F., & Xu, H. (2019). PINK1 Inhibits Local Protein Synthesis to Limit Transmission of Deleterious Mitochondrial DNA Mutations. *Molecular Cell*, *73*(6), 1127-1137.e5. https://doi.org/10.1016/j.molcel.2019.01.013
Zheng, Y., Dubois, W., Benham, C., Batchelor, E., & Levens, D. (2020). FUBP1 and FUBP2 enforce distinct epigenetic setpoints for MYC expression in primary single murine cells. *Communications Biology*, *3*(1), 545. https://doi.org/10.1038/s42003-020-01264-x
Zhou, M., Kong, B., Zhang, X., Xiao, K., Lu, J., Li, W., Li, M., Li, Z., Ji, W., Hou, J., & Xu, T. (2023). A proximity labeling strategy enables proteomic analysis of inter-organelle membrane contacts. *iScience*, *26*(7), 107159. https://doi.org/10.1016/j.isci.2023.107159
Zipor, G., Haim-Vilmovsky, L., Gelin-Licht, R., Gadir, N., Brocard, C., & Gerst, J. E. (2009). Localization of mRNAs coding for peroxisomal proteins in the yeast, Saccharomyces cerevisiae. *Proceedings of the National Academy of Sciences*, *106*(47), 19848–19853. https://doi.org/10.1073/pnas.0910754106

List of abbreviations

Abbreviation	Explanation
Blue Native PAGE	Blue native polyacrylamide gel electrophoresis
BSA	Bovine serum albumin
CLUH	Clustered mitochondria protein homolog
Cryo-EM	Cryogenic electron microscopy
DNA	Deoxyribonucleic acid
DOX	Doxycycline
DTT	Dithiothreitol
EDTA	Ethylenediaminetetraacetic acid
ER	Endoplasmic reticulum
ERM	Endoplasmic reticulum membrane
FL	Full-length
GFP	Green fluorescent protein
Hsp	Heat shock protein
Hsp70	70-kDa heat-shock protein
Hsp90	90-kDa heat-shock protein
HsTOM	Homo sapiens TOM
IM	Inner membrane
IMS	Intermembrane space
LARP	La ribonucleoprotein
LARP4	La ribonucleoprotein 4
MAVS	Mitochondrial antiviral-signaling protein
MIM	mitochondrial import machinery
mitoRNAs	Nuclear encoded mitochondrial transcripts
MOM	Mitochondrial outer membrane
mtDNA	Mitochondrial DNA genome
MTS	mitochondrial targeting sequence
OM	Outer membrane
OXPHOS	Mitochondrial oxidative phosphorylation
PABPC4L	Polyadenylate-binding protein 4-like
PAIP1	Translational activator PABP-interacting protein 1

PCR	Polymerase chain reaction
PINK1	Serine/threonine-protein kinase PINK1
PL	Proximity labeling
PPI	Protein-protein interactions
PVDF	Polyvinylidene fluoride
SDS-PAGE	Sodium dodecyl sulfate polyacrylamide gel electrophoresis
SNCA	alpha Synuclein
SYNJ2	Synaptojanin-2
SYNJ2BP	Synaptojanin 2 binding protein
TBS	Tris buffer saline
TIM	Translocase of the inner mitochondrial membrane
TMD	Transmembrane domain
TOM	Translocase of the outer membrane
TOM–CC	TOM core complex
Tom20	Mitochondrial import receptor subunit TOM20 in Saccharomyces cerevisiae
Tom22	Mitochondrial import receptor subunit TOM22 in Saccharomyces cerevisiae
Tom40	Mitochondrial import receptor subunit TOM40 in Saccharomyces cerevisiae
Tom70	Mitochondrial import receptor subunit TOM70 in Saccharomyces cerevisiae
TOMM20	Mitochondrial import receptor subunit TOM20 homolog in human
TOMM22	Mitochondrial import receptor subunit TOM22 homolog in human
TOMM40	Mitochondrial import receptor subunit TOM40 homolog in human
TOMM5	Mitochondrial import receptor subunit TOM5 homolog in human
TOMM6	Mitochondrial import receptor subunit TOM6 in Saccharomyces cerevisiae
TOMM7	Mitochondrial import receptor subunit TOM7 homolog in human
TOMM70	Mitochondrial import receptor subunit TOM70 homolog in human
VDAC	Voltage-dependent anion channel
WT	Wild type

Acknowledgment

I would like to take the opportunity to express my gratitude to everyone who contributed to the success of this work. I express my sincere gratitude to Prof. Ralf-Peter Jansen for giving me the opportunity to work on many projects, and for our scientific discussions. I am grateful to Prof. Dr. Jeffrey Gerst for being a part of my thesis advisory committee over the past years and reviewing this thesis in spite of the tight timeline. I would like to especially thank Prof. Boris Macek and Katharina Zittlau for their great and inspiring collaboration. I would also appreciate the great help from Silke Wahl and Bianca Lemke for MS samples processing. I also thank Prof. Dr. Gabriele Dodt and Prof. Dr. Philipp Kahle for kindly being in my thesis examining committee. My gratitude to MOMbrane RTG, and the Deutsche Forschungsgemeinschaft (DFG) for funding my doctoral research. Furthermore, I would like to thank the fellows of MOMbrane RTG, especially Prof. Dr. Doron Rappaport and Prof. Boris Macek for vivid discussions and learning atmosphere during our biweekly seminars and collaborating projects. Thanks to Klaudia Maruszczak, Fenja Odendall, and Anasuya Moitra for always being so helpful, cheerful, and supportive. I am thankful to Prof. Dr. Gabriele Dodt for her support regarding lab equipment and reagents. I am also grateful to Nisha Mohd Rafiq for her cheerful presence at IFIB, sharing lab equipment, lab reagents, moral support, and technical help in microscopy analysis. I learnt a lot about neuronal biology and neurodegenerative diseases from our talks. My thanks goes especially to Saroj Pandey, Karin Steiger, Ashwin Mathew for their kindness, motivation, and help at all times in the lab. I am thankful to Glencora Wolffhugel for moral support and being always there for me. I will miss our tea parties and biosafety discussions. I acknowledge my gratitude to my mentor Prof. Dr. Johannes Wöstemeyer from University of Jena, Germany. I appreciate your continuous support, guidance, and unwavering belief in me. Thank you for reviewing my thesis and always being so helpful throughout this journey. Beyond academic network, I like to thank my friends who have been my support system throughout my stay in Germany, I dedicate my thesis to my husband and brother, immensely supportive and understanding, thank you for being my strength and for your unconditional love!

Appendix

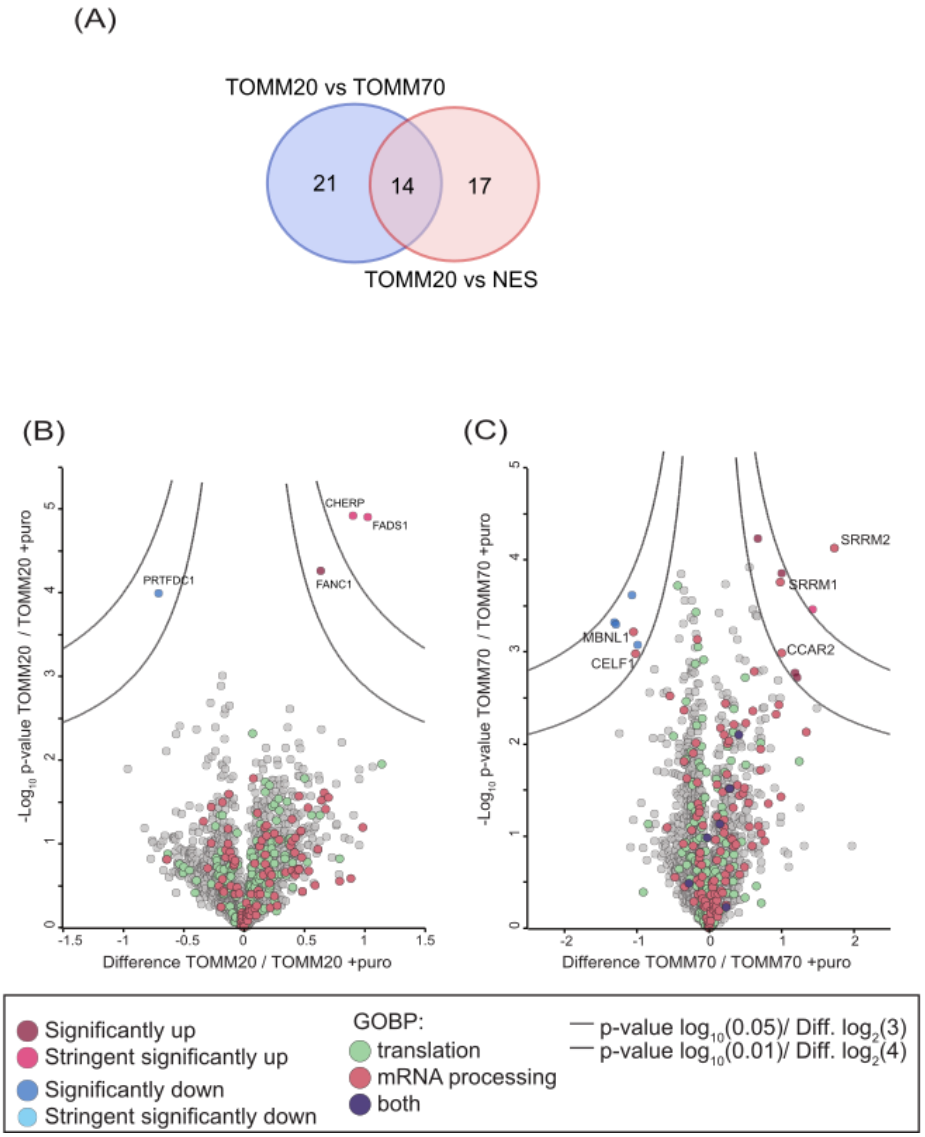

Suppl. Figure 1. Comparisons of proteins identified in various interactomes and effect of puromycin on TOMM20- and TOMM70-APEX2 interactomes.
(A) Venn diagram showing TOMM20 overlapping candidates by comparing the enriched candidates of TOMM20 in TOMM20 vs TOMM70 interactomes and TOMM20 vs NES interactome. **(B)** Volcano plots for TOMM20-APEX2 interactome against TOMM20-APEX2 interactome (+puro). **(C)** Volcano plots for TOMM70-APEX2 interactome against TOMM70-APEX2 interactome (+puro). Highlighted are the proteins annotated (based on GOBP) for translation and mRNA processing

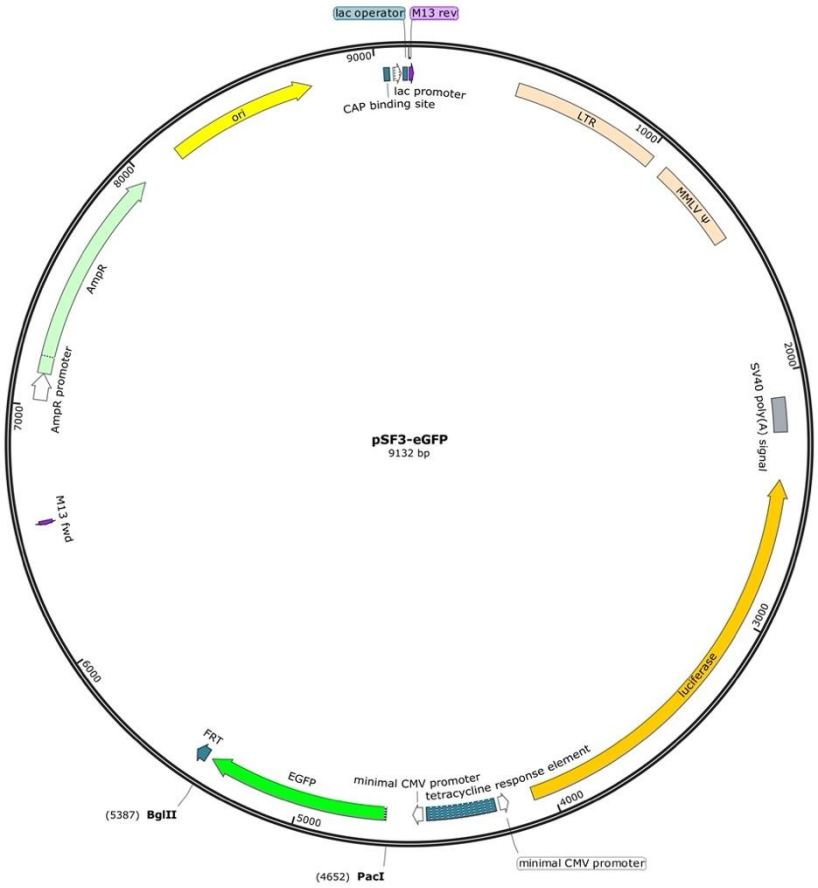

Suppl. Figure 2. Plasmid map of pSF3-GFP (RJP 2251) used as template plasmid to clone expression cassettes of corresponding fusion transgenes.

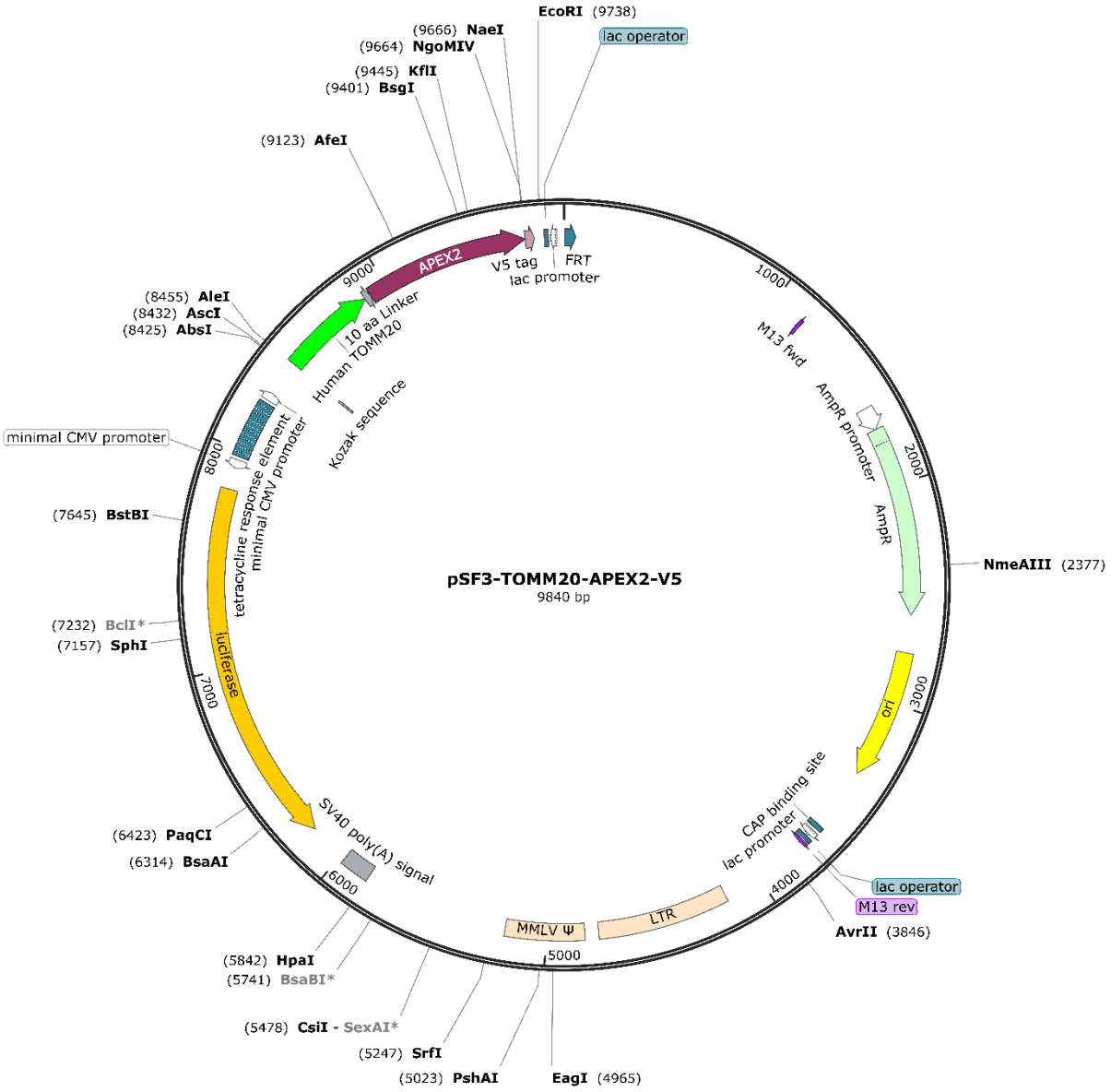

Suppl. Figure 3. Plasmid map of pSF3-TOMM20-APEX2-V5 (RJP 2303), used to express NES targeted APEX2 in HeLa cells.

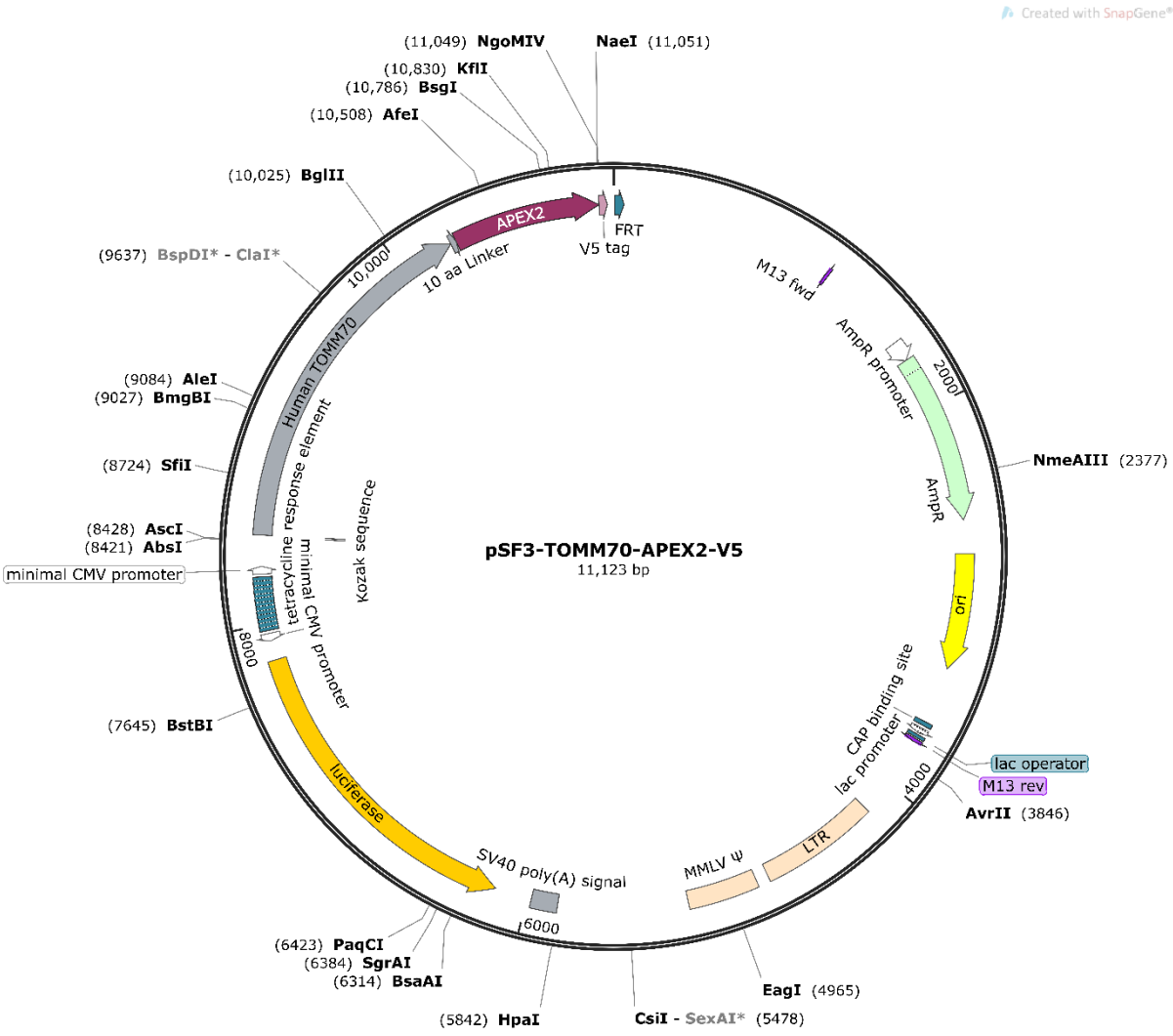

Suppl. Figure 4. Plasmid map of pSF3-TOMM70-APEX2-V5 (RJP 2307), used to express NES targeted APEX2 in HeLa cells.

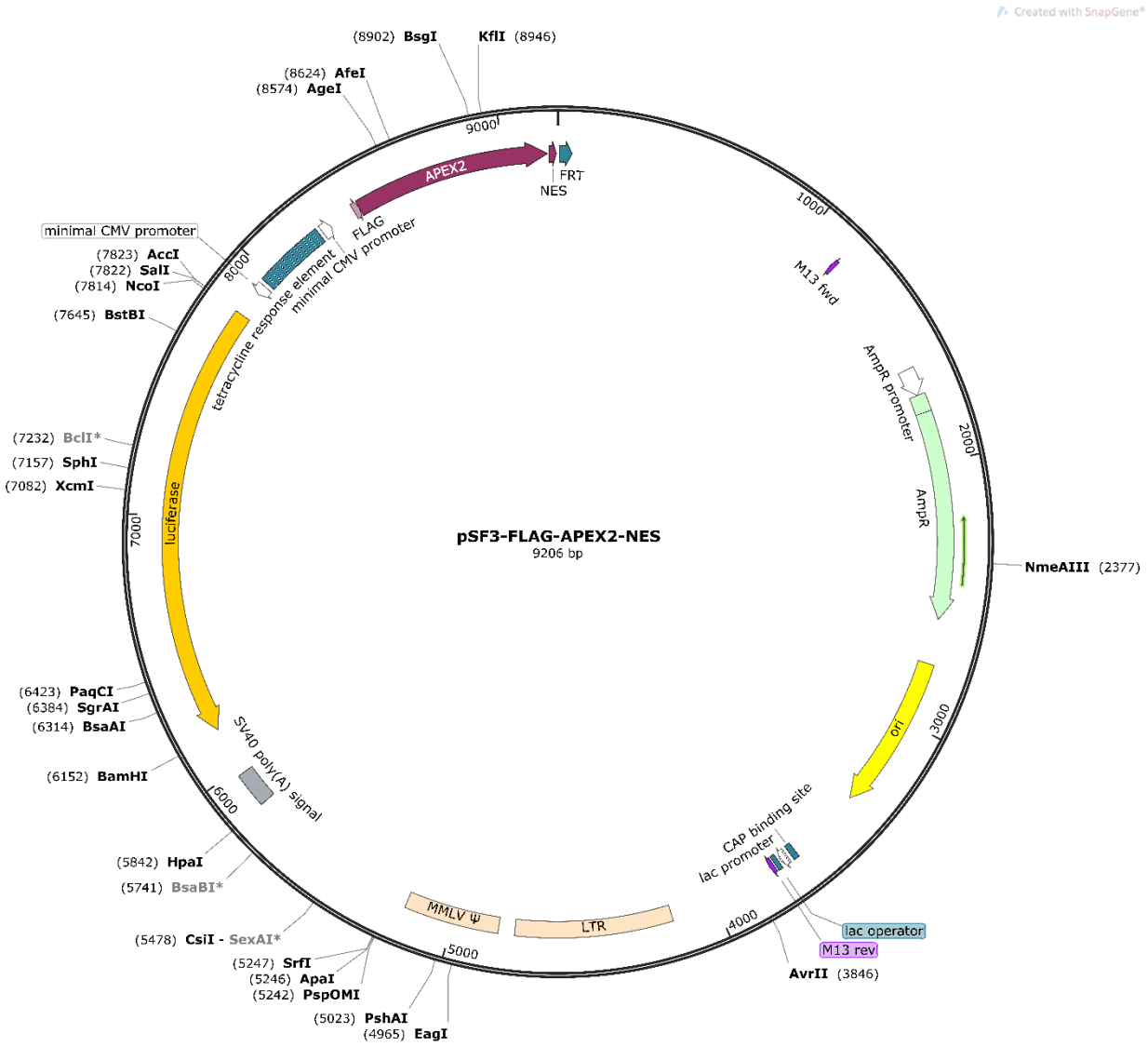

Suppl. Figure 5. Plasmid map of pSF3-FLAG-APEX2-NES (RJP 2358), used to express NES targeted APEX2 in HeLa cells.

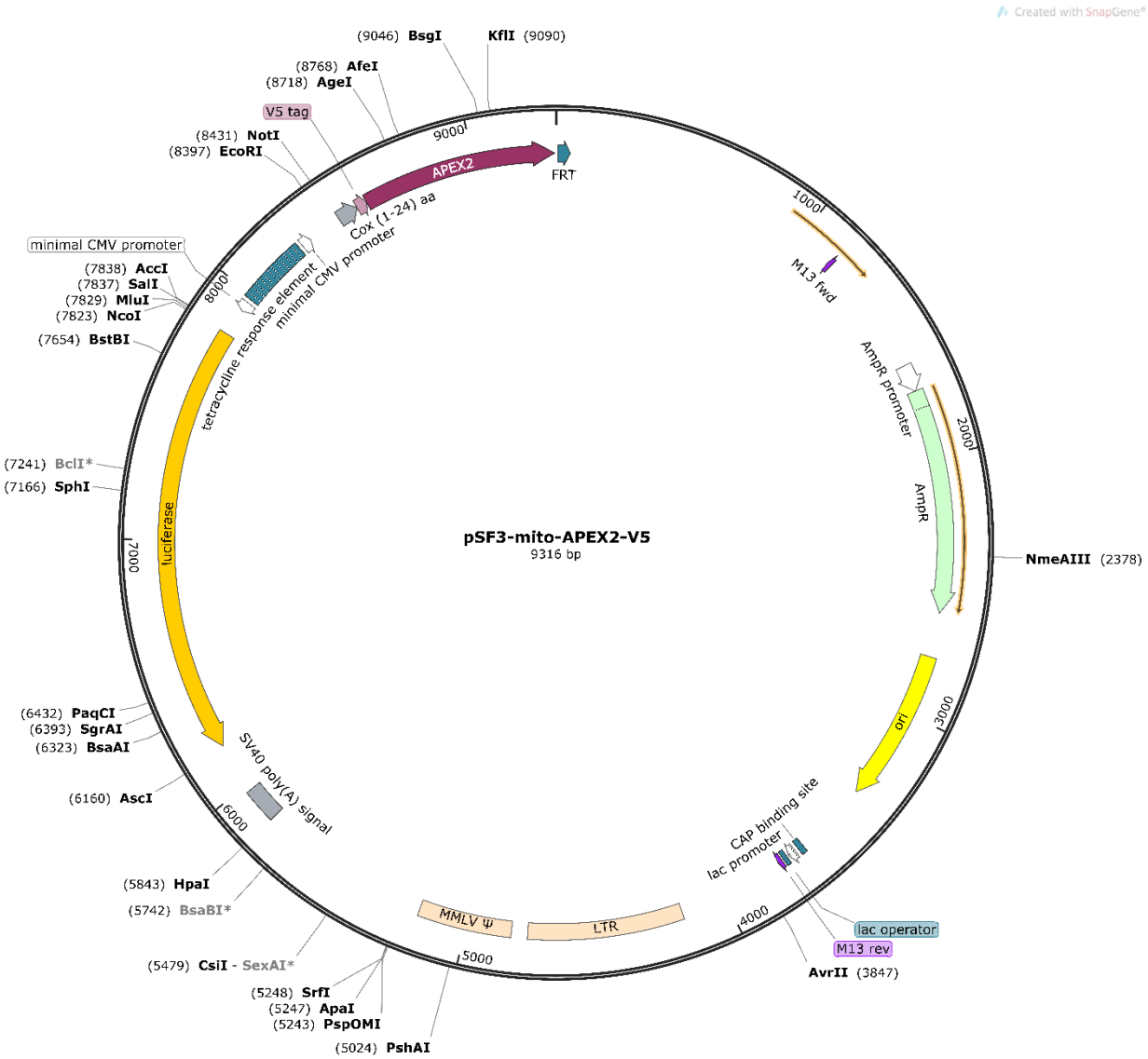

Suppl. Figure 6. Plasmid map of pSF3-mito-APEX2-V5 (RJP 2359), used to express Mito targeted APEX2 in HeLa cells.

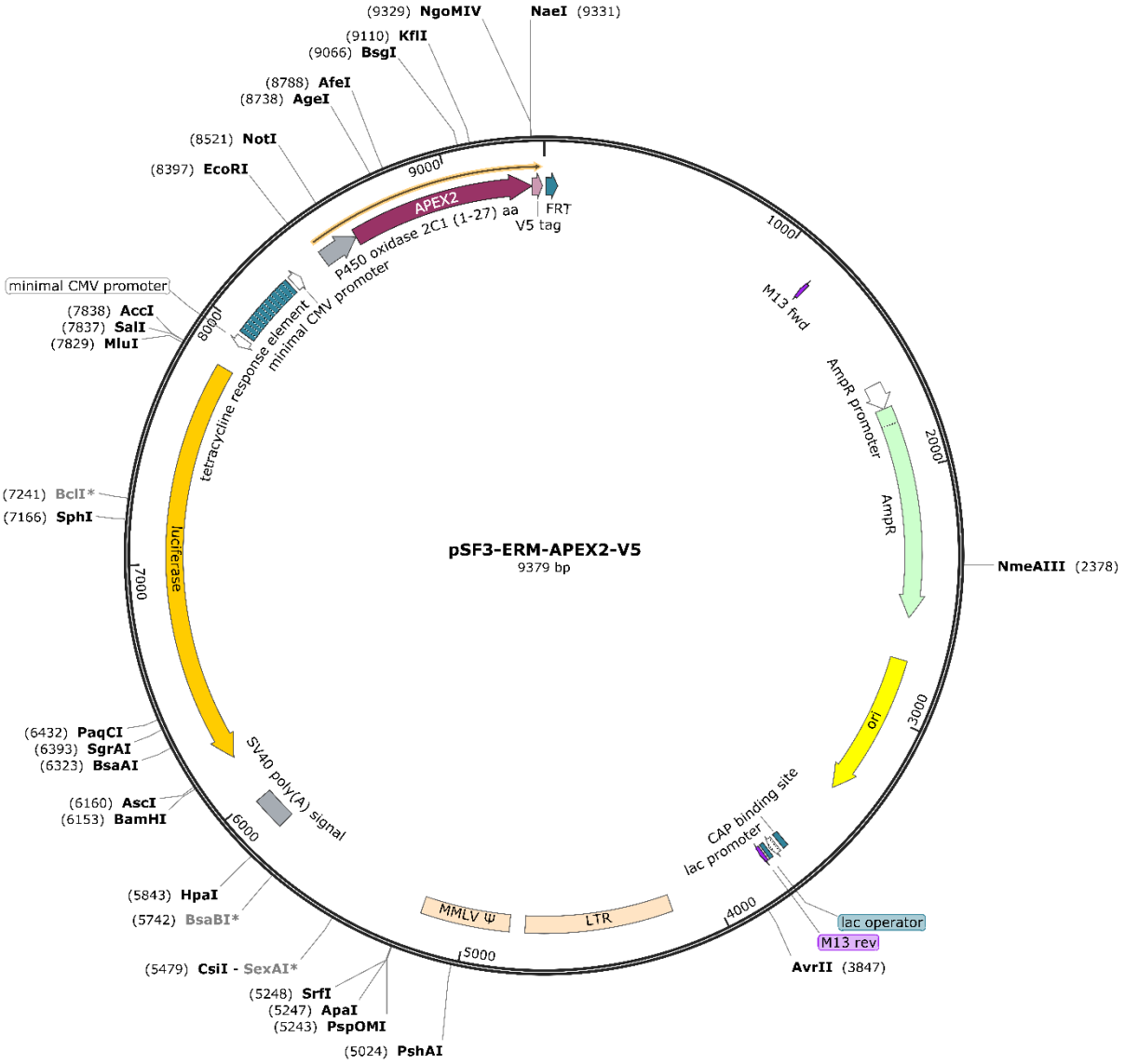

Suppl. Figure 7. Plasmid map of pSF3-ERM-APEX2-V5 (RJP 2297), used to express ERM targeted APEX2 in HeLa cells.

Supplementary tables

Supplementary Tables (1-13) are available for public access on the following repository.

https://github.com/TOMM-20-70/Thesis-supplementary-data